Doctoral   Science

2009-01-01

Enhanced Absorption Metal Oxides for Photocatalytic Applications

Reenamole Georgekutty
Technological University Dublin

Recommended Citation

Enhanced Absorption Metal Oxides for Photocatalytic Applications

Reenamole Georgekutty BSc MSc

Thesis submitted to fulfil requirements for

PhD

at Dublin Institute of Technology

Thesis Supervisors:

Dr. Michael K. Seery

Dr. Suresh C. Pillai

School of Chemical and Pharmaceutical Sciences

February 2009

ABSTRACT

Environmental pollution and industrialization on a global scale has drawn attention to the vital need for developing new hygienic and environmentally friendly purification technologies. The most common indoor and outdoor purification processes have their corresponding limitations of electricity and/or other energy sources. To address such enormous tasks, advance oxidation technology like heterogeneous photocatalytic systems via metal oxide semiconductors such as TiO_2, ZnO, that are capable to operate effectively and efficiently under UV and visible light, must be established. Due to the wide band gap of semiconductors, they are unable to absorb visible light. Hence, numerous research efforts have been done to increase the photocatalytic activity and optical absorption of semiconductors by various methods. This thesis presents the study of enhanced absorption capability of metal modified, especially silver modified, TiO_2 and ZnO and silver-ceria co-doping on TiO_2. All the experiments carried out and characterization techniques used were explained in detail.

The present work deals with the synthesis of unmodified and with various mol% of metal modified TiO_2 and ZnO. Photocatalytic activity is analysed using a model dye, rhodamine 6G (R6G). A noble metal such as silver is used as the metal modifier and optimised the concentration of silver giving the highest photcatalytic activity in both cases. The synthesis of TiO_2 through a modified sol-gel route and effect of silver modification to enhance the photocatalytic activity of TiO_2 is explored. In the case of TiO_2, two methods are adopted to introduce silver, such as the light irradiation method and the direct calcination method. Of the two methods, the latter is found to produce a more effective photocatalytic material (6–50 % improvement in catalytic efficiency),

which is attributed to the fact that the silver is homogeneously dispersed throughout the material. 5 mol% is found as the optimum giving the highest rate of photocatalytic activity. Results demonstrate that silver modification retains the anatase phase stability up to 700 °C. In addition, adsorption experiments on TiO_2 using oxalic acid illustrate that oxalic acid forms strong ring complexes on the surface of TiO_2 which undergo further degradation. Photcatalytic activity tests of various % of urea modified TiO_2 indicate urea modification can extend the anatase phase stability for higher temperatures and 1:1 TTIP:Urea modified sample at 900 °C shows high photocatalytic activity among other samples.

Analysis on the effect of silver modification on ZnO and mechanism of photocatalytic enhancement is illustrated. In the case of ZnO, a wet chemistry approach is used for the silver modification. Materials are synthesized at various temperatures ranging from 300 to 1000 °C. It is observed from the characterization that 3 mol % silver-modified ZnO at 400 °C shows approximately a four times higher rate of degradation than that of unmodified ZnO and a three times higher rate than that of commercial TiO_2 photocatalyst standard, Degussa P-25. A possible mechanism of photocatalytic activity in presence of sensitising dye is also discussed in light of photoemission studies. It is reasoned that the presence of silver facilitates the interfacial charge transfer processes in such a way to utilise the CB electrons for enhancing the photocatalytic activity.

Investigated the visible light absortption capability of TiO_2 as a result of novel silver-ceria co-doping. The effect in structural and optical properties associated with co-doping is demonstrated. Analysis on results shows silver-ceria co-doping results in a large shift in absorption towards visible wavelength resulting in visible light active

materials. Furthermore, the structural analysis clearly proves the high temperature stability of the anatase phase and it is believed that there is a silver-ceria interaction at low temperature on the TiO_2 surface.

In overview, the work produced and results derived from the current study have different potential applications in the field of semiconductor photocatalysis in the near future.
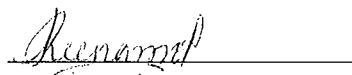
DECLARATION

I certify that this thesis which I now submit for examination for the award of PhD is entirely my own work and has not been taken from the work of others, save and to the extent that such work has been cited and acknowledged within the text of my work.

This thesis was prepared according to the regulations for postgraduate study by research of the Dublin Institute of Technology and has not been submitted in whole or in part for another award in any Institute.

The work reported on in this thesis conforms to the principles and requirements of the Institute's guidelines for ethics in research.

The Institute has permission to keep, lend or copy this thesis in whole or in part, on condition that any such use of the material of the thesis be duly acknowledged.

Signature

Reenamole Georgekutty

Date

Dedicated to my Brothers......

ACKNOWLEDGEMENTS

Nothing in the world is permanent, and we're foolish when we ask anything to last, but surely we're still more foolish not to take delight in it while we have it. If change is of the essence of existence one would have thought it only sensible to make it the premise of our philosophy.

W. Somerset Maugham

When I stand before God at the end of my life, I would hope that I would not have a single bit of talent left, and could say, 'I used everything you gave me'.

E. Bombeck

Table of Contents

ABBREVIATIONS USED

A	:	Anatase
AOP	:	Advanced oxidation process
ATR–FTIR	:	Attenuated total reflection infrared spectroscopy
AZ	:	Ag modified ZnO
BET	:	Brunauer Emmet teller
CB	:	Conduction band
DOS	:	Density of states
DRS	:	Diffuse reflectance spectroscopy
DSC	:	Differential scanning calorimetry
DSSC	:	Dye sensitized solar cell
EPA	:	Environmental protection agency
EPR	:	Electron paramagnetic resonance
FT-IR	:	Fourier transform infrared spectroscopy
g	:	Gram
HOAc	:	Acetic acid
HOMO	:	Highest occupied molecular orbital
IUPAC	:	International Union of Pure and Applied Chemistry

KBr	:	Potassium bromide
L	:	Litre
LUMO	:	Lowest unoccupied molecular orbital
PL	:	Photoluminescence
R	:	Rutile
R6G	:	Rhodamine 6G
RPM	:	Rotation per minute
SEM	:	Scanning electron microscopy
TAS	:	Transient absorption spectroscopy
TEM	:	Transmission electron microscopy
TSC	:	Trisodium Citrate
TTIP	:	Titanium tetraisopropoxide
UV	:	Ultraviolet light
VB	:	Valence band
XRD	:	X-ray diffraction

LIST OF FIGURES

LIST OF SCHEMES AND TABLES

Schemes

Tables

1. INTRODUCTION

1.1   Introduction

1.1.1   Context

Increasing contamination of ground water system and atmospheric air by organic pollutants create serious threats to living organisms as the quality of the environment is directly linked to human health. The report by the New York State Department of Environmental Conservation reveals that even babies were born with detectable levels of pollutants.[1] Ireland is not excluded from this situation. In recent decades, Ireland has faced increasing environmental pollution caused by the developments in agricultural and industrial sectors. In particular, the increases in population and urbanization have created a greater potential to spoil the green and agricultural image of the country. The rising level of pollution in rivers and lakes is one of the main environmental concerns facing the country today. While Ireland is not facing the immediate danger of extreme levels of water pollution, there is a concern that pollution levels of the Irish waters will increase substantially in the next few years if the problem is not mitigated soon. Water quality surveys from the Irish Environmental Protection Agency (EPA) show that the quality of the inland waters has decreased since they were first assessed in the 1970s.[2]

The same is true for air. According to a recent report by EPA,[3] the biggest threat facing Irish air is the emission from road traffic. Ireland has been unable to cut its production of carbon dioxide and other greenhouse gas emissions, a leading cause of global warming because of the fast growing economy and large increase in car ownership. Currently this emission is close to 70 million tons. Though the government made efforts to buy carbon credits from foreign companies and other countries that are emitting less than their specified limits to achieve an artificial cut the actual level of pollution in Ireland is expected to keep rising. Even with the reduction in emissions, the country will still be affected by climate change and heavy rainfall in the future years, because of the level of greenhouse gases already in the atmosphere. Thus, environmental pollution is

considered as a major global problem and in order to eradicate this we need a technology that is capable of destructing the pollutants efficiently and cost effectively.

1.1.2 Semiconductor photocatalysis

In order to address these significant problems, extensive research is underway to develop advanced analytical, biochemical and physicochemical methods for the characterisation and elimination of hazardous chemical compounds from air, soil and water.[4-6] In this regard, the application of photocatalysis, especially semiconductor photocatalysis has potential in tackling the problem. According to IUPAC, photocatalysis is defined as a catalytic reaction which implies the photon assisted generation of catalytically active species by the catalyst or by the substrate.[7] Hence photocatalysis is the acceleration of chemical reaction in presence of light. Among several remediation strategies available, the treatment of pollutants by semiconductor-mediated photocatalysis is one of the fastest growing areas of academic research and commercial activity over the last 20 years.[8] Moreover, the area of environmental catalysis has seen exceptional growth in past decades and still continues to display the significant applications in the 21st century, in spite of some technical difficulties toward demonstrating the commercial viabilities.

Due to the insoluble nature of the catalysts during application, semiconductor photocatalysis constitutes a heterogeneous catalytic system. Compared with traditional oxidation processes, heterogeneous photocatalysis has the following advantages:

a) It utilizes low-energy ultraviolet light with semiconductors acting as photocatalysts and leads to complete mineralization of pollutants to environmentally harmless compounds.

b) The photocatalytic processes allow thermodynamically unfavourable reactions to occur and allow destruction of non-biodegradable refractory contaminants.

c) While catalytic processes normally require high temperature or high pressure, photocatalytic oxidation is a promising technique for many purposes due to its ability to operate at or slightly above ambient conditions.

A photocatalytic system consists of semiconductor particles (photocatalysts) which are in close contact with a liquid or gaseous reaction medium. The semiconductors can act as a photocatalyst as they can be sensitized by light. On exposing the catalyst to ultraviolet light, processes such as redox reactions and molecular transformations take place which results in the detoxification of organic pollutants. Generally, a photocatalytic reaction occurs on the surface of an adsorbed phase (catalyst surface) and in the case of semiconductor photocatalysis, the photonic activity initiates the thermal activation of the catalyst.

In terms of simplicity, semiconductor photocatalysis is an efficient technology among the advance oxidation processes (AOP), because of its potential to utilise solar energy. The use of solar radiation to create energy and initiate chemical reactions has great potential in both industrial and environmental applications. The effective utilization of clean, safe, and abundant solar energy will lead to promising solutions not only for energy issues (due to the exhaustion of natural energy sources) but also for the many problems caused by environmental pollution. In addition, some of the advantages with semiconductor photocatalysts include that they are inexpensive, non-toxic, have high surface area, and exhibit tunable properties which can be modified by size reduction, doping.[9] Semiconductor photocatalysis involves a number of reactions such as photocatalytic oxidation, photocatalytic reduction, dehydrogenation, hydrogen transfer, deuterium-alkane isotopic exchange, metal deposition, water detoxification, gas-phase

4

pollutants removal and a host of other environmental applications.[9, 10] Photocatalytic oxidation is the main reaction taking place in the case of degradation of pollutants. It involves generally the heterogeneous catalytic activation of the semiconductor by irradiating light from a source of wavelength approximately greater or equal to the band gap energy of the semiconductor. A wide variety of compounds such as alkanes, alkenes, alcohols, aromatic and aliphatic alcohols, surfactants and pesticides can be degraded by the heterocatalytic oxidation.[11] For example, a general stoichiometry for the oxidation of chlorinated hydrocarbon can be written as shown in *Scheme 1.1:*

$$C_xH_yCl_z + [x + (y\text{-}z) / 4] \, O_2 \xrightarrow{\ hu, \ TiO_2\ } xCO_2 + z \, H^+ + zCl^- + (y\text{-}z/2) \, H_2O$$
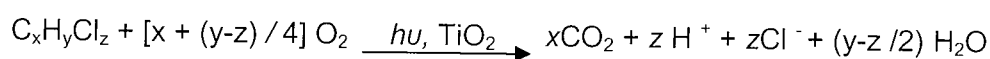
Scheme 1.1: General Scheme for oxidation of chlorinated hydrocarbon

Metal chalcogenides such as ZnS, CdS, CdSe, WS_2 and MoS_2 are also used as photocatalysts. However, metal sulfides are not stable enough for catalysis in aqueous media due to photoanodic corrosion and they are toxic. Iron oxides undergo photocathodic corrosion. ZnO is a reasonable substitute for titania, except for its property of undergoing incongruent dissolution resulting in the formation of zinc hydroxide layer on the ZnO particle leading to a slow catalyst inactivation. Among semiconductors, TiO_2 is reported to be the superior photocatalyst because of its physical and chemical stability, high catalytic activity, high oxidative power, low cost and ease of production.[12] Furthermore, the heterogeneous photocatalytic oxidation with TiO_2 satisfies the major requirements,[13] which make it competitive with other processes. They are:

- The photocatalyst should be a low cost material;

- The reaction is quite fast at mild operating conditions such as room temperature and atmospheric pressure;

5

- A wide range of organic matter can be converted to water and CO_2;

- No chemical reactant should be used and no harmful side reactions are produced.

Currently, the principle of semiconductor photocatalysis is not only important in the area of environmental purification, but also for the energy production (solar cell like DSSC), photovoltaics, electrochromic gas storage and gas sensing

1.2   Mechanism of photocatalysis

The various metal oxides such as TiO_2, ZnO, MoO_3, CeO_2, ZrO_2, WO_3, Fe_2O_3 and SnO_2 are used in semiconductor photocatalysis as they can act as sensitizer for the light induced redox reactions due to their electronic structure; filled valence band and empty conduction band.[14] When metal oxide are irradiated with light having energy $h\upsilon$ equal to or exceeding the band gap energy of the semiconductor, electrons from valence band are excited to the conduction band resulting in holes in the valence band (*Fig. 1.1*). (The band gap is the energy difference between the upper level valence band and lower level conduction band). The lifetime of this excited electron and the created positive hole should be long enough to enable their participation in reduction and oxidation reactions. In addition, both charges must migrate to the surface of the semiconductor particle to be available to the surrounding medium.
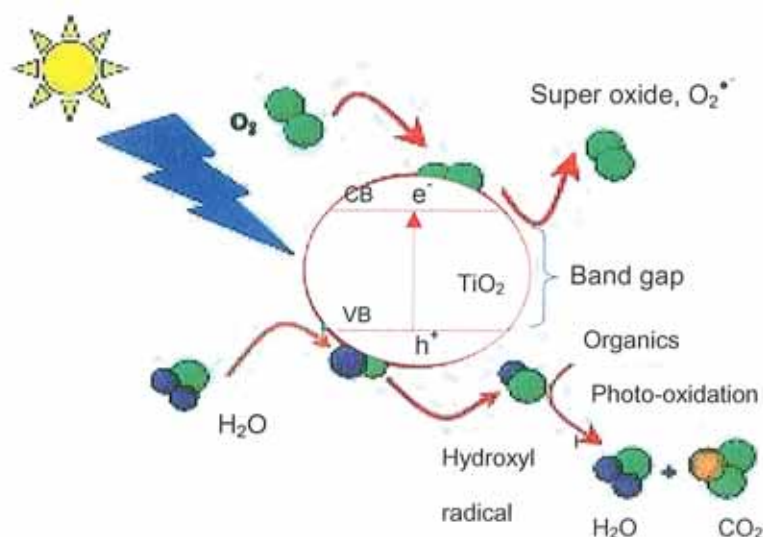
Figure 1.1: Mechanism of semiconductor photocatalysis

The conduction band electrons and valence band holes formed as a result of the light excitation can recombine and discharge the input energy as heat, get trapped in meta-stable surface states, or can react with electron donors and electron acceptors adsorbed on the semiconductor surface.[15] The characteristic feature of semi-conducting metal oxides is the strong oxidising power of their holes. The redox potential for photo-generated holes is +2.53 V versus the standard hydrogen electrode (SHE). They can react with water molecules in a one-electron[†] oxidation step to produce highly active hydroxyl radicals ($\cdot$OH) which can degrade the organic contaminants in to CO_2, water and mineral acids. Recently, Nakato *et al.* investigated the photooxidation of water adsorbed on the TiO_2 surface by *in situ* FT-IR absorption and photoluminescence measurements and concluded that the oxygen photo-evolution is initiated by a nucleophilic attack of a H_2O molecule on a photo-generated h^+ at a

---

[†] Two-electron oxidation reactions were also reported.

surface lattice O site, not by oxidation of a surface OH group by the hole,[16] whereas the conduction band electrons can reduce appropriate electron acceptor molecules.[17] In order for oxidation to occur effectively, the photo-generated electrons must be captured. Generally, atmospheric oxygen acts as the electron acceptor by forming the super oxide ions $O_2\bullet^-$ because the conduction band of TiO_2 is nearly isoenergetic with the reduction potential of oxygen. It is often found that the photocatalytic activity is nearly or completely suppressed in the absence of oxygen, possibly because of the back-electron transfer from active species present on the photocatalytic surface. In addition, the concentration of oxygen has a significant effect in the relative rate of photocatalysed degradation. In other words, if there is a two-electron reduction of oxygen, H_2O_2 is formed and this H_2O_2 may also facilitate the degradation of organics and inorganic species by acting as a direct electron acceptor.[18] Depending upon the exact conditions, the holes, •OH radicals, $O_2\bullet^-$, H_2O_2 and oxygen itself can play important roles in the photocatalytic reaction mechanisms.

The possible events in semiconductor photocatalysis and their lifetimes are shown in *Scheme 1.2.*

Electronic processes	Lifetime of species (s)
a) Charge carrier generation $TiO_2 + h\nu \longrightarrow h_{VB}^+ + e_{CB}^-$	10^{-15} (very fast)
b) OH• formation at the TiO_2 surface $h_{VB}^+ + Ti^{IV}OH \longrightarrow \{Ti^{IV}OH^\bullet\}^+$	10^{-9} (fast)
c) Charge trapping $e_{CB}^- + Ti^{IV}OH \longrightarrow \{Ti^{III}OH\}$ $e_{CB}^- + Ti^{IV} \longrightarrow Ti^{III}$	10^{-10} (dynamic) 10^{-8} (Irreversible)
d) Charge –carrier recombination $e_{CB}^- + \{Ti^{IV}OH^\bullet\}^+ \longrightarrow Ti^{IV}OH$ $h_{VB}^+ + \{Ti^{III}OH\} \longrightarrow Ti^{IV}OH$	10^{-7} (slow) 10^{-9} (fast)

Scheme 1.2: Electronic events and lifetimes on light absorption by TiO_2

TiOH represents the primary hydrated surface functionality of TiO_2, h_{VB}^+ is a valence band hole, e_{CB}^- is a conduction band electron and $\{Ti^{III}OH\}$ is the surface trapped conduction band electron.

The rate of the photocatalytic reaction is determined by the illuminated surface area of photocatalysts, light irradiance, reactants adsorption rate, electron-hole recombination rate and the various properties of photocatalysts.[19-21] Studies show that there is a linear relationship between the photocatalytic rate and the amount of substrate adsorbed on the surface of the photocatalyst. The higher the surface area of the photocatalyst, the faster the rate of reaction of e^- and h^+ with the adsorbed substrates because of the larger number of substrates that surrounds the $e^- - h^+$ pairs. Unlike the reaction of electrons and holes, it is difficult to evaluate the recombination rate directly. It is assumed that recombination takes place at crystal defects.[22] The surface of the crystal can be considered a defective site and catalysts with higher surface area will have a higher recombination rate. But if the surface reaction predominates the recombination reaction, the catalyst with higher surface area is better and *vice versa*. The crystal defect can be reduced by calcination without a large reduction in the surface area of the photocatalyst.

Overall, the rate is not significantly great due to the low photoefficiency. Thus commercialization of photocatalytic processes is still in its infancy.

1.3 TiO$_2$ as a photocatalyst

1.3.1 Introduction

Semiconductor photocatalysis with a primary focus on TiO_2 as a durable photocatalyst has been applied to a variety of problems of environmental interest. TiO_2 is the oxide form of titanium, the fourth most abundant structural metal in the earth's crust. It is a wide band gap semiconductor with band gap energy of ~ 3.2 eV, which corresponds to the UV light of wavelength 380 nm. The high catalytic activity, *i.e.* high oxidative power and photostability, make titanium dioxide a suitable material for use in photocatalysis.

10

Furthermore, it offers tremendous hope in helping ease the energy crisis through effective utilization of solar energy based on photovoltaic and water-splitting devices.[23] Since Fujishima and Honda demonstrated the TiO_2-photoassisted electrochemical splitting of water into hydrogen and oxygen in 1972, the interest in photocatalysis using TiO_2 has attracted much attention particularly in the field of photovoltaic and environmental treatments. They report the photosplitting of water by TiO_2 is similar to the photosynthesis in a plant's leaf, where both are absorbing light and produce oxygen.[24] This event marked the beginning of a new era in heterogeneous photocatalysis. A good reason for the use of photocatalyst titanium dioxide is that it has immediate effect even with small quantities.

1.3.2 Structural and Electronic Properties

Titania is a polymorphic substance present in three crystalline phases; anatase, rutile, and brookite; each with different structure and properties. Among these crystalline forms, rutile is thermodynamically the most stable, whereas anatase and brookite are metastable and transform to rutile on high temperature heating. Titania in the rutile form has been widely used as pigments, cosmetic ingredient and as a catalyst support. The brookite form has not attracted much attention from investigators because of its instability in a wide range of temperatures. The nanoscale anatase form has been favoured in the field of photocatalysis due to its wider band gap and large surface area.
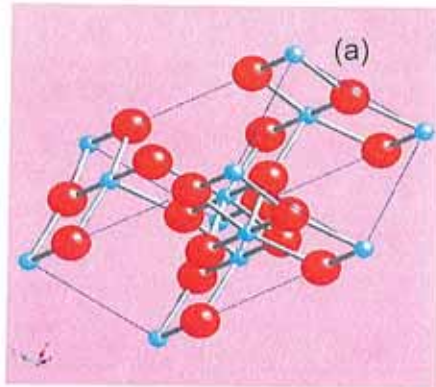
Structure:	Tetragonal
Lattice-	a =3.784A°
Constants :	c=9.515A°
Density:	3.79 g/cm³
Ti-O bond	1.934 A° (4)
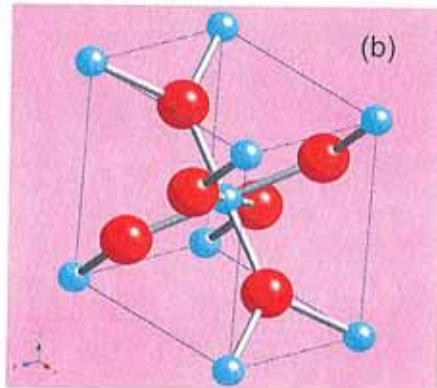
Structure:	Tetragonal
Lattice-	a =4.593A°
Constants :	c=2.959A°
Density:	4.13 g/cm³
Ti-O bond	1.949 A° (4)
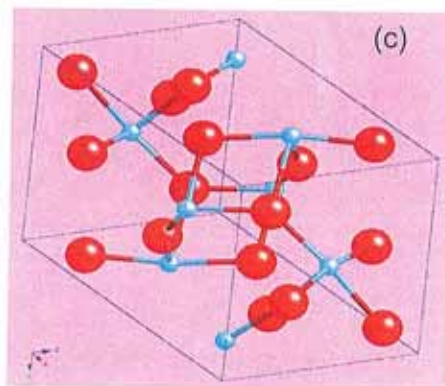
Structure:	Orthorhombic
Lattice-	a =9.184A°
Constants :	b=5.447A°
	c= 5.145 A°
Density:	3.99 g/cm³
Ti-O bond	1.92 A° -1.98 A°

Figure 1.2 Crystal structure and parameters of TiO_2 (a) unit cell of anatase (b) unit cell of rutile (c) unit cell of brookite.

Fig.1.2 shows the crystal structure of TiO_2. Anatase and rutile are in tetragonal structure brookite is orthorhombic. Anatase and rutile are made up of TiO_6 octahedra,

12

where each Ti^{4+} ion is surrounded by an octahedron of six O_2^- ions and the oxygen atom is linked with three Ti atoms. The two crystal structures differ in the distortion of each octahedron and by the assembly pattern of the octahedra chains. The Ti-Ti distances in anatase are larger, whereas the Ti-O distances are shorter than those in rutile. In the rutile structure, each octahedron is in contact with 10 neighbour octahedrons (two sharing edge oxygen pairs and eight sharing corner oxygen atoms), while, in the anatase structure, each octahedron is in contact with eight neighbours (four sharing an edge and four sharing a corner). The electronic structure of TiO_2 has been studied by various instrumental techniques such as X-ray photoelectron spectroscopy, X-ray absorption and emission spectroscopy. The two crystal structures; anatase and rutile, differ by the distortion of each TiO_6 octahedron and by the assembly pattern of the octahedra chains. These differences in lattice structures cause different mass densities and electronic band structures between the two forms of TiO_2. The brookite form of TiO_2 has a more complex structure, with eight formula units in the orthorhombic cell which can spontaneously transform to rutile at ~750 °C. The interatomic distances and Ti-O-Ti bond angles are similar to those of rutile and anatase. The essential difference is that there are six different Ti-O bonds ranging from 1.87 to 2.04 Å.

At room temperatures, titania exists in anatase phase and at high temperatures it exists as rutile. Anatase to rutile transformation is irreversible and exothermic in nature.[25] It involves an overall contraction of oxygen and a movement of ions so that a co-operative rearrangement of Ti^{4+} and O^{2-} occur. The transformation implies that two of the six Ti-O bonds of anatase structure break to form rutile structure.[26] Hwu *et al.* found the crystal structure of TiO_2 nanoparticles depended largely on the preparation method.[27] For small nanoparticles (<50 nm) anatase seemed more stable and transformed to rutile at 700 °C. However, Banfield *et al.* observed that the prepared

TiO$_2$ transformed to rutile after reaching a certain particle size and the rutile became more stable than anatase for particle size >14 nm.[28] Once the rutile was formed it grew much faster than anatase. Both anatase and rutile particle sizes increase with increasing temperature. But the growth rate is different with rutile having a much higher growth rate than anatase.

1.3.3 Optical properties of titania

The mechanism of light absorption in pure TiO$_2$ is the direct inter-band electron transition. The indirect transitions are allowed due to a large dipole matrix element and a large density state for the electrons in the valence band. An enhancement in this absorption is expected for small TiO$_2$ nanocrystals as well as in porous and microcrystalline semiconductors. The electron transfer at any point in the conduction band will become possible when hν = E_g + W_c, where W$_c$ is the width of conduction band. Sato and Sakai made an analysis on the band gap of various structured TiO$_2$ and showed that the band gap of TiO$_2$ nanosheets were larger than that of bulk TiO$_2$. It is well-known that for nanoparticles the band gap energy increases and the energy band becomes more discrete with decreasing size.

Bavykin et al.[29] studied the optical absorption and photoluminescence of colloidal TiO$_2$ nanotubes with internal diameter in the range of 2.5 - 5 nm, and found that in spite of different diameters, all the nanotubes had similar optical properties. In a theoretical study conducted by Enyashin and Seifert recently, the band structures for anatase nanotubes, nanostrips, and nanorolls were similar to the density of states (DoS) of the corresponding bulk phase.[30] The valence band of both bulk TiO$_2$ and their nanostructures was composed of 3d Ti-2p O states, and the lower part of the conduction band was formed by 3d Ti states. The differences between these

14

nanostructures were insignificant. All anatase systems were semiconductors with a wide direct band gap.

The process of recombination and being trapped by surface adsorbed species between the formed charge carriers as a result of light absorption are competitive and it will determine the overall efficiency for various applications of TiO_2 nanoparticles. Electron paramagnetic resonance (EPR) studies show that the excited electrons are trapped as two Ti (III) centers, while the holes were trapped as oxygen-centered radicals covalently linked to surface titanium atoms.[31, 32] Howe and Gratzel found that irradiation at 4.2 K in vacuum produced electrons trapped at Ti^{4+} sites within the bulk and holes trapped at lattice oxide ions immediately below the surface, which decayed rapidly in the dark at 4.2 K. In the presence of O_2, trapped electrons were removed and the trapped holes were stable to 77 K. Serpon found that O_2 was an efficient scavenger of conduction band electrons which eventually resulted in extended surface reconstruction involving Ti–OH functionalities[33] and the trapping of electrons as Ti^{3+} species occurred with a time scale of 30 ps and more than 90% of photogenerated electron/hole pairs recombined within 10 ps.[34] Berger *et al.* studied the UV light induced electron-hole pair excitation in anatase TiO_2 nanoparticles by using EPR spectroscopy and it was found that photogenerated electrons were either trapped at localized sites, giving paramagnetic Ti^{3+} centres or remained in the conduction band as EPR silent species.

1.3.4 Synthetic methods of titania

There are many methods to prepare titania. Some important methods are briefly outlined below.

1.3.4.1 Sol-Gel method

The sol-gel method is a versatile method for the preparation of titania nanomaterials. In a typical process, a sol is formed from the hydrolysis and polymerisation of titania precursors, which are usually metal alkoxide. Polycondensation and loss of solvent lead to the transition from sol to solid gel phase. The hydrolysis and condensation are responsible in the transformation of metal alkoxide precursors to a metal-oxo macromolecular network. The recombination of these metal-oxo polymers leads to the production of well dispersed structures which occupy the whole volume. One of the advantages of this method is that, from this sol, fine coatings of titania material can be prepared. Moreover, the nanomaterial prepared through this method have fully hydroxylated surfaces which will strongly influence the photocatalytic properties. The development of Ti–O-Ti chains is favoured with a low content of water, a low hydrolysis rate and excess titanium alkoxide. The presence of large quantities of Ti–OH and insufficient formation of three dimensional polymeric skeletons lead to loosely packed first-order particles. Polymeric Ti-O-Ti chains are developed in the presence of a large excess of water.

As well as for the preparation of highly crystalline anatase TiO_2 nanoparticles with different sizes and shapes,[35] the sol-gel method has also been widely applied to prepare composite and metal-doped materials. Because of these advantages, this work also uses the sol-gel method for the synthesis of metal oxide nanoparticles.

1.3.4.2 Hydrothermal method

Hydrothermal synthesis is normally conducted in pressure vessels with or without Teflon under controlled temperature and pressure and with the reactions conducted in aqueous solutions. The temperature can be elevated to reach the vapour pressure of

16

saturation. The temperature and amount of solution added largely determine the internal pressure produced. It is a method used for the production of small particles in the ceramic industry. For example, TiO_2 nanoparticles can be prepared by hydrothermal reaction of titanium alkoxide in acidic-ethanol water solution. Reports show that the particle size can be controlled by adjusting the concentration of the Ti precursor and the composition of the solvent system.[36] In addition to TiO_2 nanoparticles, TiO_2 nanorods,[37-39] nanowires,[40, 41] nanotubes[42] etc have been prepared through the hydrothermal method. This method started to be used widely to prepare TiO_2 nanotubes since it was introduced by Kasuga et al. in 1998.[43-45]

1.3.4.3 Solvothermal method

The solvothermal method is almost similar to hydrothermal method except that the solvent used is non-aqueous. The temperature can be higher, as a variety of solvents with high boiling point can be chosen. This method has been found to be a versatile method for the preparation of TiO_2 nanoparticles such as nanorods[46] and nanowires[47] with narrow size distribution and dispersity by controlling the hydrolyzation reaction.

1.3.4.4 Direct oxidation reaction

TiO_2 nanomaterials can be prepared by the oxidation of titanium metal using oxidants under anodization. For example, crystalline TiO_2 nanorods have been obtained by direct oxidation of titanium metal plate with hydrogen peroxide.[48, 49] Peng and Chen reported that, at high temperatures, acetone can be used as the oxygen source to oxidise the Ti plate.[50] Highly dense and well aligned TiO_2 nanotubes were obtained with

acetone as oxygen source where Ti cations diffused to the oxide surface and reacted with adsorbed acetone species.

1.3.4.5 Chemical vapour deposition

This method is normally used to prepare coatings, free standing bodies, films and fibres. In this process, material in its vapour state is condensed to form solid phase material. It usually takes place within a vacuum chamber. If no chemical reaction occurs, this process is called physical vapour deposition. The phase and surface morphology of the TiO_2 can be tuned by changing the reaction conditions such as vaporising temperature, pH, pressure etc in the chamber.

1.3.4.6 Electro-deposition

This method is also used to prepare coatings, especially metallic coatings, on a surface. The substrate to be coated is used as the cathode and immersed in a solution containing metal ions to be deposited. By heating the deposited substrate to remove the template, pure TiO_2 can be obtained.

1.3.4.7 Sonochemical method

This method has been applied to prepare various TiO_2 nanomaterials by several researchers.[51-53] Preparation of anatase, rutile and their mixtures were reported by Huang et al. from various precursors using ultrasonic radiation.[54] Zhu et al. observed the formation of TiO_2 whiskers and nanotubes when TiO_2 was sonicated in aqueous NaOH and followed by washing with deionised water and HNO_3 mixture.[55]

18

1.3.4.8 Microwave method

Materials having dielectric properties can be prepared by applying high-energy electromagnetic waves. The major advantages for using this method in the industrial fields are rapid heat transfer and selective or volumetric heating. Formation of high quality TiO_2 nanorods[56] and nanotubes[57] with crystal phases of anatase, rutile and their mixtures were reported by several groups.

1.3.5 Modification of Titania

Most of the applications of TiO_2 nanomaterials are closely related to their optical properties. One of the goals for the improvement in the performance of TiO_2 nanomaterials is to increase their optical response by shifting the onset of the absorption from the UV region to visible region. There are several ways to achieve this aim. Firstly, doping TiO_2 nanomaterial with other elements can narrow the electronic properties and thus alter the optical properties of TiO_2 nanomaterials. Secondly, sensitizing TiO_2 with other inorganic or organic compounds having absorption in visible region can improve its optical activity in the visible light region. Thirdly, coupling collective oscillations of the electrons in the conduction band of metal nanoparticle surfaces to those in the conduction band of TiO_2 nanomaterials in metal-TiO_2 nanocomposites can improve the performance. In addition, the modification of the TiO_2 nanomaterials surface with other semiconductors can alter the charge-transfer properties.

1.3.5.1 Synthesis of doped TiO₂ nanomaterials

The optical properties of the nanomaterials are largely determined by its underlying electronic structure. The electronic properties of a material are closely related to its chemical composition (chemical nature of the bonds between the atoms or ions), its atomic arrangement, and its physical dimension (confinement of carriers) for nanometer-sized materials. The chemical composition of TiO_2 can be altered by doping. Studies show that it is easier to substitute the Ti^{4+} cation in TiO_2 with other transition metals, and it is more difficult to replace the O^{2-} anion with other anions due to differences in charge states and ionic radii. Doping can be performed by metals or nonmetals. Choi *et al.* performed a systematic study of TiO_2 nanoparticles doped with 21 metal ions by the sol-gel method and found the presence of metal ion dopants significantly influenced the photoreactivity, charge carrier recombination rates, and interfacial electrontransfer rates.[58] Li *et al.* developed La^{3+}- doped TiO_2 by the sol-gel process and found that the lanthanum doping could inhibit the phase transformation of TiO_2, enhance the thermal stability of the TiO_2, reduce the crystallite size, and increase the Ti^{3+} content on the surface.[59] TiO_2 nanoparticles doped with Cr and V ions with an ion-implantation method was reported by Anpo *et al.*[60] All of these studies observed a red shift in the band gap transition or a visible light absorption in metal-doped TiO_2. This red shift was attributed to the charge-transfer transition between the *d* electrons of the dopant and the CB (or VB) of TiO_2. Metal-ion doped TiO_2 prepared by ion implantation with various transition-metal ions such as V, Cr, Mn, Fe, and Ni was found to have a large shift in the absorption band toward the visible light region.

Recent theoretical and experimental studies have shown that the desired band gap narrowing of TiO_2 can also be achieved by using non-metal dopants. It is found that doping with various non-metals such as B, C, N, F, S, Cl, and Br could improve the photocatalytic activity of TiO_2 nanomaterials. Asahi and co-workers calculated the

20

electronic band structures of anatase TiO_2 with different substitutional dopants, including B, C,[61] N,[62] F,[63, 64] and S.[65, 66] It was found that C-doping introduced deep states in the gap.[67] In the case of N-doping, it was found that the substitutional doping of N was the most effective in the band gap narrowing because its p states mixed with O $2p$ states. S-doping introduces a similar band gap narrowing and the mixing of the sulfur $3p$ states with the valence band was found to contribute to the narrowing of band gap. When F replaced the O in the TiO_2 lattice, the F $2p$ states were localized below the O $2p$ valence states without any mixing with VB or CB and as a result additional states appeared below CB edge, thus reducing the effective band gap for effective visible light absorption.[68]

1.3.5.2 Modification of titania by sensitization

Dye sensitization is one of the viable alternative methods for the modification of semiconductors to make them active in the visible light. In such cases, the sensitizer is anchored onto the surface of the semiconductors. When molecules are adhered on the surface of semiconductors, their translational mobility is considerably reduced. This extends the range of excitation energies towards visible region. Various dyes such as erythrosine B, cosin, rose bengal, thionine, chlorophylline, carbocyanin etc have been reportedly employed as sensitizers. Dye sensitized solar cell is an example of the use of this principle.

The narrow band gap semiconductors have been used as sensitizers to improve the optical absorption capability of TiO_2. Vogal et al studied the sensitization of TiO_2 by CdS, PbS, Ag_2S, etc and optimised for efficient charge separation and found that CdS could significantly improve the photostablity.[69] Sant and Kamat found that charge transfer occurred only when TiO_2 nanoparticles were sufficiently large (>1.2 nm) so that

the conduction band of the nanoparticles was located below that of CdS nanoparticles.[70] Kamat *et al.* recently reported the sensitization of mesoscopic TiO_2 films using bifunctional surface modifiers (SHR- COOH) linked with CdSe nanoparticles. Upon visible light excitation, CdSe nanoparticles injected electrons into TiO_2 nanocrystallites.[71]

Noble metals were also found to be important sensitizing modifiers. Tian and Tatsuma found that nanoporous TiO_2 films loaded with Ag and Au nanoparticles exhibit negative potential changes and anodic currents in response to visible light irradiation, with potential applications for photovoltaic cells, photocatalysts, and plasmon sensors.[72] Cozzoli *et al.* found that, following UV illumination, TiO_2 nanorods sensitized with Ag or Au nanoparticles could sustain a higher degree of conduction band electron accumulation than pure TiO_2.[73] Kawahara *et al.* proposed the mechanism of charge separation at the interface between Ag and TiO_2 nanoparticles.[74] They found that, in the multicolour photochromism of TiO_2, nanoporous films loaded with photocatalytically deposited Ag nanoparticles, visible light-induced electron transfer from Ag to oxygen molecules played an essential role.

1.3.6 Applications of TiO_2 nanomaterial photocatalysts

The existing and promising applications of TiO_2 nanomaterials include paint, toothpaste, UV protection, photocatalysis, photovoltaics, sensing, and electrochromics as well as photochromics. The major environmental photocatalytic applications are shown in the diagram below (*Fig. 1.3*). As a result of its high refractive index, it is used as anti-reflection coating in silicon solar cells and in many thin-film optical devices.[75] TiO_2 is successfully used as a gas sensor[76] (due to the dependence of the electric conductivity on the ambient gas composition) and is utilized in the determination of

22

oxygen[77] and CO[78] concentrations at high temperatures (>600 °C) and simultaneously determining CO/O_2 and CO/CH_4 concentrations.[79] Due to its hemocompatibility with the human body, TiO_2 is used as a biomaterial (as bone substituent and reinforcing mechanical supports). The ability to control photocatalytic activity is very important in applications such as the utilization of TiO_2 in paint pigments[80] and cosmetics.[81] A low photoactivity is preferred for these applications in order to prevent the physical loss of pigment when the surface is degraded and to reduce the UVC induced dimer formation which can damage the DNA cells.

Air purification
Decomposition of aldehyde
Removal of NO_x

Water purification
Decomposition of organic materials
Degradation of environmental hormones

TiO₂ + Light

Anti-fogging Anti-contamination (Self-cleaning)
Decomposition of oil
Superhydrophilic effect

Anti-bacteria Sterilization
Sterilization of Escherichia coli and MRSA
Degradation of virus

Figure 1.3: Fundamental environmental fields in application of photocatalyst. [46]

Photocatalysis is not adequate to break down large quantities of a substance at once, but it is highly effective in breaking down growing substances, which initially have a small quantity, such as bacteria and virus. It already has been proven to be useful for the destruction of micro-organisms such as bacteria,[82] and viruses,[83] for the inactivation of cancer cells,[84] for odour control,[85] for the production of gas[86, 87] for

23

cleaning dirt[88] and for disinfection of waterborne pathogens from drinking water for developing countries and from biomedical devices.[89-92]

The major findings which led to the development of TiO_2 photocatalysis are:

- **1972** - The first photo-electrochemical cell for water splitting is reported by Fujishima and Honda using a rutile TiO_2 photoanode.

- **1977** - Schrauzer and Guth[93] reported the photocatalytic reduction of molecular nitrogen to ammonia over iron-doped TiO_2 and Frank and Bard[94] examined the reduction of CN^- in water, which is the first consideration of TiO_2 in environmental purification.

- **1978** - An alternative photoinduced Kolbe reaction[95] (the first organic photosynthetic reaction), ($CH_3COOH \rightarrow CH_4 + CO_2$) which opens the field of organic photosynthesis.

- **1983** – Ollis[96] reported the semiconductor-sensitized reactions for organic pollutant oxidative mineralization.

- **1985** - Application of TiO_2 as microbiocide,[97] effective in photo-killing of *Lactobacillus acidophilus, Saccharomyces cerevisiae* and *Escherichia coli.*

- **1986** - Fujishima *et al*[98] reported the first use of TiO_2 in photo-killing of tumour cells (HeLa cells).

- **1991** - O'Regan and Gratzel[99] reported an efficient solar cell using nanosized TiO_2 particles.

- **1995** - Negishi *et al*[100] developed highly transparent photocatalytic sol-gel coatings of TiO_2.

- **1998** - Wang *et al.*[101] explored the anti-fogging and self-cleaning properties by developing highly hydrophilic TiO_2 surfaces.

- **2001** – Asahi *et al.* reported[67] visible light activity of N-doped TiO_2.

As well as environmental applications, the use of TiO_2 as nanocrystalline electrodes in the field of photovoltaics have been studied widely. Dye sensitised solar cells (DSSC) is one of the developing applications in this area. In the past decades, research focussed on the optimisation of the organic dyes in DSSC, while more recently attention has been paid to making use of various types of TiO_2 such as mesoporous, nanotube, anatase-rutile hybrid, core-shell structure *etc* as electrode material. The use of photocatalytic activity for water splitting is another important application since Fujishima and Honda reported it. Catalysts such as Pt and NiO are often loaded on the surface of TiO_2 in order to introduce active surface sites for H_2 evolution. Syama and Arakawa found that addition of carbonate salts to Pt-loaded TiO_2 suspensions led to highly efficient water splitting.[102] Borgarello *et al.* reported that water cleavage could be induced with visible light in colloidal solutions of Cr-doped TiO_2 nanoparticles deposited with ultrafine Pt or RuO_2.[103]

Nanocrystalline TiO_2 electrodes have been applied in the electrochromic display devices. Among those the electrochromism of nanocrystalline TiO_2 electrodes in Li containing electrolytes related to the reversible insertion of Li^+ into the anatase lattice of the nanoparticles[104] and nanocrystalline TiO_2 electrodes modified with viologens and/or anthrachinons equipped with a surface anchoring group were widely studied and reported.[105] Moreover TiO_2 have been widely studied as sensors for various gases. The

hydrogen-sensing capabilities of the sensors were largely recovered by ultraviolet (UV) light exposure after being completely extinguished by immersion of the sensor in motor oil. Many types of TiO_2 nanomaterial-based room-temperature hydrogen sensors are based on Schottky barrier modulation of devices like Pd/TiO_2 or Pt/TiO_2.[78, 106, 107] Oxygen sensors based on TiO_2 nanomaterials include TiO_{2-x},[108] TiO_2-Nb_2O_5,[109] CeO_2-TiO_2,[110] and Ta-Nb-,[111] Cr and Pt-doped TiO_2.[112]

1.3.7 The present situation with TiO_2 photocatalysis

Semiconductor photocatalysis has progressed so much that commercial devices based on this technology are appearing on the international markets[113] and one area appears particularly promising is the use of this technology for water purification. According to the research reports, over 800 contaminants can be removed by photocatalysis.[114] Photocatalysis has not only been proven to remove pollutants from water, but also colour, taste and odour.[115] The recent development of practical applications of photocatalytic activity of TiO_2 according to the above research reports are already shown in *Fig. 1.3*. Most of the studies about the photocatalysis of TiO_2 are focused on powdered TiO_2. But for practical applications, this is a problem due to post treatment separation requirements of the mixture. This could be overcome by immobilizing TiO_2 particles as thin films on solid substrate though the film-type photocatalysts normally have lower surface areas than powders. In spite of such technical difficulties, the photocatalytic activity of titania extends its application in the form of thin coatings of the material exhibiting self-cleaning and disinfecting properties under exposure to UV radiation as the use of the material in the powder form is difficult to reuse. The antibacterial activity of titania makes the thin films worthy in applications such as preparing medical devices, food preparation surfaces, air conditioning filters, and

sanitary ware surfaces *etc*. When microorganisms are in contact with the TiO_2 surface that is exposed to UV light of wavelength below 385 nm, hydroxyl radicals are formed and break down the cell wall and outer membrane, allowing cell contents to leak out and TiO_2 particles to enter, thereby causing cell damage and death in the presence of water.[116]

The recently discovered 'wettability', or 'super-hydrophilicity', presents a large range of applications in cleaning and anti-fogging surfaces. Generally, when moist air comes in contact with glass, small droplets of water are formed and the glass becomes fogged. On titanium dioxide coated glass, the water forms a continuous flat sheet, so that there is no fogging. An application of this is the 'self-cleaning' windows. The formed thin water sheet also easily lifts the dirt and grime from the surface and washes it off effectively.

The photo-induced super-hydrophilicity is an intrinsic property of the TiO_2 and the mechanism for this process was proposed on the basis of the reconstruction of the surface hydroxyl groups under UV irradiation.[117] Photoinduced super-hydrophilicity is accompanied by photocatalytic activity, as both phenomena originating from the same property; so the surface adhered contaminants will be either photodegraded or washed away by water. The mechanism involves the reduction of Ti(IV) cations to Ti(III) by electrons and simultaneous trapping of holes at lattice sites (usually bridging oxygen) or close to the surface of the semiconductor. Such trapped holes weaken the bond between the associated titanium and lattice oxygen, allowing oxygen atoms to be liberated, thus creating oxygen vacancies. The subsequent dissociative adsorption of water at the site renders it more hydroxylated. An increased amount of chemisorbed – OH leads to an increase of van der Waals forces and hydrogen bonding interactions

between H_2O and $-OH$. Water can easily spread across the surface and hydrophilic properties will be enhanced.
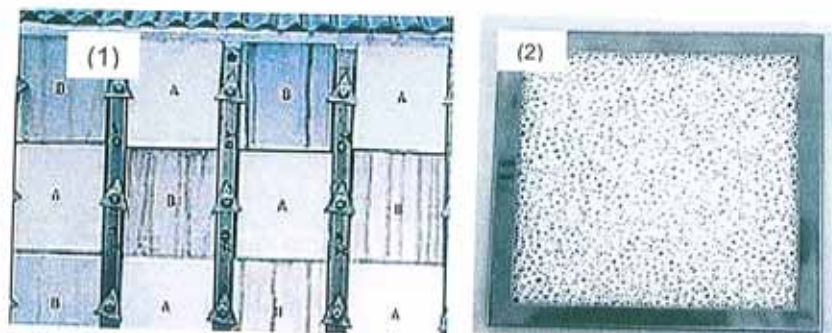
Figure 1.4: (1) Self cleaning effect -TiO_2 coated wall tiles A and ordinary tiles B, (2) TiO_2 based porous ceramic filters for air cleaning.[118]

The use of titania coated ceramic tiles in a hospital can reduce the spread of infections to patients by improving the hygienic conditions. The property like photocatalytic oxidation has been applied to remove and decompose the pollutants in indoor air. In the case of air purification, the TiO_2 reactors trap and chemically oxidise the organic compounds, converting them primarily to CO_2 and water. Because of this, they can be integrated in to new and existing heating, ventilation and air-conditioning systems.

In the thirty-plus years of research, the study of photocatalysis has run into a practical-use phase so that coating products and air cleaning equipments using TiO_2 have started to come onto the market. The commercialization of TiO_2-based photocatalytic products commenced in the mid-1990's in Japan.[119] However, this industry has grown very rapidly, and more than 2000 companies have joined in this new industry, whose products are mainly used in different categories, *i.e.* exterior construction materials, interior furnishing materials, road construction materials, purification facilities,

household goods, *etc.* The market share of purification facilities grew at the highest rate, from 9% in 2002 to 33% in 2003, which was mainly due to the contribution of air purification products, including air cleaners and air conditioners. TOTO Ltd. is the main producer of TiO_2-based self-cleaning tiles in Japan. Its self-cleaning tiles have been applied on more than 5000 buildings in Japan according to data for 2003.[120] However, a recent report by JTDA (Japan Titanium Dioxide Association), reveal that Japan's production of TiO_2 was 253,259 tonnes in the year to end-March 2006, representing a 0.6% fall from the previous year.[121]

1.4 ZnO as a photocatalyst
1.4.1 Introduction

ZnO is another semiconductor and has a wurtzite structure with a wide band gap of 3.3 eV. It appears to be a suitable alternative to TiO_2; however, ZnO is unstable with respect to incongruous dissolution yield $Zn(OH)_2$ on the ZnO particle surfaces and thus leading to catalyst inactivation over time.[122] It offers significant opportunity in providing electronic, photonic and spin-based functionality (spintronics) because of its direct wide band gap and large exciton binding energy ~60 meV. This makes it worthy in the potential and established hi-tech applications such as piezoelectric transducers, ceramics, optical coatings, high speed and display devices,[123-126] gas sensors,[127] varistors,[128-130] photocatalysis[131] and photovoltaics.[132] The high exciton binding energy of ZnO, which renders it more applicable for making room-temperature UV laser devices. In addition, the high chemical stability and low toxicity together make ZnO suitable for UV screening applications. In such applications, ZnO is found to be better than TiO_2 due to its broader absorption of UV light, *i.e.* ZnO absorbs both UVA and UVB radiation where as TiO_2 absorbs only UVA and it has a lower refractive index.

Moreover, because of its non-central symmetry, ZnO is piezoelectric, which is a key property in building electromechanical coupled sensors and transducers. Finally, ZnO is bio-safe and biocompatible, and can be used for biomedical applications without coating. With these three unique characteristics, ZnO could be one of the most important nanomaterials in future research and applications.

ZnO also reported as a photocatalyst and has the same reaction mechanism of TiO_2 because of its electronic structure. In addition, in terms of studying the mechanism of photocatalysis, ZnO offers some advantages over TiO_2. Among these is the fact that ZnO is that it can emit quite strong flourascence, due to the recombination of electron-hole pairs. It facilitates the mechanistic study of interfacial charge transfer processes and thereby photocatalysis. This property has also been used to sense the presence of organic molecules in its immediate vicinity.[133] Many reports over the last few decades show that ZnO can effectively degrade the organic and inorganic pollutants in the presence of light.[134, 135] Also, some studies demonstrated that illuminated n-type semiconductors such as ZnO, TiO_2, CdS, and WO_3 can be used to drive the photochemical reduction of dissolved metals including noble metals, with consequent deposition and accumulation of reduced product of the photocatalyst. This property and possibility of a general precious metal recovery scheme heightens the interest in potential use of heterogeneous photocatalysis.[136]

Though ZnO is good wide band gap semiconductor which possesses the same characteristic properties of TiO_2, it is only recently that research has begun to exploit it as photcatalyst for environmental purification processes. Previous studies show ZnO as an effective photocatalyst for the photocatalytic degradation of various azo-dyes under UV light irradiation.[137, 138] Studies have also been conducted using ZnO under

sunlight[139, 140] and good results have been obtained. Their applications remain limited only by pH as the photocatalytic degradation capacity of the ZnO nanoparticles was higher than that of the ZnO nano-crystalline particles.

1.4.2 Structural properties and synthetic methods of ZnO

ZnO crystallizes in wurtzite structure which is a hexagonal lattice consisting of Zn^{2+} and O^{2-} such that each Zn ion is surrounded by tetrahedral of O^{2-} ions and vice versa. This tetrahedral co-ordination gives rise to polar symmetry along the hexagonal axis which is responsible for the different properties of ZnO. A unit cell of ZnO is shown in *Fig.1.5*. The lattice parameters of a hexagonal unit cell are; a = 3.2495 Å, c = 5.206 Å and density 5.605 g/cm³ The optical properties of ZnO are highly influenced by the energy band structure and these lattice parameters. Because of the partial ionic nature of ZnO, the top of the valence band, or highest occupied molecular orbital (HOMO), is formed from the 2p levels of O^{2-} and the bottom of the conduction band, or the lowest unoccupied orbital (LUMO), is formed from the 4s levels of Zn^{2+}. The various electronic transitions between these energy levels make it to be a luminescent material and suitable for further piezoelectric or pyroelectric and optical device applications.
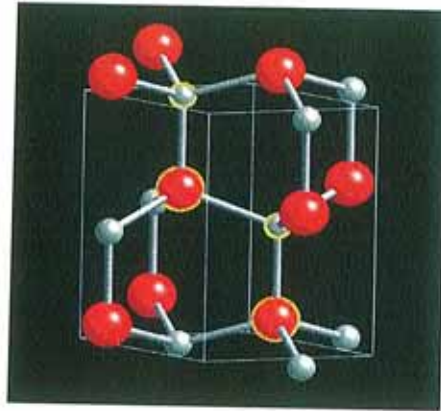
Figure 1.5 Unit cell structure of wurtzite ZnO. Large spheres represents oxygen.[141]

Photoluminescence is utilised to detect the emission properties of ZnO. UV and green emission are the two main emissions observed in ZnO and the intensities of which are dependants on crystal quality. It is imperative to know the excitation and recombination processes to improve the PL and further applications. The properties of ZnO particles are highly dependent upon particle size, shape, and surface characteristics. Recently, research is concentrating on exploiting the size and shape dependant properties of ZnO by synthesising various nanostructures such as nanorods, nanoflower, nanosheets, vertically aligned nanosheets, nanowires, nanotips, nanotubes *etc.* Several fabrication techniques have been developed to prepare ZnO structures with well-defined shapes, such as vapor-phase evaporation,[142, 143] metal-organic vapor-phase epitaxy,[144] templatebased synthesis,[145] and laser ablation *etc.*[146]

Vapour phase evaporation is the simplest and most widely-used method where the generated zinc vapours as a result of heating are deposited on a substrate surface at low temperature. Various sized nanowires, nanotubes, nanorods, nanotips *etc* were prepared by this method.

32

The development of the wet-chemistry approach, the one which we chose for the present study, to synthesis ZnO particles with controllable sizes and shapes is more desirable in terms of simplicity, efficiency, and low cost.[147-149] This method is based on hydrothermal decomposition. $Zn(OH)_2$ or zinc salts such as $Zn(CH_3COO)_2$ or $Zn(NO_3)_2$ etc. were used as precursors along with water as reaction medium and organic reagents as surfactant. Different nanowhiskers had been obtained in different solution systems.[150, 151]

In addition to photocatalysis, ZnO has potential in solar energy applications to fabricate the solar energy devices because of the longer lifetime of electron compared to TiO_2. Several attempts were made[152] to improve the solar efficiency of DSSC made of ZnO electrodes since 1968 and the highest efficiency reported up to date is about 7.2% using porous single crystal.[153] Another issue is to synthesis p-type ZnO which is desired not only for electronic applications but also enhanced photocatalysis. Impurity doping is one suitable method to develop p-type conductivity and also for light-harvesting nature. For the present study, as in the case of TiO_2, silver was chosen as a dopant or modifier to tune the optical and electronic properties of ZnO for efficient photocatalysis.

1.5   Problems with current technology

Given the extensive research already carried out for both TiO_2 and ZnO, the current situation is that the technology is limited by only a few problems. As discussed, a semiconductor photocatalyst should be chemically stable, biologically inert, easy to produce and use, activated by sunlight, able to efficiently catalyze reactions, inexpensive, and without risks for the environment or humans. Titanium dioxide (with

sizes ranging from clusters to colloids, powders and large single crystals) is close to being an ideal photocatalyst, displaying all the above properties.

However, even though it is a good photocatalyst, its applications are limited because of its inability to absorb visible light efficiently. As discussed, the mechanism of the photocatalytic reaction involves the absorption of light having energy greater than or equal to the band gap energy of the semiconductor, leading to the formation of electron-hole pairs which are responsible for subsequent degradation reactions. The light required by anatase TiO_2, which is the most photoactive phase of TiO_2, is UV light with wavelength shorter than 380 nm – corresponding to the band gap energy (3.2 eV) of TiO_2. But the total solar spectrum consists of only 3-5 % UV light.[154] Hence the effective utilisation of solar energy which comes above 400 nm becomes difficult. In this scenario, one of the major challenges for the scientific community involved in photocatalytic research is to increase the spectral sensitivity of photocatalysts to visible light.

Secondly, the nature of surface adsorbed species have significant importance in photocatalytic action. A photocatalyst is characterised by its ability to adsorb simultaneously two reactants which can be oxidised or reduced. The ability of a semiconductor to undergo photoinduced electron transfer to an adsorbed particle is governed by the band energy positions of the semiconductor and the redox potential of the adsorbates. The band gaps of various semiconductors are shown below (Table 1.1). The energy level at the bottom of conduction band is the reduction potential of photoelectrons and the energy level at the top of valence band determines the oxidizing ability of photo-holes; each value reflecting the ability of the system to promote reductions and oxidations. Hence, a reduction in the energy gap between VB and CB, which facilitate the easy excitation by visible light and oxidation reaction by VB

holes, is of significant importance for the effective photcatalytic processes. The formation of hydroxyl radical at the surface takes place by trapping the holes, causes the VB holes to be in lower potential and which allows it to react with target substrate. In addition, the trapping reaction of CB electrons is quite influential in determining the photonic conversion efficiency.

Table 1.1: Table showing the band gap of various semiconductors.

Semiconductor	Valence band (V vs NHE)	Conductance band (V vs NHE)	Band gap (eV)	Band gap wavelength (nm)
TiO_2	+3.1	-0.1	3.2	387
SnO_2	+4.1	+0.3	3.9	318
ZnO	+3.0	-0.2	3.2	387
ZnS	+1.4	-2.3	3.7	335
WO_3	+3.0	+0.2	2.8	443
CdS	+2.1	-0.4	2.5	496
CdSe	+1.6	-0.1	1.7	729

Thirdly, one significant factor that reduces the photocatalytic activity of TiO_2 is the efficient rate of recombination of photogenerated electrons and holes.[155] As indicated earlier (*Scheme 1.2*), the photogenerated electrons and holes are highly reactive and they can initiate many chemical reactions before they recombine. If a suitable scavenger or surface defect is available to trap the electron and hole, recombination is inhibited and subsequent redox reactions can occur. Photoactivity of the semiconductors is a photochemical process, where the separation and recombination of photoinduced charge carriers are in competition and photocatalytic activity is effective when separation between the electrons and holes are maximum. Many approaches have been applied by researchers to reduce the recombination reactions.

Such efforts include the surface modification of TiO_2 with noble metals or an oxide and simultaneous scavenging of electrons and holes by the surface adsorbed species.[156] Recent studies show that modification of semiconductor with metals such as Ag, Au, Pt etc. can improve the photocatalytic efficiency by inhibiting the recombination.[157] More recently, some groups reported that the substituted nitrogen acted as an inhibitor for electron-hole recombination.

1.6 Research priorities and overview of thesis

As was stated, there is a considerable priority in the research of semiconductor photocatalysis to develop a system which is capable of using natural sunlight for purification processes. In particular, this work has centred on metal oxide semiconductors to find how they can be efficient photocatalysts and to assign the photocatalytic degradation mechanism with a selected dye. One possible approach to overcome the above mentioned obstacles is to make TiO_2 photocatalytically active beyond its absorption threshold of 400 nm by creating energy levels within the band gap or by sufficiently shifting the conduction band (CB) and/or the valence band (VB) so that photons of lower energy are able to excite electrons. In order to make this dream true, several different approaches have been proposed. A detailed description has already been discussed in Section 1.3.5. One of them involves the synthesis of modified TiO_2 by controlling the particle size, crystallinity and crystalline phase. The contribution to this part is to synthesise metal oxides such as TiO_2 and ZnO, which were selected for the current studies, in a modified way.

It is essential to reduce the band gap of titania and thereby the electron-hole recombination, so that it can be active in the visible region. Doping can either add an energy level filled with electrons in the band gap which can be easily excited into the

conduction band (n-type) or add a level of extra holes in the band gap to allow the excitation of valence band electrons, to create mobile holes in the valence band (p-type). The main purpose of doping is to induce a bathochromic shift (*i.e.* a decrease of the band gap or introduction of intra-band gap states) which results in more visible light absorption. Hence, by doping with certain metals such as transition metals, the band-gap energy of TiO_2 will be reduced so that visible light is capable of supplying enough energy to generate e^-/h^+ pairs. For all these purposes, a noble metal – silver – is chosen as a modifier, and analysed the effects of silver modification in absorption capability, band gap narrowing, opto-electronic properties of both TiO_2 and ZnO.

In conclusion, not only the low cost and chemical stability of metal oxides and their semi-conducting properties can make them very attractive for photocatalytic applications. Additional questions need to be addressed. How can we make these materials be used for efficient visible light photocatalysis? How can the opto-electro-chemical properties of metal oxides be controlled by simple chemical means to improve performance? How can a large number of new modified metal oxides be synthesized and how can we decide the exact mechanism of degradation reaction of various pollutants? These are the questions which are addressed in this thesis. The thesis is organized in to 6 chapters.

Chapter 1 sketches an outline the importance of semiconductor photocatalysis in the area of environmental purification and energy production. The basic mechanism of photocatalysis, its advantages compared the traditional purification processes, current limitation, and motivations of the research are also discussed.

Chapter 2 presents the materials and experimental set-up used for the synthesis and photocatalytic activity test. The various techniques used for the characterisation of the synthesised materials are also presented.

Chapter 3 explains the synthesis and characterisation of silver modified TiO_2. The optimised conditions and the effect of silver in textural and photocatalytic properties of TiO_2 is also analysed. The photocatalytic activity analysis of work carried out at *Institute fur Technische Chemie,* Hannover, Germany, about the surface adsorption properties TiO_2 is discussed.

Chapter 4 provides an overview on the use of ZnO as a photocatalyst and explores the effect of silver modification on ZnO and its photcatalytic activity. A mechanistic study of photocatalysis is explained.

Chapter 5 presents a study about the effect of co-doping inTiO_2 on its photo-electronic and photcatalytic properties.

Chapter 6 concludes with some suggestion for future research based on preliminary results of some experiments on sensing property of ZnO and nano-silver preparation.

2. EXPERIMENTAL AND

CHARACTERISATION TECHNIQUES

2.1 Chemicals Used

The reagents titanium tetraisopropoxide (97%), acetic acid (99.7%), silver nitrate (99%), cerium (III) nitrate hexahydrate (99%), zinc acetate dihydrate (98%), oxalic acid (97%), ethanol (reagent grade), potassium chloride (99%), sodium borohydride (99%), potassium bromide (99.9%), ethylene glycol (99%), vitamin C (analytical reagent grade) and trisodium citrate (99%) were purchased from Sigma-Aldrich and used as received. Rhodamine 6G (analytical reagent grade) was purchased from Eastman and used as received. Deionised water was used in all experiments.

2.2 Synthesis of Nanomaterials

2.2.1 Synthesis of TiO$_2$

Titanium isopropoxide (25 mL, 90 mM) was added to glacial acetic acid (48 mL, 800 mM) with stirring. De-ionised water (150mL) was added to the partially hydrolysed titanium isopropoxide-acetic acid mixture drop-wise with vigorous stirring. In the final solution, the titanium isopropoxide, acetic acid and water were in 1:10:100 molar ratios. The solution was stirred for up to 8 h to get a clear transparent sol and allowed to dry at 100 °C in an air oven for overnight after which it was calcined at the required temperature (such as 600 and 700 °C) in air for 2 h at a ramp rate of 5 °C

2.2.2 Synthesis of silver modified TiO$_2$

Silver modified titania was prepared by adding various amounts of silver nitrate corresponding to different mol % of silver (1, 2, 3, 5 and 10 mol %) to the sol containing partially hydrolysed titanium isopropoxide-acetic acid mixture (prepared as described in *2.2.1*) under vigorous stirring.[158] For photoreuced silver modification, the sol was then irradiated[159, 160] with a 250 W bulb for 0 – 60 minutes. The distance between the bulb

and the beaker containing sol was about 7 cm.[161] After irradiation, the stirred sol was kept in an oven set at 100 °C until all the solvent evaporated. The dried powders were crushed in to fine powders with a pestle and mortar and calcined at 600 and 700 °C for 2 h at a ramp rate of 5 °C per minute. A parallel experiment without irradiation by the bulb yields silver-modified titania where the silver was not reduced prior to calcination.

2.2.3 Synthesis of cerium modified TiO$_2$

To the titania sol prepared as described in *2.2.1,* various amounts of cerium nitrate hexahydrate were added with stirring so that the concentration of ceria in the resulting material would be 0, 0.05, 0.1, 0.2, 0.5,1, 2 and 3 mol %. The TTIP, HOAC and H$_2$O were in the ratio of 1:10:100. The sol was allowed to dry at 100 °C in an air oven for overnight and dried samples were calcined at 600 °C for 2 h.

2.2.4 Synthesis of ZnO

Zinc acetate (10.98 g, 50 mM) was dissolved in ethanol (500 mL) at 60 °C in a rotary evaporator and stirred for 30 min. Oxalic acid (12.55 g, 100 mM) dissolved in ethanol (200 mL) at 60 °C was slowly added to the warm ethanolic solution of zinc acetate. The mixture was stirred for 2 h, after which time a thick white gel formed. This was allowed to dry at 80 °C overnight. The dried xerogel was calcined at different temperatures (300 °C – 1000 °C) for 2 h to yield ZnO powder.[162]

2.2.5 Synthesis of silver modified ZnO

For silver modified ZnO, various amounts of silver nitrate corresponding to 1, 3, 5 and 10 mol % of silver dissolved in ethanol were added to the zinc acetate-oxalic

41

acid solution (prepared as described in *2.2.4*) and continued the stirring. This was dried and calcined at different temperatures from 300 – 1000 °C.

2.2.6 Synthesis of silver – ceria co-doped TiO₂

In the co-doped samples the amount of cerium was kept constant (1 mol %) and various mol % of silver (1, 3 and 5 mol %) were used as co-dopant. For a typical experiment to prepare 1:1 silver-ceria co-doped TiO₂, silver nitrate (0.065 g) dissolved in water (33.5 mL) (*i.e.* solution A) was mixed with a solution of cerium nitrate hexahydrate (0.166 g) dissolved in water (33.5 mL) (*i.e.* solution B). The mixture of solution A and B was added drop-wise to the partially hydrolysed titanium tetra isopropoxide-acetic acid mixture prepared as in the section *2.2.1* and stirred for 6 h for homogenization. The prepared sol was allowed to dry at 100 °C overnight. The dried samples were calcined at various temperatures in the range 400 – 900 °C.

Similar experiments were conducted to prepare co-doped samples with a silver concentration of 3 and 5 mol % as well as a sample where the silver – cerium mol % was 3 mol % silver : 3 mol % cerium.

2.2.7 Preparation of nanosilver sol having various size and shape

Silver nanoparticles were prepared through a citrate stabilized single-step method. A small amount of NaBH₄ was used for the in-situ generation of silver seeds, which grows on further addition of AgNO₃. Vitamin C and trisodium citrate (TSC) were used to control the shape of nanoparticles. Experiments were conducted by varying the concentration of reagents and it was concluded the concentrations for a typical

synthesis as TSC (10 mL, 2.5×10^{-2} M) and $NaBH_4$ (100 µL, 0.05 M) which were were mixed with water (120 mL). Silver nitrate (10 mL, 0.05 M) was added drop wise to the above solution with stirring. This results in the formation of stable yellow silver sol.

2.2.8 Synthesis of silver modified TiO_2 and ZnO using nanosilver sol

The various coloured (shaped) silver sols prepared as described in *2.2.7* were used as the silver source for the modification of both TiO_2 and ZnO. 1 and 5 mol% silver modified TiO_2 samples were prepared by mixing TiO_2 with corresponding amount of the above prepared silver sol. In a typical experiment to synthesise 5 mol% silver doped TiO_2, anatase TiO_2 (1 g) prepared as described in *2.2.1* was mixed with above prepared yellow silver sol (201.6 mL). The mixture was stirred for 2 h in the dark, centrifuged, washed several times with water and dried at room temperature. For 1 mol% silver doped TiO_2, the corresponding volume of the prepared yellow sol (40.2 mL) was used.

Both 5 mol% and 1 mol% silver doped ZnO were also prepared similarly by using ZnO prepared as in *2.2.4*.

2.3 Fabrication of Titania Thin Films

Thin films were prepared from TiO_2 and silver modified TiO_2 sol prepared as described in sections *2.2.1* and *2.2.2*. Before coating the sample, the pre-treatment of the glass slide was necessary to remove impurities and to make the glass perfectly wetting. The glass slides were boiled in concentrated H_2SO_4 for 30 min, followed by washing with distilled water to remove the acidity completely. H_2SO_4 will selectively extract the free Na-ions embedded in the glass slide and converted in to the soluble sodium sulfate.[163]

The glass slides were ultra-sonicated in isopropanol-water mixture for 20 min and subsequently dried in an air oven at 100 °C.

Table 2.1 Samples prepared as powders for the study and their abbreviations.

Sample Composition	Temperature (°C)	Abbreviation
1 mol % Ag – TiO_2	600 & 700	1Ag-T
3 mol % Ag – TiO_2		3Ag-T
5 mol % Ag – TiO_2		5Ag-T
10 mol % Ag – TiO_2		10AgT
0.1% Ce – TiO_2	600	0.1Ce-T
0.2% Ce – TiO_2		0.2Ce-T
1% Ce – TiO_2		1Ce-T
2% Ce – TiO_2		2Ce-T
3% Ce – TiO_2		3Ce-T
1% Ag – ZnO	400 - 1000	1AZ
3% Ag – ZnO		3AZ
5% Ag – ZnO		5AZ
10% Ag – ZnO		10AZ
1% Ag – 1% Ce – TiO_2	400 - 1000	1:1 ACT
3% Ag – 1% Ce – TiO_2		3:1 ACT
5% Ag – 1% Ce – TiO_2		5:1 ACT
3% Ag – 3% Ce – TiO_2		3:3 ACT

The coatings were prepared by dip coating and drop-spin coater equipment. For dip coating, glass slides were dipped in sol for 30 sec and withdrawned at speed of 1mm/sec. For spin coating, the pre-treated glass slides having 3.8cm length and breadth were mounted on the rotating disk of spin coater (PI- KEM, Chemat Technology, Spin-coater, KW-4A) equipment and about 1 mL of the prepared titania sol was dropped on it. Then it was rotated with a rotation speed of 2000 RPM for 2 min. The slides were dried and thus 3 – 5 layers of coatings were prepared (*Fig. 2.1*). Glass slides were dried in an oven at 80 °C between each coating. The coated material was calcined at 500 °C for 2 h with a ramp rate of 1 °C/min.
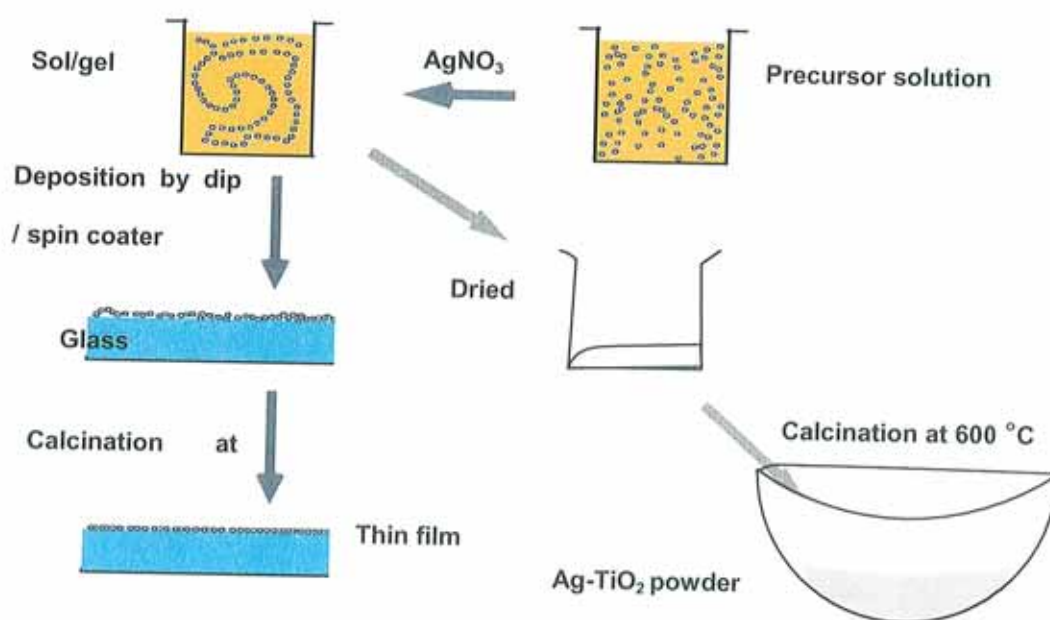
Figure 2.1: Schematic illustration of fabrication of thin film and corresponding powders

2.4 Photocatalytic Activity Evaluation

The photocatalytic activities of the materials were studied by examining the degradation reaction of a model dye rhodamine 6G (R6G). For powder samples, about 0.06 g of titania sample was dispersed in 50 mL of R6G solution (50 mL, 5×10^{-6} M).

The suspension was irradiated with light using Q-Sun solar test chamber (0.68 W/ m² at 340 nm). The Q-sun chamber is a solar light simulator consists of Xenon arc lamp that reproduces the effect of full spectrum sunlight and can filter the desired light (*Fig. 2.2*). Degradation was monitored by collecting aliquots at increasing time intervals. The aliquots were centrifuged and absorption spectra were recorded using Perkin Elmer Lambda 900 spectrophotometer.

The rate of degradation was assumed to obey (pseudo) first-order kinetics and hence the rate constant for degradation, k, was obtained from the first-order plot of kinetic analysis according to the *Equation 2.1*

$$\ln\left(\frac{A_0}{A}\right) = kt$$
<div align="right">*Equation 2.1*</div>

where A_0 is the initial absorbance, A is the absorbance after a time (t) of the R6G dye degradation, and k is the first order rate constant.

The effect of intensity of irradiance of Q-Sun chamber in the photocatalytic activity also were analysed by studying the degradation of R6G using various irradiation intensity such as 0.6, 0.5, and 0.4 W/m². Terrestrial activity of the highly active silver modified sample and the standard TiO_2 was determined by carrying out the reaction under Dublin summer sunlight at noon. The intensity of the sunlight was determined by a Solar Light Co. Broadband radiometer PMA 2107 (Philadelphia) which gave approximately 12.4 W/m² across the 260 – 400nm wave band.

For photocatalytic activity test for the materials coated on glass slides, the prepared slides (2 – 3 slides in 50 mL) were placed in R6G solution having concentration 5×10^{-7} M concentration and exposed to light irradiation in Q-Sun chamber. The samples were

collected at each time intervals and measured the decrease in absorbance at 525 nm with UV-vis absorption spectrometer

Figure 2.2: Picture of the Q-sun solar chamber used for the photocatalytic light irradiation experiments.

2.5 ATR – FTIR Study of the Adsorption of Oxalic Acid on TiO$_2$

Attenuated Total Reflection (ATR)-FTIR spectroscopy has been shown to be an extremely useful tool for studies of adsorption of molecules and ions from solution.[164, 165] The present study about the adsorption of oxalic acid on anatase TiO$_2$ was done at Institute fur Technische Chemie, Hannover University, Germany as a part of Short Term Scientific Mission (supported by COST Action-540). The Fourier Transform Infrared (FTIR) spectrometer was a BOMEM MB 122 equipped with a liquid N$_2$ cooled mercury – cadmium – telluride (MCT) detector as shown in *Fig. 2.3.* Two horizontal and trapezoidal ATR units, *ATR-1* and *ATR-2*, were mounted in the optical path of the equipment for different experiments. *ATR-1* was used for the experiments in a batch cell reactor and *ATR-2* was used for the experiments in a flow cell reactor.

47
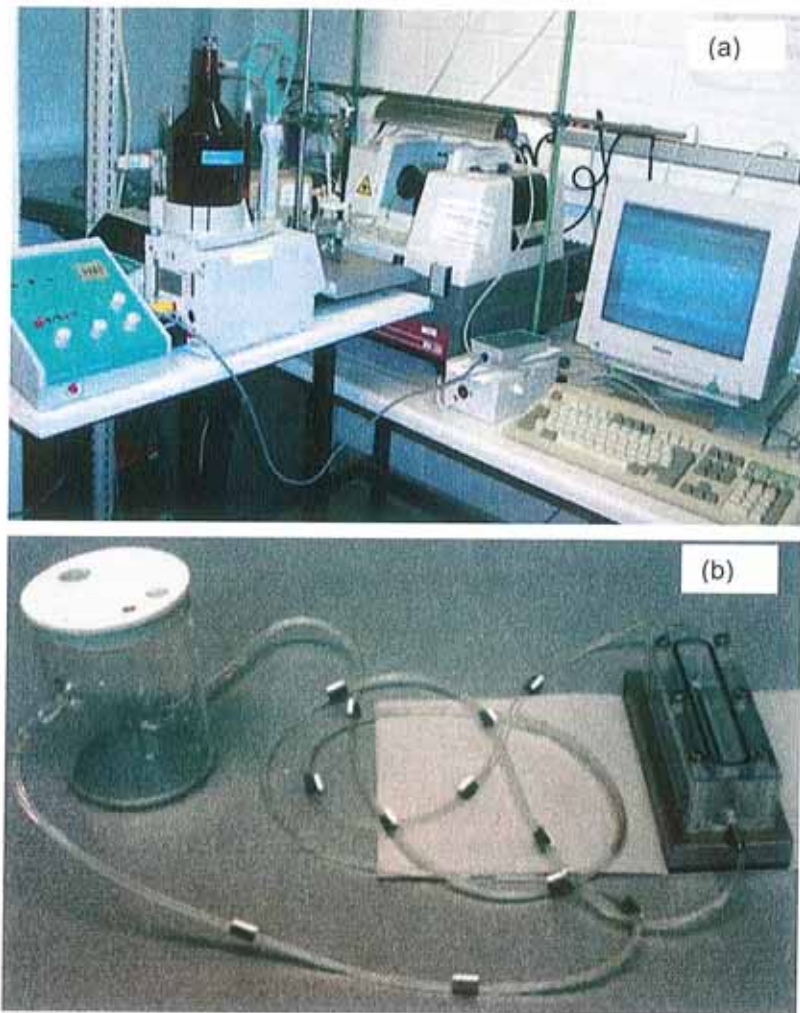
Figure 2.3: (a) The experimental set up of the ATR-FTIR analysis for the study of adsorption of oxalic acid and (b) flow cell reactor with ZnSe prism

Before preparation of the TiO_2 thin layers, the ATR ZnSe prism surface was cleaned by polishing with 1 µm diamond paste (Metadi II, polishing grade) and rinsed with methanol and deionised water. This cleaning procedure was important since the formation of a precipitate on the ZnSe crystal was observed, after long irradiation times, and could only be removed by polishing the crystal with diamond paste.

A thin layer of immobilized TiO_2 particles was deposited on the surface of the ATR ZnSe crystal in the following way: a TiO_2 suspension was prepared at a concentration of 4.24 g/L and dispersed by sonication for 15 min in an ultrasonic cleaning bath. An aliquot of 400 µL of this suspension was placed on the surface of the crystal. With the tip of the pipette this small volume was spread in order to evenly cover the surface of the crystal. The thin layer of suspension was directly evaporated to dryness at room temperature overnight in a semi-opened desiccator. The coverage of the final dry layer of particles obtained is roughly about 2.3 g/m^2.

The TiO_2-coated crystal was equilibrated with a circulating, oxalic acid-free, aqueous solution for 30 min; and then with KCl (0.01M) solution. During this period, sequential spectra were collected at time intervals of approximate 4 minutes. Each final spectrum consists of 10 sub files which is the average of 250 scans. When the last spectrum had been recorded, the UV(A) lamp was turned on and another sequence of spectra was recorded during 30 min at the same time intervals. These two groups of spectra are considered as the blank reference spectra in the dark and under UV(A) illumination, respectively. The background was subtracted and baseline correction was made due to instrumental instabilities. The pH of the circulating solution was adjusted to 3.6 during the experiment and the spectrometer was constantly purged with argon to avoid H_2O and CO_2 contamination.[166] (A. J. McQuillan, Adv. Mater., 2001, 13, 1034).

Following the recording of the blank references, the circulating solution was replaced by the test solution of oxalic acid (ca. 30 mL, 2 mM) and a new set of spectra was collected in a similar way. For the current study, in order to determine the optimum concentration of TiO_2 to be used for the thin film preparation, various concentrations of both TiO_2 and oxalic acid were tested.

2.6 Characterisation Techniques

2.6.1 XRD analysis

X-ray diffraction (XRD) is a versatile, non-destructive technique that reveals detailed information about the chemical composition and crystallographic structure of natural and synthetic materials. The X-ray analysis of pure powdered sample is the fingerprint of that material and this technique is ideally suited for characterisation and identification of polycrystalline phases. For the current analysis, samples were prepared by smearing the powder crushed in acetone on a clean glass plate and X-ray patterns were collected using a Siemens D 500 X-ray diffractometer, with a diffraction angle range 2θ = 10 − 70° using Cu K$_\alpha$ radiation.

The mass fraction of rutile in the calcined samples was calculated by Spurr formula (*Eqn. 2.2*),[167]

$$X_R = \frac{1}{1 + 0.8(I_A / I_R)}$$
Equation 2.2

which is the relationship between integrated intensities of anatase (101) and rutile (110) peaks where I_A and I_R are the integrated peak intensities of anatase and rutile peaks respectively. Particle size (D) was determined by the Scherrer equation (*Eqn. 2.3*).

$$D = \left(\frac{k\lambda}{\beta \cos \theta} \right)$$
Equation 2.3

k is the shape factor, λ is the wavelength of X-ray radiation which is 1.54 Å and β is the full width at half maximum of the main intensity peak. The line broadening β is measured from the increased peak width at half the peak height and is obtained from Warren formula $\beta^2 = \beta_M{}^2 - \beta_S{}^2$ where β_M is the measured peak width and β_S is the

corresponding width of a peak of a standard material whose particle size is greater than 200 nm.

For ZnO, the particle size (D) of the samples were estimated using the same formula, by measuring the line broadening of (101) intensity peak.

2.6.2 UV-visible absorption / transmission spectroscopy

The photocatalytic activity of titania and silver modified titania were measured by taking the absorption spectra of titania – R6G mixtures on increasing irradiation times. The solution collected after light irradiation from Q-Sun solar chamber was centrifuged and the clear solutions were taken for the measurement. The decrease in absorbance at 525 nm was noted to monitor the degradation of R6G. The absorption spectra were recorded using Perkin Elmer Lambda 900 spectrophotometer in the range of 300 – 600 nm. In the case of coatings, transmission spectra of the films, which are the ratio of amount of light transmitted through the sample and the light transmitted through the blank, were recorded from the same instrument. An uncoated glass slide was used as blank. From the transmission data, absorbance is calculated by the relation,

$$A = -\log (\% \text{ transmittance}) \qquad Eqn. \quad 2.4$$

2.6.3 Diffuse reflectance spectroscopy

In order to calculate the effect of silver doping in the band gap of the prepared material, diffuse reflectance spectra were recorded using Perkin Elmer Lambda 900 spectrophotometer. The instrument was set in a scanning range of 200 - 800 nm. The samples were prepared in pellet form having uniform thickness by mixing with KBr. From the diffuse reflectance spectra, band gaps of the samples were calculated as follows. The reflectance spectrum was fitted by a sigmoidal fitting technique. The

fit gives various straight lines along the reflectance spectrum. The line extrapolates the wavelength scale give the specific wavelength of absorption. Dividing 1040 by the obtained wavelength will give the band gap energy value.

2.6.4 Transmission electron microscopy

Transmission Electron Microscopy (TEM) provides the information about the surface morphology in nanometre scale. It is a powerful tool for the observation of crystal defects, grain boundaries, interfaces, line and planar defects. The TiO_2 samples were prepared by dispersing the powder in ethanol and ultra-sonicated for 10 min. The carbon coated Cu-grid was dipped in the solution, so that the particles were stacked on the grid. The TEM images for the present study were collected from JEOL 100 CX transmission electron microscope.

2.6.5 Scanning electron microscopy

Scanning Electron Microscopy (SEM) is a good technique to produce high-resolution images of a sample surface. Due to the manner in which the image is created, SEM images have a characteristic three-dimensional appearance and are useful for judging the surface morphology of the sample. For the current study, SEM images were collected from Trinity College, Dublin using a Hitachi 4300 Field Emission Scanning Electron Microscope (FESEM) which was operated at 20 kV.

2.6.6 Differential scanning calorimetry (DSC)

The phase changes occurring in the materials during the heat treatment were analysed by differential scanning calorimetry (DSC). DSC is a thermo-analytical technique where the heat lost or gained (exo/endothermic) in a sample is measured relative to a

reference sample as a function of increasing temperature. DSC measurements were carried out with a Rheometric Scientific DSC QC. About 6 mg of the dried sample was heated from room temperature (25 °C to 500 °C at a constant heating rate of 10 °C/min).

2.6.7 Fourier transform infrared spectroscopy

IR Spectroscopy is an extremely effective method for determining the presence or absence of a wide variety of functional groups in a molecule. Also it gives an insight on the various type of bonding in the semiconductors. The formation of nanosized TiO_2, ZnO and corresponding silver modified materials was confirmed by measuring the FTIR spectra of ZnO and silver modified ZnO samples using a GX-FTIR spectrophotometer in the wavenumber range 4000 – 400 cm^{-1}, using 20 scans per sample. The samples were prepared as pellet by mixing with KBr in a 1:200 ratio.

2.6.8 Raman spectroscopy

Raman scattering is a strong candidate to be the technique of choice for characterization of metal oxides. It can provide plenty of information about crystal structure and elementary excitons. One of the advantages of Raman spectroscopy is that very low frequency vibrational modes can be observed. It was an additional tool to probe the phase formation. Raman scattering from semiconductors less than 100 nm in diameter is affected by the finite size of the scatterer. Raman spectra of the present samples were collected from an Instruments S. A. Labram 1B spectrometer, with an excitation wavelength of 514 nm (50 mW).

2.6.9 Photoluminescence

Photoluminescence spectroscopy is a contactless, non-destructive method of probing the electronic structure of materials. Photoluminescence relates to the difference in

energy levels between the two electron states involved in the transition between the excited state and the equilibrium state. The quantity of the emitted light is related to the relative contribution of the radiative process. Analysis of photoluminescence helps to understand the underlying physics of the recombination mechanism. It will give an insight to the mechanism of interfacial electron transfer. Room temperature photoluminescence spectra of the prepared samples were obtained from Perkin Elmer Luminescence Spectrometer (LS50B). About 1 mg of the sample was dispersed in 2:1 ratio of ethylene glycol-water mixture and ultrasonicated for 30 min before recording the emission spectra. The excitation wavelength was 325 nm, and spectra (uncorrected) were obtained in the range 350 – 600 nm.

2.6.10 BET specific surface area analysis (nitrogen sorption studies)

The tendency of all solid surfaces to attract surrounding gas molecules gives rise to a process called gas sorption. Monitoring the gas sorption process provides a wealth of useful information about the characteristics of solids such as surface area and pore size. Surface area is calculated from the monolayer amount, using the B.E.T. (Brunauer, Emmett and Teller) method. Before performing a surface area analysis or pore size measurement, solid surfaces (adsorbent) must be freed from contaminants such as water and oils. Surface cleaning (degassing) is most often carried out by placing a sample of the solid in a glass cell and heating it under a vacuum at 300 °C for 2 h. The cleaned sample is brought to a constant temperature by means of an external bath, typically a Dewar flask containing liquid nitrogen. Small amounts of a nitrogen gas (the absorbate) are admitted in steps into the evacuated sample chamber. The variation of adsorption with pressure at a given constant temperature is expressed graphically and is known as adsorption isotherm.

Nitrogen sorption studies of the corresponding samples were carried out using BET analyser Quantachrome 2000e. In BET theory, it is assumed that multilayer adsorption can take place since the solid surface possesses uniform localized sites. The surface area was calculated using the BET surface area equation (*Eqn. 2.5*),

$$\cdot \quad \frac{P/P_0}{V(1-P/P_0)} = \frac{1}{V_m c} + \frac{c-1}{V_m c}\left(\frac{P}{P_0}\right) \qquad \text{Equation 2.5}$$

V is the volume of the gas adsorbed at pressure P; V_m is the volume adsorbed when the solid surface is completely covered with a monolayer of adsorbed gas molecules and c is a constant depending upon the nature of the gas.

Since c and V_m are constant for a given gas solid system, a plot of $\left(\dfrac{P}{V(P_0 - P)}\right)$ against P/P_0 would be a straight line, allowing V_m to be calculated from the intercept and slope. The total surface area of the sample can be calculated using the equation,

$$S = \frac{V_m N_A A}{M} \qquad \text{Equation 2.6}$$

Where N_A is Avogadro's number, A is the cross sectional area of a single molecule of the adsorbate and M is the molecular weight of the adsorbate. The BET surface area of the sample is usually expressed in m^2/g.

3. SILVER MODIFIED TiO$_2$ PHOTOCATALYSTS

3.1 Introduction

Among the many candidates for photocatalysts, TiO_2 is the most widely used material for industrial applications. More significantly, it has been used as a white pigment since ancient times and thus its safety to humans and the environment is guaranteed by history. This stable filler and colorant has been widely used to make products as diverse as paper, plastics, lipstick, toothpaste, and pharmaceutical tablets. Titania occurs mainly in minerals like rutile, ilmenite, leucoxene, anatase, brookite, perovskite and sphene. Among the three crystalline forms, rutile is the most stable form and major ore of titania and anatase is the most used form for technological applications. In addition, TiO_2 nanoparticles in the 10 – 50 nm range possess unusual properties and can be used in various applications. The properties are related to the atomic structure. Its wide band gap property makes TiO_2 a substitute for silicon to make solar power cells, as well as battery storage media.[168]

As described in *Chapter 1*, the mechanism of photocatalysis involves the excitation of valence electrons to the conduction band by absorbing the UV light, resulting in the formation of holes in the valence band. As well as the energy of incident light, the photocatalytic efficiency depends on the rate of recombination of photoexcited electrons and holes. However, the lifetimes of these species are very small and in the absence of suitable scavengers, they will dissipate the stored energy within a few nanoseconds by recombination. This is ascribed to the electron/phonon interactions[169] – they relax to the bottom of the conduction band and to the upper edge of the valence band respectively. Generally, in TiO_2 semiconductor photocatalysis, the incidence of recombination between the photogenerated electrons and holes is high which reduces the efficiency of photocatalytic process. The electron-hole recombination is on the order of < 30 ps and so efficiency is very low. It is imperative for efficient photocatalytic

processes to have the charge carriers separated as far as possible and the efficiency of photocatalysis depends on how well one can prevent this recombination. Deep electron traps and high surface acidity are needed to lengthen the lifetime of photoexcited electrons and holes and to ensure better adsorption of organic substances on the surface. Many studies have been carried out to improve the photocatalytic activity by reducing the recombination reaction. Doping is found to be an effective tool to increase the photocatalytic efficiency. Several metals were used for doping especially Pt, Li^+, Zn^{2+}, Cd^{2+}, Mn^{2+}, Ce^{3+}, Cr^{3+}, Fe^{3+} and Al^{3+}.[170-172] Platinization of titania had been proposed in 1978 for the photocatalytic transformation of acetic acid.[173] The presence of transition metals may increase the photocatalytic activity by scavenging electrons that reduce the recombination of charges and favour the formation of hydroxyl radical. Details have already been explained in *Chapter 1*.

According to previous reports, insertion of noble metals is very effective for enhanced photocatalysis[58, 174] as they inhibit the electron-hole recombination and research in this area made great progress. Particularly, it is found that deposition with silver has been of considerable interest because of its potential applications. Fujishima *et al.,* in 2003, explored the multicolour photochromism property of silver loaded TiO_2 with the aim of practical applicability in the photochromic display devices, smart windows *etc.*[175] The importance in medical applications of silver and antibacterial activity of TiO_2 led researchers to think about to manufacture the silver modified titania coated sanitary wares,[176] medical devices, food preparation surfaces, air conditioning filters, *etc.* Silver can trap the excited electrons from TiO_2 with holes available for the degradation of organic species. It also results in the extension of their wavelength response towards the visible region.[177] Moreover, silver particles can facilitate the electron excitation by

creating a local electric field,[178] and plasmon resonance effect in metallic silver particles shows a reasonable enhancement in this electric field.[179] The effect of Ag doping on titania and its photocatalytic activity by UV irradiation was studied by Chao et al[180] (using a sol-gel method) and they found that Ag doping promotes the anatase to rutile transformation, which is attributed to the increase in specific surface area which causes the improvement in photocatalytic activity and enhances the electron-hole pair separation. However, there are some contradictory results also reported showing the decreased activity of silver modified titania.[181] This may be due to the method preparation, nature of organic molecules, photoreaction medium or the metal content and its dispersion. Although there has been extensive research on silver modified titania, the exact mechanism and the role of silver is still under debate.

Here in our research lab, we made an attempt to modify the semiconductors such as TiO_2 and ZnO by using noble metals like silver. This chapter describes, a comparative study of the photcatalytic activity of solar initiated photocatalytic activity of sol-gel titania with silver nitrate added in various amounts. The silver ion was either reduced during the synthesis phase by irradiating the sample with light (pre-irradiated) or formed during calcination of the sol-gel material *via* decomposition of silver nitrate (not pre-irradiated; *Scheme 3.3*). The detailed electronic, optical and structural properties of the silver modified TiO_2 and the effect of silver modification on increasing the photocatalytic efficiency were also described. In a separate section, the photocatalytic activity study of N-doped titania (collaborative work) is also discussed.

In addition to the modification of titania, some surface characteristic analysis of pure anatase titania has also been done as a part of a Short Term Scientific Mission funded

by COST Action- 540 at Institute fur Technische Chemie, Leibniz Universitat, Hannover, Germany. There are many factors that affect efficiency of photocatalytic activity. In the case of environmental application, a proper understanding of the reaction mechanisms in the semiconductor photocatalysis will lead to the development of efficient photocatalytic systems specific to particular chemical species and new photocatalysts based on the TiO_2 nanomaterials. Study of the surface characteristics and its interaction with substrates can provide information about the photocatalytic reaction mechanism. Recent studies show attenuated total reflection infrared spectroscopy (ATR–FTIR) as a good tool to interpret the structural and thermodynamic information about the surface complexes which is formed by the interaction of TiO_2 with light.[165] Also it sheds light on the dynamics of mass transfer across the TiO_2 – aqueous solution interface, when the interfacial species undergo chemical changes caused by light induced heterogeneous oxidation. One of the advantages of the ATR spectroscopy is that *in situ* spectra of adsorbed species can be recorded easily at a given metal oxide surface.

3.2 Results

3.2.1 Crystallinity

XRD of the modified and unmodified titania samples irradiated with light for 40 min to reduce the silver nitrate and calcined at 600 °C and 700 °C are shown below (*Fig. 3.1*). The materials show a high degree of crystallinity and existence of fully anatase phase at 600 °C. The chosen calcination temperature was 600 °C as this temperature was found to have highest photocatalytic activity among samples calcined at different temperatures, due to the fact that the material is in the anatase phase and is highly crystalline.[182] However, there are no obvious peaks showing the presence of silver in

the XRD of silver modified titania samples calcined at 600 °C, which indicates that the discrete silver particles are homogeneously distributed in the titania matrix. This conclusion is further verified by studying an XRD of Ag-TiO$_2$ calcined at 700 °C which shows the presence of peaks corresponding to the metallic silver at 38.2, 44.4 and 64.5. Interestingly, the presence of small amounts of silver (1 mol %, 3 mol %) result in the anatase to rutile phase transformation occurring at a higher temperature. This differs from other work where addition of silver resulted in the rutile phase forming at 500 °C.[183] There was no measurable difference in the XRD spectra due to pre-irradiation of samples.
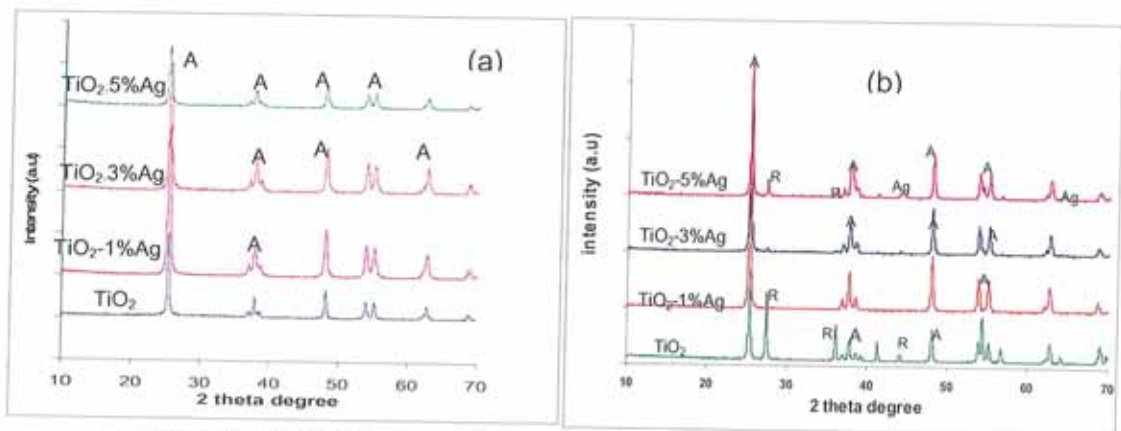
Figure 3.1: XRD of unmodified and various mol % silver modified titania at (a) 600 °C (b) 700 °C. (A, Anatase; R, Rutile)

In samples calcined at 700 °C, silver peaks are detected and this also in a good agreement with the values of peaks obtaining by calcination of silver nitrate alone. The 700 °C sample indicates that at this higher temperature, the silver particles homogeneously distributed throughout the TiO$_2$ matrix begin to diffuse towards the edges of the material forming agglomerates. In order to study the effect of silver on particle size, crystallite sizes were calculated from the XRD spectra (*Table 3.1*). It was found that the particle size reduces as a result of Ag addition. However, there is no

61

significant reduction in particle size observed with increasing silver amounts after this initial reduction.

Table 3.1: Crystallite sizes calculated from XRD.

Mol % Ag	Crystallite Size (nm) ± 5 % error	
	600 °C	700 °C
0	27.57	33.93 (A)/40.53 (R)(48% R)
1	18.76	32.66
3	19.30	30.65
5	19.42	33.99 (A)/45.24(R) (13% R)

3.2.2 Visible light absorption

Diffuse reflectance spectroscopy (DRS) and transmission spectroscopy were used to record the transmission of the films and absorbance of the powders respectively. In all cases, increasing amounts of silver results in shifting of the absorption band into the visible region. Reflectance spectra of the powders show an increased visible absorption of the powders as a result of increasing levels of doping. From the spectra it is seen that, the addition of silver extend the absorption towards the visible region. A consistent decrease in the percentage of reflectance as a result of the increased amount of silver could also been observed, which depict the enhanced absorption capability of the silver modified titania material.
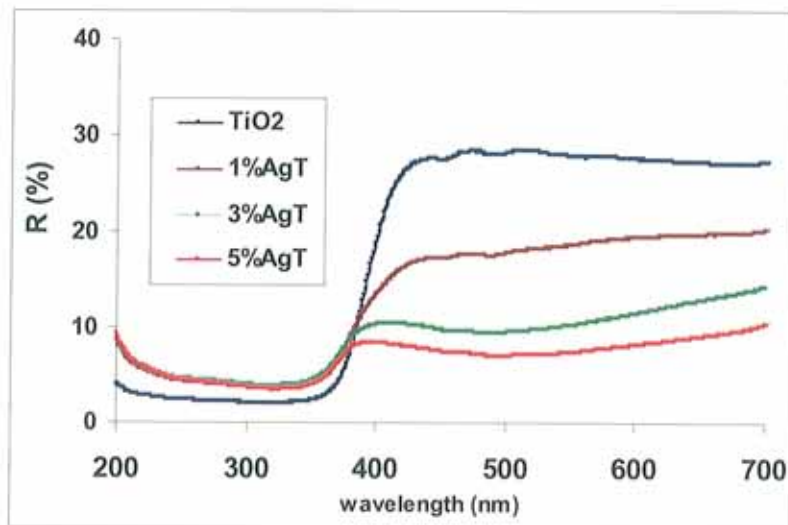
Figure 3.2: Diffuse reflectance spectra of TiO$_2$ and silver modified TiO$_2$ at 600 °C.

Moreover, the transmission spectra of the thin films show the presence of a band at ~ 400 nm, which is due to the surface plasmon resonance of the silver metal (*Fig. 3.3*). It is noted that upon illumination of TiO$_2$ / AgNO$_3$ solution during the preparation time stable colloidal solutions were obtained which displays the progressive evolution of characteristic silver surface plasmon band at 400 nm. This is indicative of the formation of nanometer sized silver metal corresponding to a size of approximately 20 nm,[184] which exhibit unique optical properties in the visible region. These silver nanoparticles can easily disperse into the TiO$_2$ matrix. At this plasmon band resonance frequency, there would be efficient visible light absorption. The light absorption by silver can be controlled by the modifying the size and shape of silver particles. Size and shape dependent absorption properties of silver have already been reported.[185]
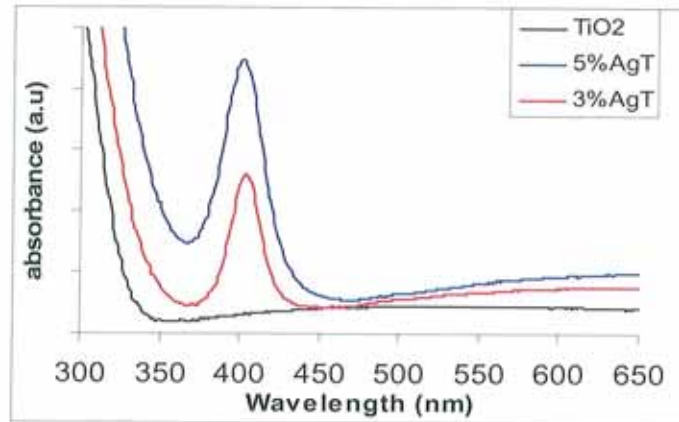
Figure 3.3: Transmission spectra (A = -logT) of unmodified and
silver modified titania thin films

3.2.3 SEM analysis

The surface morphology of unmodified and silver modified titania materials were given below (*Fig. 3.4*). The addition of silver causes the surface morphology of titania to change. During calcination at 600 °C, the presence of silver promotes the anatase phase to form clusters.
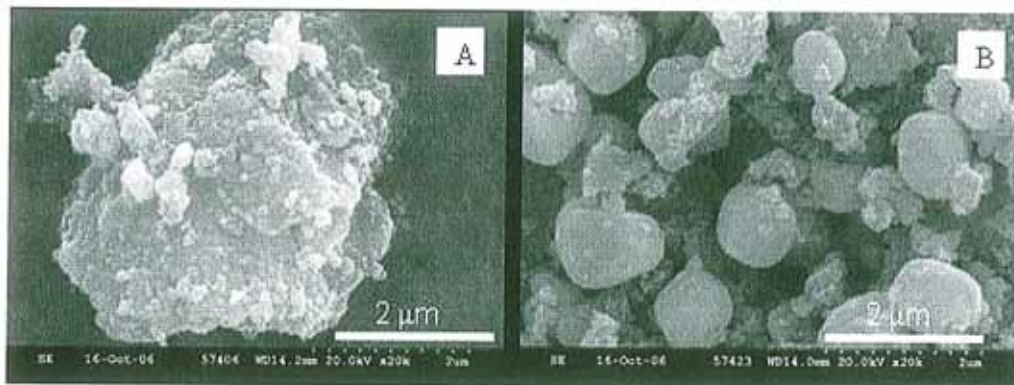
Figure 3.4: SEM images of (A) Unmodified TiO$_2$ and (B) 5% Ag modified TiO$_2$ at 600 °C.

3.2.4 TEM analysis

Transmission electron microscopic observations of a typical unmodified and 5 % silver deposited titania calcined at 600 °C are shown below (*Fig. 3.5*). The crystalline morphology agrees with the results obtained from X-ray analysis. As calculated from the XRD, 5 mol % silver deposited titania at 600 °C shows the lowest anatase grain size ~20 nm where as the unmodified titania shows the particle sizes of ~30 nm. With anatase grain size decreasing, the specific surface area of the material increases which facilitate the requirements of photocatalysis.
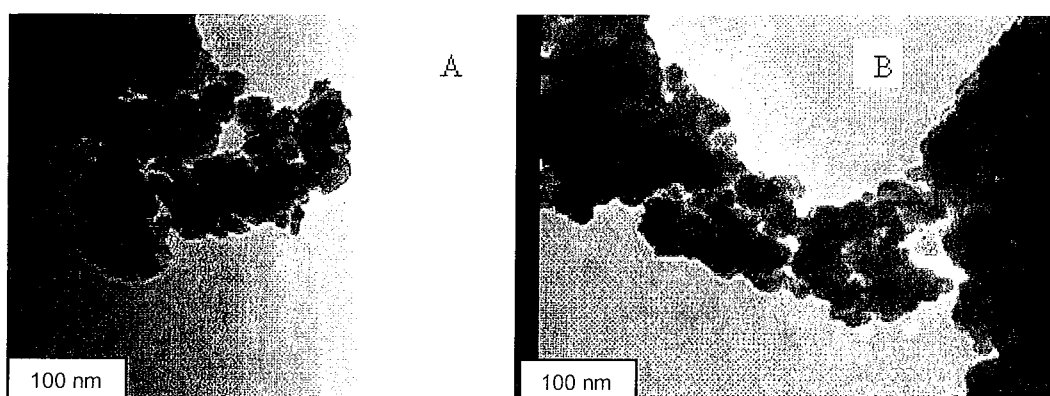
Figure 3.5: TEM photographs of (A) unmodified and (B) silver modified titania

at 600 °C.

3.2.5 Photocatalytic studies and kinetic analysis

In order to examine the photocatalytic activity of the materials prepared the effect of photodegradation of R6G in presence of the unmodified and silver modified materials was studied. Silver metal can be incorporated by photoreduction of Ag^+,[186] or by allowing the silver salt to decompose during calcination.[187] In order to examine the effect of pre-irradiation, we prepared two parallel sets of modified materials (the

experimental details are given in *Chapter 2*) – the first where the silver nitrate was added and the solution irradiated for 0 – 60 min before drying and calcination, the second where the silver nitrate was added and the material dried and calcined without irradiation. The results of this study are shown in Table 3.2.

Table 3.2: The rate constant for degradation of R6G for samples with different mol percentages of silver – after pre-experimental irradiation to reduce $AgNO_3$ and sample which were directly calcinated.

Ag (mol %)	Rate constant (min^{-1})	
	No pre-irradiation	Pre-irradiation (60min)
0	0.06	--
1	0.16 ± 0.02	0.10 ± 0.01
2	0.18 ± 0.02	0.17 ± 0.02
3	0.24 ± 0.02	0.21 ± 0.03
5	0.34 ± 0.03	0.24 ± 0.03
10	0.07 ± 0.03	0.06 ± 0.03

According to kinetic analysis, for both pre-irradiated and non-irradiated samples, the activity of the catalyst is enhanced significantly on addition of silver, with the degradation rate increasing from 0.06 min^{-1} to 0.24 min^{-1} for the pre-irradiated samples and to 0.34 min^{-1} for the non pre-irradiated samples, corresponding to half lives of 12.0, 2.8 and 2.4 min respectively (*Fig. 3.6*). When comparing the effects of pre-irradiation, the samples that were not pre-irradiated showed a slight enhancement over those which were pre-irradiated, although the enhancement was not large. According to our study, it is clear that with the increase in the time of pre-irradiation, the amount of photo

reduced Ag increases and which causes the growth of silver clusters and thereby decreasing the active sites for the photocatalytic reaction. This is confirmed by varying the pre-irradiation time of the 5 % Ag-TiO$_2$ sample, which shows the rate of degradation decrease from no pre-irradiation (0.34 min^{-1}) through 20 (0.28 min^{-1}), 40 (0.27 min^{-1}) and 60 minutes pre-irradiation (0.24 min^{-1}).
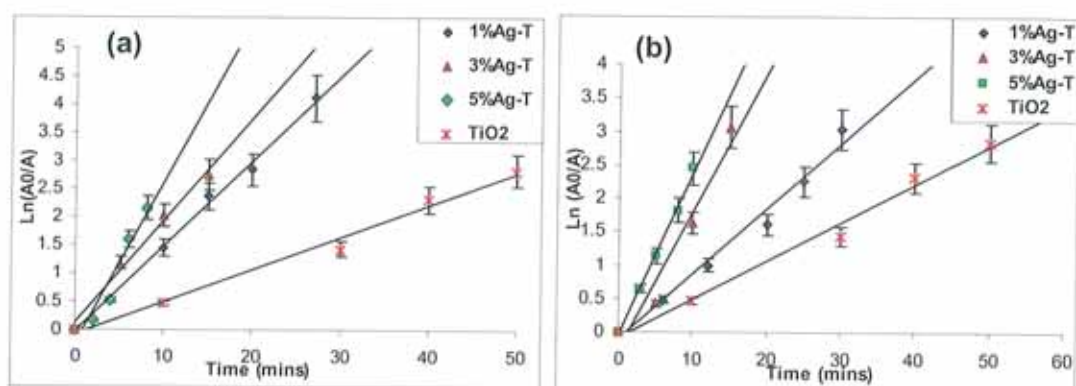
Figure 3.6: Kinetic analysis showing the effect of increasing concentration of Ag on the rate of degradation of R6G where the preparation method involved (a) no pre-irradiation and (b) with pre-irradiation

From the degradation studies, it is found that silver modification made substantial increase in the photocatalytic activity of titania. 5 mol % silver modified titania shows a higher photocatalytic activity among other samples (*Fig. 3.7*). The unmodified titania degrades the R6G within 50 – 60 min where as the 5 % silver modified titania requires only 10 min to effect degradation. In order to optimise the amount of silver to give the highest photocatalytic activity, photocatalytic degradation study with 10 mol % silver modified titania have been completed and it shows a decrease in the photocatalytic activity as compared to 5 mol % silver modified sample.
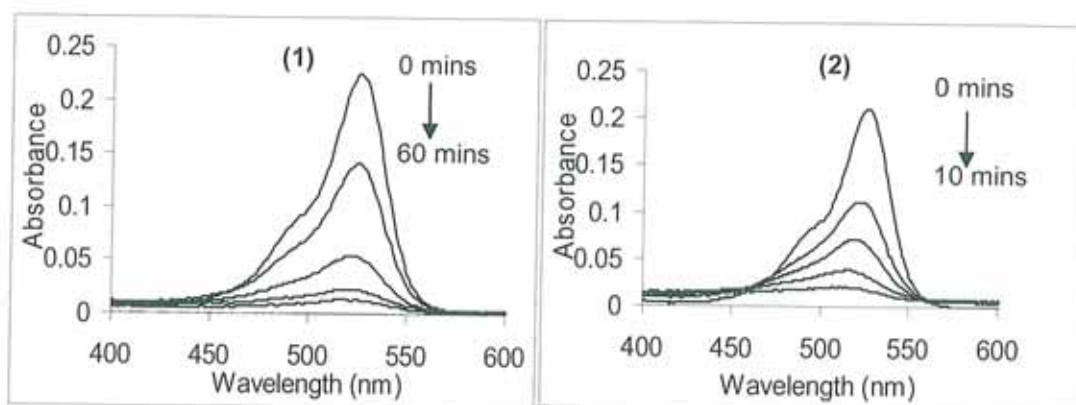
Figure 3.7: Absorption spectra of the degradation of R6G in presence of (1) TiO$_2$ and (2) 5 mol % Ag added TiO$_2$.

Fig. 3.8 shows the rate constant of degradation as a function of mol % of silver. As observed in the transmission and DRS spectra, increasing amounts of silver result in increased visible light absorption and hence enhanced photocatalytic activity. The optimum concentration of silver giving the good photocatalytic activity is found to be 5 mol % and after the optimum it starts to decrease.
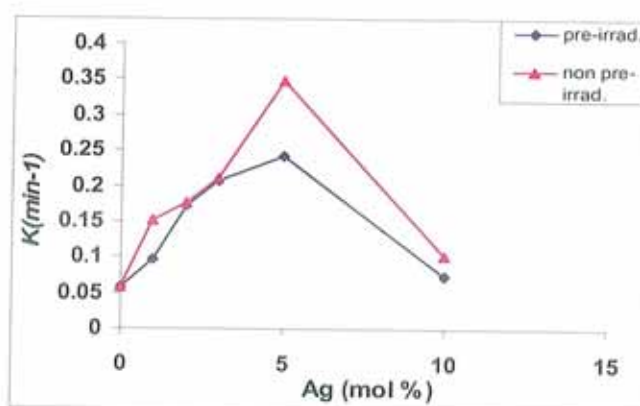
Figure 3.8: Plot of rate constants of degradation against mol % of Ag with pre-irradiated and non pre-irradiated samples.

3.2.6 Sunlight as a light source

The above experiments were conducted in a Q-Sun solar chamber which models the solar spectrum, at a power corresponding to noon time, summer day, in Florida. Similar experiments were carried out with solutions of R6G in the presence of titania and silver modified titania (5%) placed in a sunny window behind glass in Dublin. The kinetic analysis showing the rate of reaction with unmodified titania and 5 mol % Ag modified titania, (pre-irradiated) is given below (*Fig. 3.9*). In this case, rate constants for decomposition of rhodamine are 1.95×10^{-2} min and 1.3×10^{-2} min for modified and unmodified titania respectively, corresponding to half lives of 35 min and 52 min. These studies show these materials to be active in climates such as Ireland.
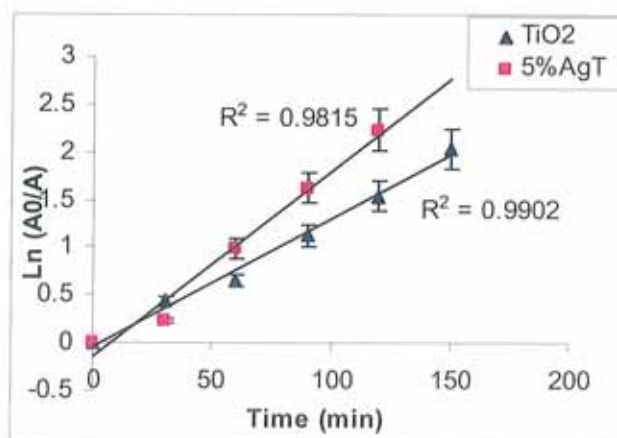
Figure 3.9: Comparison of kinetics of TiO_2 and 5% Ag-TiO_2 in degradation of R6G with sunlight as a light source.

The degradation of R6G was examined in the presence of silver nanoparticles and in the absence of titania. Minimal degradation was observed over 6h irradiation in the Q-Sun chamber, indicating the requirement of the presence of titania for the photocatalytic mechanism.

Degradation experiments were carried out with thin films of 3% and 5% silver modified titania in Q-Sun chamber. It is found that the coatings are active in degrading the dye.

The 5% Ag modified titania thin film degrading the dye with a rate of 9.5 x 10^{-3} min^{-1} where as the 3% Ag modified titania degrading the dye with a rate of 9.1 x 10^{-3} min^{-1}.

3.2.7 ATR-FTIR analysis on the adsorption of oxalic acid on anatase TiO$_2$

The experimental set-up and detailed explanation about the adsorption of oxalic acid on pure anatase TiO$_2$ has already been presented in *Chapter 2*. A detailed study about the surface adsorbed characteristic species on TiO$_2$ during light irradiation was not possible due to the short period of visit; the results obtained are presented here. Oxalic acid was selected as a model adsorbent. It is reported that oxalic acid induces a new channel for electron-hole recombination during the arrival and absorption of UV(A) photons. This is assumed to occur at adsorption sites which can act efficiently as traps for the photogenerated electron-hole species.[188] TiO$_2$ (from suspensions of 0.03, 0.07 and 0.1 M) thin films having various concentrations were prepared and analysed the adsorption of oxalic acid in dark and light conditions. The evolution of FTIR spectra of adsorption of oxalic acid on TiO$_2$ and 5 mol% silver modified TiO$_2$ with 0.1 M concentrations, which is a roughly optimised concentration, both in dark and light conditions are shown in *Fig. 3.10*. There are four prominent peaks at 1697 cm^{-1}, 1635 cm^{-1}, 1420 cm^{-1}, and 1270 cm^{-1}, which can be identified from the spectra below.
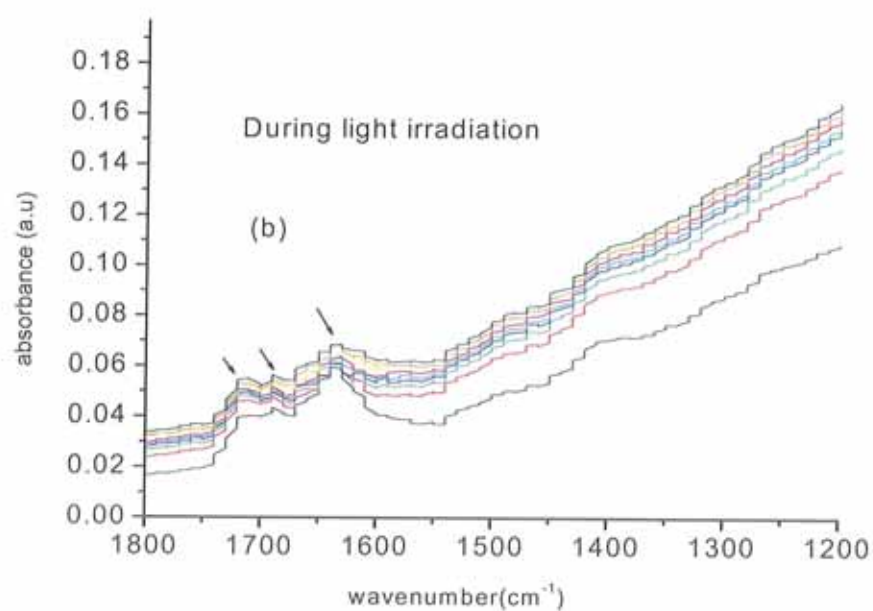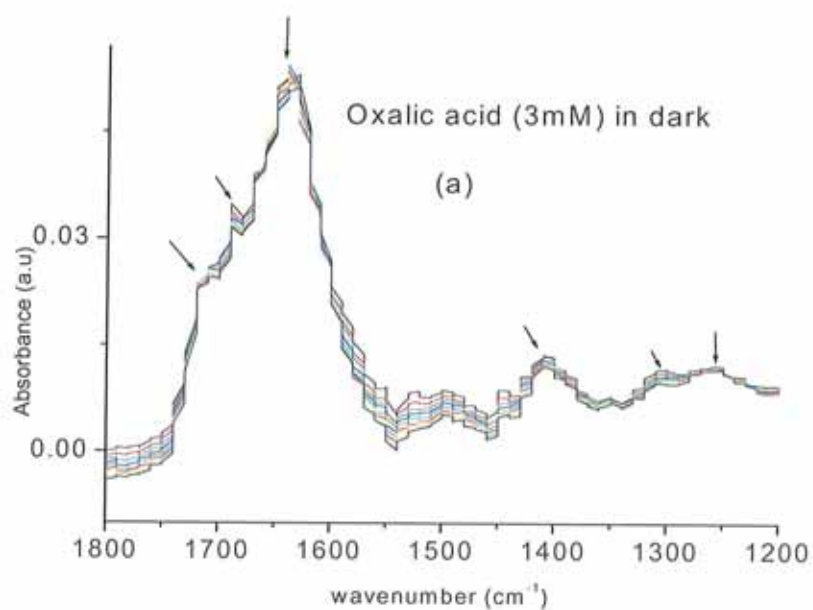
Figure 3.10: ATR-FTIR spectra of adsorption of oxalic acid on TiO_2 (0.1 M) thin film (a) dark (b) during light irradiation.

Similar experiments were carried out using 5 mole % silver modified TiO_2 and the spectra are shown *Fig.3.11*. The general shape of the resulting spectra closely resembles the absorbance spectra of oxalic acid on pure anatase TiO_2. However, there are some shifts in the band positions of prominent peaks such as 1709, 1673 and 1627 cm^{-1}. In addition, the intensity of peak at 1420 cm^{-1} is slightly increased. The minor spectral shifts in the frequencies of the bands are most likely due to slight changes in the bulk or surface properties of the system under steady state light illumination. It has been previously shown that change in binding modes can also cause the changes in the shifts in spectral evolution.

For comparison, the analysis of oxalic acid adsorption on a standard commercial TiO_2, PC 500, has been done using the similar experimental conditions. The concentration of the suspension of TiO_2 was 0.03 M and the oxalic acid concentration was 2 mM. The spectra *Fig 3.12 (b)* shows no significant change during the light irradiation. The mode of binding of oxalate molecules on PC 500 is seems to be same both in dark and light. In the case of oxalate heterogeneous photolytic oxidation, no intermediates are expected to be formed. The product formed upon hole capture, the radical anion $C_2O_4^{\cdot-}$, rapidly injects an electron into the conduction band of TiO_2, yielding two equivalents of CO_2.[189]
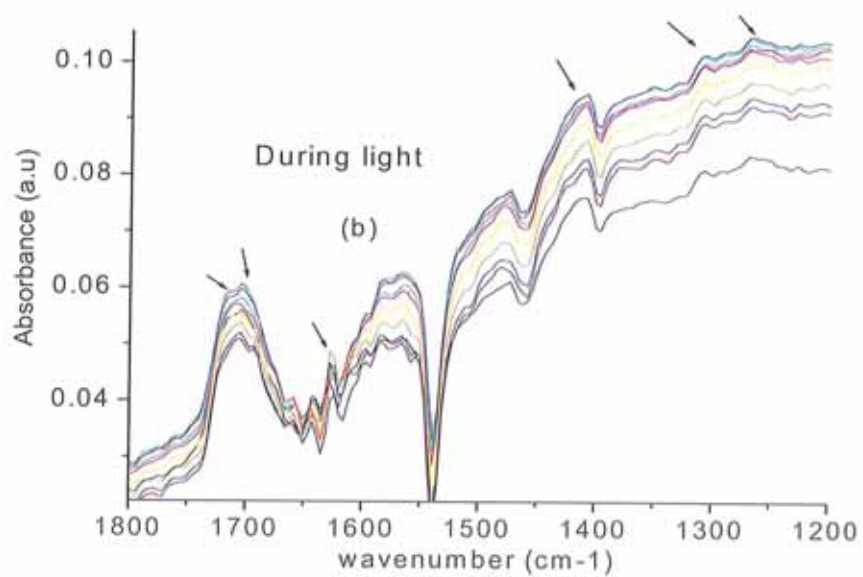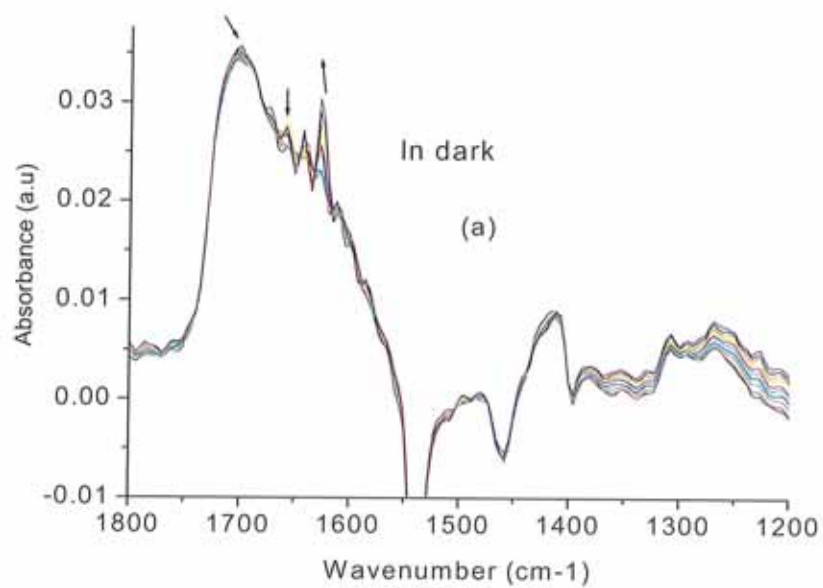
Figure 3.11: ATR–FTIR spectral evolution of adsorption of oxalic acid on 5 mole% silver modified anatase TiO_2 in (a) dark (b) during light irradiation.
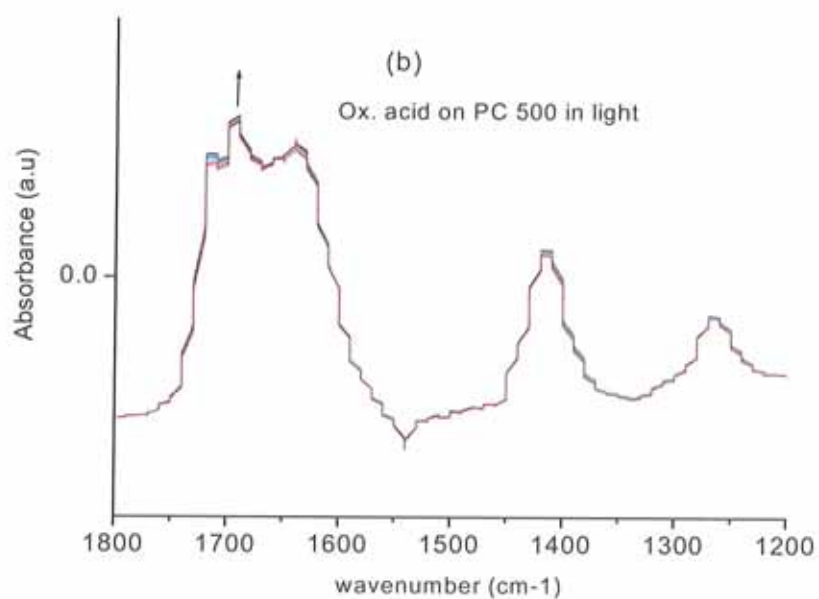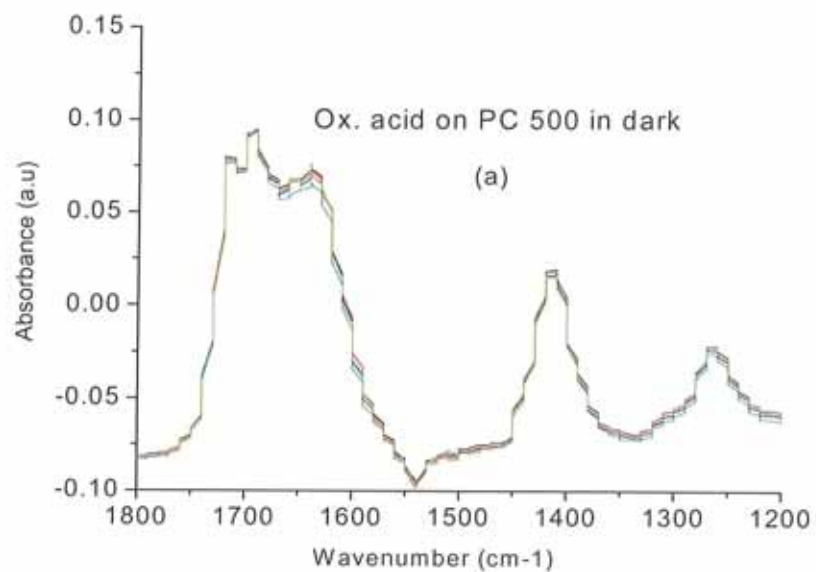
Figure 3.12: ATR-FTIR spectral evolution of adsorption of oxalic acid on a standard TiO₂, PC 500 (0.07M), in (a) dark and (b) during light irradiation

In order to determine the optimised concentration of TiO_2, we measured the spectral evolution of oxalic acid adsorption with various concentrations (0.07, 0.01 M) of TiO_2. *Fig. 3.13* shows the evolution of oxalic acid adsorption spectra on TiO_2 having 0.07 M concentration.
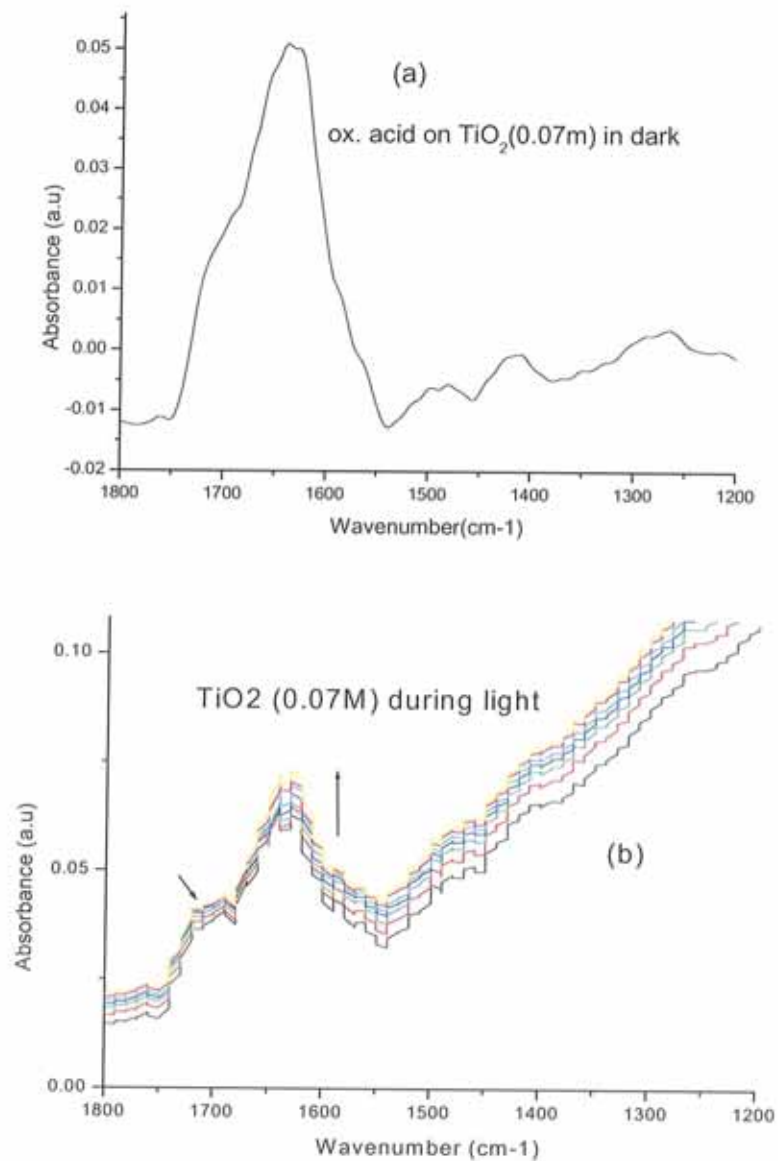
Figure 3.13: ATR-FTIR spectral evolution of adsorption of oxalic acid on TiO_2 thin film of concentration 0.07 M in (a) dark and (b) light irradiation.

3.3 Discussion

3.3.1 Synthetic procedure of silver modification

Titania can be prepared by different methods such as inert gas condensation, $TiCl_4$ oxidation, oxidation – hydrothermal synthesis of metallic Ti, hydrolysis precipitation of titanium alkoxide or chlorides [sol-gel process] *etc*. Among these, sol-gel process provides excellent chemical homogeneity and the possibility of deriving unique metastable structures at low reaction temperatures. TiO_2 nanocrystals prepared by the sol-gel route have fully hydroxylated surfaces and these hydroxyls have strong influence on the catalytic and photocatalytic properties such as electron transfer rates and reducing properties. One of the advantages with sol prepared via sol-gel process is that chemically homogeneous coatings and powders with a wide variety of useful applications can be prepared. Sol-gel processes usually involve various metal alkoxide molecules that are hydrolyzed under controlled conditions and then subsequently reacted to condense with each other to form metal-oxygen-metal bridging units.

The synthesis of TiO_2 in the present study involves the chemical modification of Titanium isopropoxide (Ti(iOPr)$_4$) precursor and its hydrolysis followed by condensation reaction. Glacial acetic acid was used as the chemical modifier which stabilizes the sol by modifying the coordination sphere of titanium.[190, 191] Acetic acid (HOAc) is a popular modifier because it can easily dissolve a wide variety of different precursor molecules, helping enable the creation of a multitude of multi-cation solutions.[192, 193]

The reactivity of Ti(OPr)$_4$ towards acetic acid can be described in terms of the nucleophilic substitution of (i-OPr) by (OAc) groups. Acetates are stronger ligands. They are also able to behave as bi-dentate species and give rise to acetate bridges. Moreover, (Ti (iOPr)$_4$) is monomeric and the Ti atom exhibits a coordination number of

76

4 because of the steric hindrance of (OPr) groups. Consequently the metal atom is able to increase its coordination number upon complexation with acetates leading to six coordinate titanium species. The addition of acetic acid leads the reaction to be exothermic and this increase in Ti coordination leads to a decrease of the overall reactivity of the modified molecular precursor. This is the first step of the modification which involves the removal of isopropoxy group by the acetate group from acetic acid and forming a soluble species, metal alkoxo-acetate, having lower activity than the starting precursor.[194-196] According to Birnie *et al.*, isopropyl acetate ester forms in these mixtures and serves as an indicator of the extent of condensation between the titanium precursors.[197] It has been proven that up to two acetate groups will be accepted and the liberated isopropoxy group remain in the solution as isopropanol according to the *Fig. 3.14*. There are reports which show even with high concentrations of acetic acid, the IR signal of the Ti-bonded isopropoxy groups persists indicating that their complete replacement by acetates is never attained.[198] Livage and co-workers[199] and Sanchez and co-workers[200] also made analysis on this type of modification reactions by using ^{13}C NMR, XANES *etc.* From the study it was concluded that the chemical environments of carboxylic and methyl carbons in acetic acid (HOAc) are altered after the reaction with Ti (*i*OPr)$_4$ due to the bonding with titanium and that both terminal and bridging *i*-OPr groups are present.

The second stage of the process is the reaction between isopropoxy and acetate groups to form ester in the solution. In addition, there is a lesser possibility for the direct esterification (*Scheme 3.1*) between isopropanol and acetic acid and trans-esterification (*Scheme 3.2*).

*i*PrOH + HOAc → *i* PrOAc + H$_2$O (esterification) **Scheme 3.1**

$$Ti\!-\!OiPr + Ti\!-\!OAc \rightarrow i\,PrOAc + Ti\!-\!O\!-\!Ti \quad \text{(transesterification)}$$
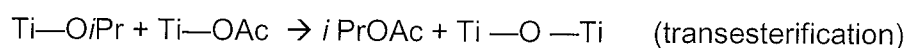
The water thus formed helps to hydrolyse the Ti bound isopropyl groups. But literature reports show that for the formation of anatase by this method of preparation, the release of water due to the esterification or trans-esterification is minimised.[198, 201] Hence, in the present case with the subsequent stages of the process, the isopropoxy groups may also be removed by alkoxolation. After the controlled addition of H_2O, loss of acetate group occurs which are replaced by hydroxyl groups which can condense by edge-sharing dimer between two octahedrons forming, Ti—O—Ti oxobridges. But this hydrolysis is preferential, whereas the bridging acetate ligands remain bonded to titanium throughout the condensation process. Condensation takes place through olation reactions (hydroxy bridge is formed between two metal centres) due to the higher lability of water with respect to -OH, -iOPr, and monodentate and/ or bidentate acetate ligands. The key advantage of the modification of $Ti(iOPr)_4$ with acetic acid is that it reduces the availability of groups that hydrolyze and condense easily through the formation of the $Ti(OCOCH_3)(iOPr)_2$ complex. Therefore, the use of acetic acid as modifier allows the control of both the degree of condensation and oligomerization and leads to the preferential crystallization of TiO_2 in the anatase phase. Without the controlled condensation reactions, an agglomerated amorphous mass of particles is immediately obtained after the addition of water. The condensed sol-gel on drying at 100 °C, leads in the loss of two equivalents of H_2O results in the formation of titanium dioxide powder. A possible mechanism of structural evolution of Ti—O—Ti anatase network during the acetic acid modification of TTIP reported by Parra *et al.*[198] is shown below.
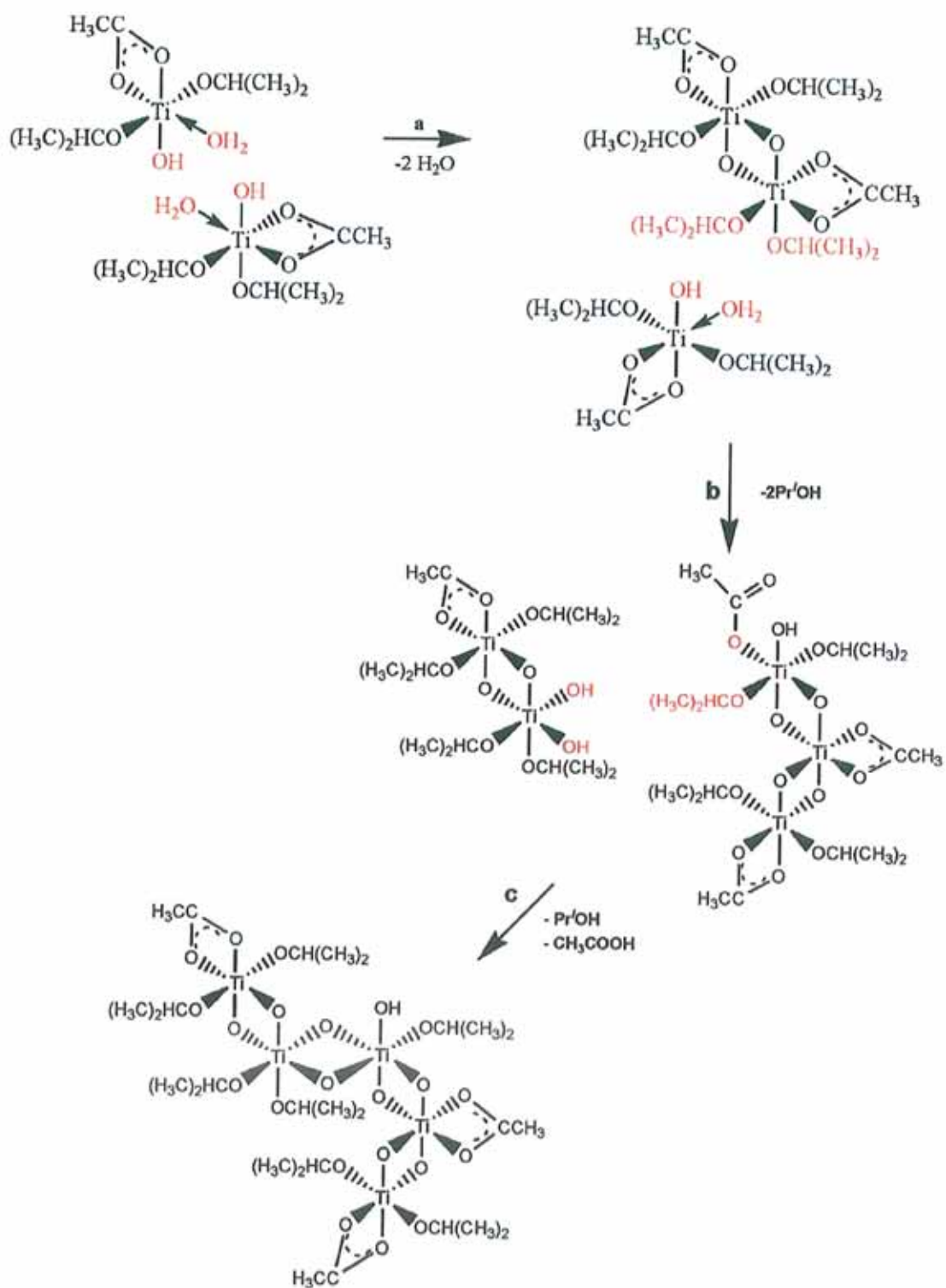
Figure 3.14: Schematic showing of the possible reaction pathway between acetic acid and TTIP.[198]

Controlling materials at the nano-level makes it possible to improve the properties and functionality for environmental applications. Common sol-gel methods employing direct addition of water molecules in a sol can lead to TiO_2 material with uncontrolled structure due to the rapid hydrolysis and condensation reactions between the highly reactive titania precursor and water. On the other hand, the acetic acid modified sol-gel synthetic route provide stability to the Ti-O-Ti network and hence the enhanced mechanical, thermal and catalytic properties. Acetic acid also serves as a chelating ligand to stabilize the hydrolysis-condensation process and minimize the agglomeration of titania particles.[202]

For inserting silver into the titania matrix, two methods were used and compared for introducing metallic silver into the TiO_2 material. The first was the *in-situ* reduction of $AgNO_3$ material to Ag^0 by irradiating the silver nitrate added titania sol samples with light for a fixed time. The second was to directly calcinate the silver added dried titania gel sample (*Scheme 3.3* below).

$$TTIP \xrightarrow[\text{AgNO}_3]{\text{HOAc + H}_2\text{O}} \begin{array}{c} TiO_2 \text{ precursor} \\ + \\ AgNO_3 \end{array}$$

light / calcination → "Pre-irradiated"

no light / calcination → "Not pre-irradiated"
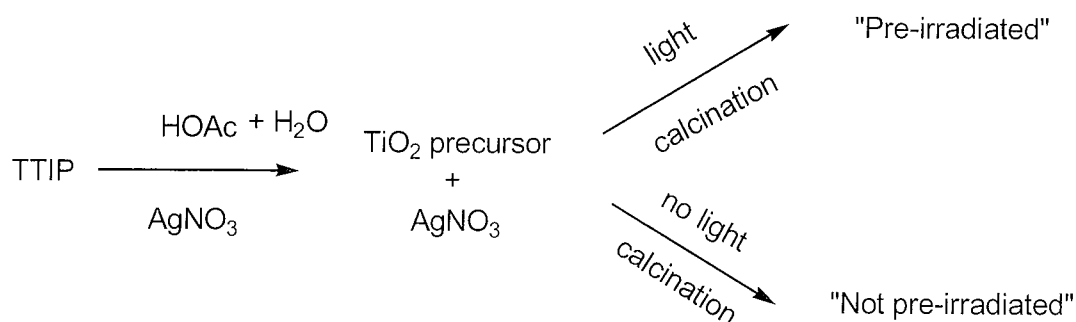
Scheme 3.3

According to the photocatalytic activity results the samples prepared by the direct calcination (not pre-irradiated) method shows a slightly better activity than the samples prepared through light reduction. In the second method, it was expected that direct calcination allows the thermal decomposition of the silver nitrate according to the *Scheme 3.4*:

$$AgNO_3 \rightarrow Ag_2O \rightarrow Ag \qquad \textbf{\textit{Scheme 3.4}}$$
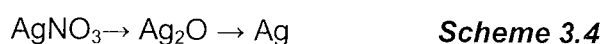
The radius of Ag^+ ions (126 pm) is much larger than that of Ti^{4+} (68 pm) and so the Ag^+ ions introduced by the sol–gel process would not enter into the lattice of anatase phase. During calcination, these uniformly dispersed Ag^+ ions would gradually migrate from the volume of the TiO_2 to the surface by enhancing their crystallinity, resulting in silver deposited on the surface on calcination.[203] It is known that silver particles deposited on the surface of the titania can act as electron–hole separation centres.[204] In addition, there may be residual Ag^+ ions within the material, acting as efficient electron traps may contribute to the enhanced photocatalytic activity of these samples over the pre-irradiated samples. This results in the formation of Schottky barrier at the $Ag–TiO_2$ contact region, which improves the photocatalytic activity.[205] For the pre-irradiated samples, it is proposed that the main reason for reduced efficiency as compared to directly calcinated samples is that in the case of titania, photoreduced Ag *cannot* be highly dispersed in the surface of TiO_2, so that the amount of active sites on the $Ag–TiO_2$ surface cannot significantly increase and thereby electronic structure of TiO_2 does not change significantly.[183] The levelling off in the photocatalytic activity on further increasing amount of silver is most likely due to the fact that as the concentration of silver becomes large, it results in one of a number of effects: (i) it acts as a barrier preventing light absorption by titania, (ii) it prevents the organic substrate

from contacting the titania surface and (iii) the silver may become a significant centre for electron–hole recombination.

3.3.2 Characterisation of the material

The preparation method used to synthesise titania and silver modified titania involves the use of acetic acid and titanium isopropoxide. This method has advantages over other methods in that the anatase to rutile transformation temperature is delayed until approximately 700 °C. It has been established that strong acids and high temperatures promote the protonation of Ti—O—Ti bridges and activate redissolution-precipitation reactions that ultimately lead to rutile. In contrast, in mildly acidic media and low temperatures, the solid precipitates into small particles that are almost insoluble in the liquid; therefore Ostwald ripening is negligible and anatase, the precipitated phase, is preserved.[206] After the optimisation about the silver insertion method, the samples selected for the present study and referred about are the direct calcinated samples. All the samples in the present study at 600 °C shows anatase phase. Other studies in this area have reported that the anatase to rutile transformation for silver modified titania can occur at lower temperatures with increment in doping level of silver.[183] As anatase is reported to be the more photoactive form of titania, this method allows us to prepare high temperature stable silver-modified anatase material.

The amorphous phase, which is detrimental to the photocatalytic activity, will be converted in to crystalline phase during heat treatment.[207, 208] Photocatalytic activity of amorphous titania is negligible[209] because of the reduced crystallinity and thereby reduced surface area compared to that of nanocrystalline anatase titania, which has a greater surface area than that of rutile. The larger surface area is a major factor in photocatalytic activity as it allows the increased adsorption of water, oxygen and

pollutants which will increase the rate of photocatalysis. The increased activity of anatase is believed to be due to the high crystallinity and higher surface area. There are theoretical aspects related to the band theory to account for this. Conduction band edges of anatase and rutile are nearly at the same level of electron energy, whereas the edges of valence band of anatase lays 0.14 - 0.21 eV lower than rutile (Fig. 3.15). Therefore the photo-reduction power of anatase and rutile are equal but the oxidation power of anatase is significantly higher than rutile. This makes anatase attractive for phototcatalytic oxidation reactions. Moreover, anatase exhibits a lower electron-hole recombination rate with respect to rutile. The higher energy position of the anatase conduction band could be the reason, because it increases the driving force for the electron transfer to surrounding oxygen.
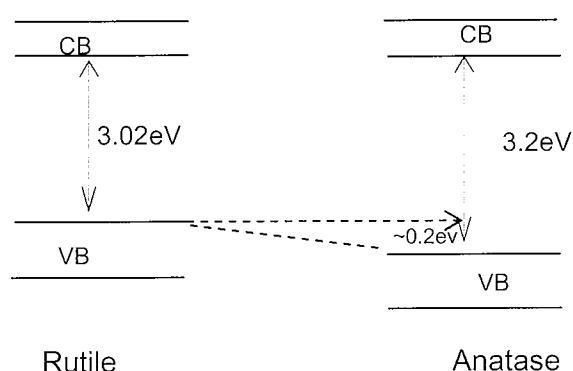
Figure 3.15: Schematic representation of band gap of anatase and rutile.

In addition, rutile usually showed agglomeration and larger particle size than those of anatase since rutile is normally prepared by calcination of anatase at high temperatures. Rutile is a thermodynamically stable phase and possesses a smaller band gap than that of anatase phase. Consequently, rutile titania possesses better

photo-absorption property in visible light, while it limits the activity by reduced surface area.

XRD analysis was also performed to determine the effect of silver addition in the phase transformation at higher temperature. When temperature goes higher – 700 °C –the anatase –rutile transformation intiates. Anatase to rutile transformation occurs by the diffusion of atoms mainly through the grain boundaries. The sol-gel method of preparation is reported to be efficient for the production of large amount of local defects, like grain boundaries owing to its capability to produce large amounts of hydroxyls. The hydroxyls will stabilize the Ti^{3+} ions which is responsible for the high activity of the material. The unmodified sol-gel titania contain 48.7 % rutile at 700 °C where as 5 mol% silver modified titania sample at 700 °C contains only 13.2% rutile. Furthermore, the 1% and 3% Ag modified titania still exist in the anatase phase at 700 °C. Hence with the suitable amount of silver, the anatase to rutile transformation is pushed to an even higher temperature. Due to the mismatch of the ionic radius of Ag^+ ions (126 pm) and that of Ti^{4+} (68 pm) there is a chance for the silver to go to the interstitials and anatase grain boundaries. This encourages the slow rate of grain growth at high temperature by increasing the diffusion barrier at the Ti—Ti grain contact which is needed for the grain growth and thus rutile formation. In the case of 1 and 3 mol% silver modified titania, anatase-rutile transformation is retarded at 700 °C because it is difficult to break the Ti-O bond which is necessary for the anatase – rutile transformation as this suitable amount of silver strengthens the Ti—O bond. Similar cases were reported where the anatase-rutile transformation of the system was studied with La and Ce as the modifier.[210]

This method provides for homogeneously distributed silver in samples calcined at 600 °C, as the presence of silver metal is only detectable in the 5% Ag TiO$_2$ sample calcined at 700 °C. The metallic silver will form at the temperature range of 200 - 400 °C. If it already contains the metallic silver, during further calcination - *i.e.* 600 °C – it will form clusters and allow the surface morphology of titania to change, which can be observed from SEM (*Fig. 3.4*). The texture and morphology of the silver layer deposited on the titania surface are very important parameters and might influence the photocatalytic activity. Moreover, presence of silver results in the increase of anion vacancies and defects at the surface which would promote the sintering of anatase grain as observed from the SEM images (*Fig. 3.4*). Also, the Ag–O bonding is much weaker than Ti–O bonding and Ag atom possesses higher surface free energy than the TiO$_2$.[187] Hence during calcination the Ag atoms have a tendency to aggregate into metallic Ag clusters. This is further examined by carrying out an experiment using 50:50 TiO$_2$: Ag mixture, calcined at 600 °C and it was found that there were no silver oxide peaks or any other phases such as silver titanate present. Instead peaks corresponding to metallic silver were obtained. The observation obtained from TEM images show good agreement with the XRD. As is clear from Table *3.1* which tabulates the results of crystallite sizes calculated from the powder X-ray analysis of the materials, all the silver modified titania material shows a decrease in the crystallite size which agrees with the results obtained from TEM analysis. The addition of an optimum amount of silver leads to the homogeneous distribution of the modifier and grain size to decrease.

The modification in the textural properties of titania using silver makes it absorb more visible light and thereby enhance the photocatalytic activity which is clear from the diffuse reflectance spectra of the powdered material and transmission spectra of the corresponding thin films. Because of the selected preparation method, the *in-situ*

formed and well dispersed silver nanoparticles were able to show the optical excitation of the plasmon, in fact a single silver nanoparticle interacts with light more efficiently than the particles of the same dimension composed of any known organic or inorganic polymers. This excitation of plasmon resonance leads to oscillating local electrons surrounding silver nanoparticles and thus extends to semiconductor interface in such a way to enhance its light absorption capability.

3.3.3 Mechanism of degradation

The photocatalytic degradation of R6G in presence silver modified titania takes place in a different manner. Analysis on the decolourisation of rhodamine dye show that 5 mol% silver modified titania among the silver modified material is more highly active than the unmodified titania. The 5 mol% silver modified TiO_2, which is the highly photocatalytically active one, at 600 °C shows no peaks of metallic silver as it is well dispersed throughout the material. Though there is no indication of metallic silver at 600 °C, these samples show good photocatalytic activity compared to the others. In the process of photocatalysis, the photogenerated electrons and holes are trapped on the surface and form paramagnetic species.[211, 212] The photocatalytic reactions arise from the reaction of these radicals with some reactant molecules on TiO_2 surface.[32] Silver plays an important role in the enhancement of photocatalysis. Even though the prepared photocatalyst contains silver in the metallic form, it can act as an electron sink. When the degradation mixture is irradiated with light, the electrons excited from the valence band of TiO_2, gets trapped by the silver leading the created hole to go for the degradation of rhodamine (Fig. 3.16). Electron transfer from conduction band of TiO_2 to the metallic silver particles at the solution interface is possible, because the Fermi level of TiO_2 is higher than that of silver metal.[213]
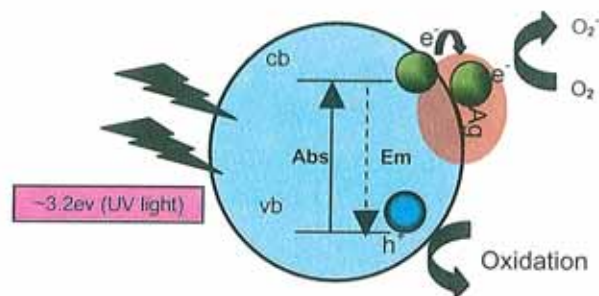
Figure 3.16: Schematic diagram of mechanism of degradation of rhodamine in presence of Ag modified TiO₂

When the number of silver clusters is small and the photogenerated electrons efficiently transfer to silver clusters, better separation of electrons and holes would be achieved with increase of silver loading up to the optimum content such as 1 and 3 mol %. These electrons could react with adsorbed molecular oxygen or surface Ti^{4+} to form reactive species $O_2^{\cdot-}$ and reactive centre surface Ti^{3+}, respectively, meanwhile the amount of recombination centres of inner Ti^{3+} decreased. In addition, the loaded silver particle can transfer one electron to adsorbed oxygen molecular to form $O_2^{\cdot-}$ or to the TiO_2 surface Ti^{4+} to form surface Ti^{3+}. This is assuming that the recombination was slowed down and the generation of $O_2^{\cdot-}$ and surface Ti^{3+} was accelerated. The yield of produced h^+ would also be increased.

It has been reported that the photodegradation of rhodamine results from both the de-ethylation and degradation of rhodamine chromophore.[214] De-ethylation occurs on the surface and rhodamine degradation is mainly a bulk solution process. According to Amal and co-workers[215, 216] the enhancing effect of silver deposits on TiO_2 mainly

87

depends on the molecular structure of substrate to be oxidised. The more C=O or C–O bond that a molecule possesses, the more probable the enhancement of degradation in presence of silver. In addition, de-ethylation (a surface bound process) is characterised by a blue shift in the absorption spectrum of rhodamine on degradation.[217] In these samples, the silver modified titania all show significant blue shifts, whereas the titania shows little or no shift. This leads to the conclusion that the silver samples achieve higher surface adsorption and hence result in better photodegradation. These materials are visible light active. There are two parallel mechanisms which may result in electron population of the conduction band of the material — (i) that the R6G absorbs visible light and injects an electron into the conduction band of the titania material and (ii) that the material itself absorbs visible light, probably facilitated by the surface plasmon absorption of the silver modified materials. It is probable that the two mechanisms are happening in parallel and there are debates on the suitability of coloured dyes such as methylene blue for photocatalytic studies.[218] However, as important as the materials ability to absorb visible light is its ability to retain charge separation and limit recombination. In comparing these materials, we are comparing not only visible light activation, but also efficiency of the materials to subsequently form hydroxyl radicals. Therefore, photosensitisation, if it is occurring, would enhance both titania samples and silver modified samples. The role of silver is to limit the recombination rate and subsequently allowing the holes for the oxidative degradation reaction to occur.

3.3.4 ATR-FTIR analysis on the surface adsorption of oxalic acid on anatase TiO$_2$

It has been pointed out previously that photocatalytic degradation reactions are sensitive to the existence of surface or dissolved complexes[219] and not only to the capacity of the oxide to generate holes and electrons.[220] Thus, the understanding of the structure and reactivity of these surface complexes will help to improve the applications of TiO$_2$ based catalysts. In the present study, oxalic acid was chosen as a model adsorbate to study these phenomena under UV(A) illumination, because it is the smallest di-carboxylic acid, it is an intermediate product in the degradation of more complex compounds. Thermal decomposition of solid or gaseous oxalic acid[221, 222] yields CO$_2$ and formic acid. Its solutions in organic solvents decompose thermally to CO$_2$ and formic acid being the latter about half dehydrated to CO when the acid is dissolved in water.[223, 224] This process is found to be complete in concentrated sulfuric acid.[225] Formic acid, CO$_2$, CO and H$_2$O were found in the photolysis of gaseous oxalic acid.[226] However, formic acid and CO was not detected in irradiated aqueous solutions of oxalic acid or photocatalytic degradation reactions in aqueous suspensions of TiO$_2$.[205, 227] There are many arguments about the intermediates formed on the TiO$_2$ – oxalic acid interface. The surface speciation of oxalic acid must consist of at least more than one adsorbed structure.

From the present study, spectra of adsorption of oxalic acid on anatase TiO$_2$ (*Fig. 3.10 a*) show four prominent peaks at 1697 cm^{-1}, 1635 cm^{-1}, 1420 cm^{-1}, and 1270 cm^{-1}. Bands in the region between 1800 and 1600 cm^{-1} can usually be assigned to carbonyl (C=O) stretching vibrations, and hence the lines at 1717 and 1697 cm^{-1} are assigned accordingly. Their splitting is interpreted by the coupling of two slightly different C=O groups. The peak at 1635 cm^{-1} can be attributed to the asymmetric stretching of the O–C=O bonds.[228] In the region between 1500 and 1200 cm^{-1}, two less intense bands are

observed around 1420 and 1270 cm⁻¹, with a shoulder at 1310 cm⁻¹ on the latter, that are ascribed to the symmetric stretching modes of C–O, C–C and O–C=O bonds in the first case, and the symmetric stretching modes of C–O bonds together with the bending mode of the O–C=O bonds in the latter. These results agree with spectra corresponding to the three surface complexes that have previously been identified for the adsorption of oxalic acid onto titania surfaces.[229, 230] The proposed structure of those surface adsorbed species and their calculated spectra by Mendive *et al.* is shown in *Fig. 3.17*
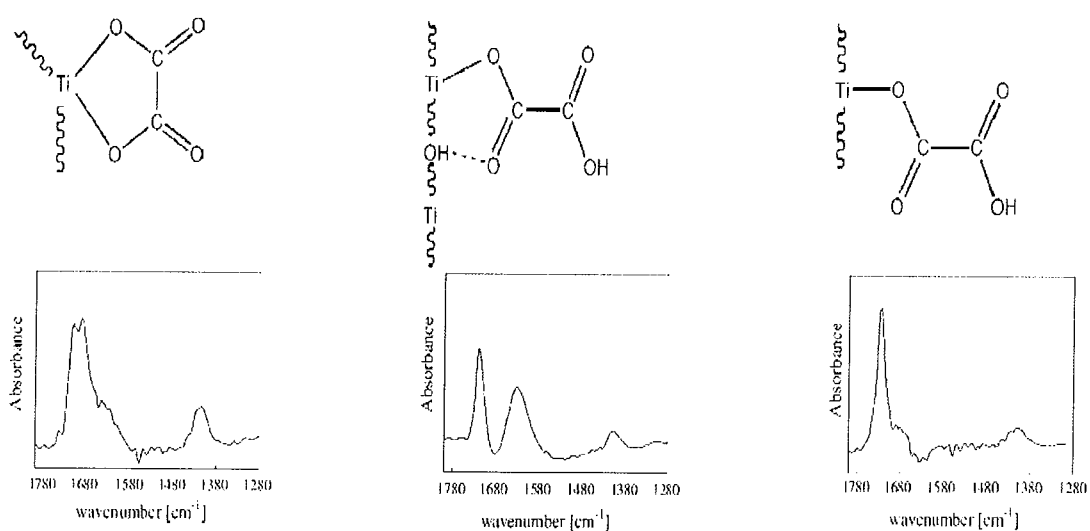
Figure 3.17: Possible structure of surface adsorbed oxalic acid species on TiO₂ and their calculated spectra by Mendive et al.

The carbonyl peaks in the region 1800-1600 cm⁻¹ remains the same while the molecular zone from 1500 to 1200 cm⁻¹, containing C–C, C–O stretching modes and bending modes of C–C–O, O–C=O and/or O–C–O shows a slight difference. The peaks corresponding to the oxalate species on anatase TiO₂ obtained in this study

shows similarity to those of other studies performed under similar conditions,[229-231] and there is general agreement that oxalate forms strong surface complexes, with a major fraction of 5-ring bidentate chelating and/or 6-ring bidentate bridging structures. Due to the lack of other experimental evidence, only thing we could assume is our similarity in spectra with those of Mendive *et al.*

In the spectra *Fig. 3.10 (b)*, it shows only the presence of well defined peaks at 1635, 1690, and 1717 cm^{-1}. All other peaks which present in the dark conditions disappeared. A reduction of the concentration of adsorbed oxalate molecules is therefore expected if oxalate is photocatalytically degraded under UV(A) illumination. Thus, under light illumination, a decrease in intensity of the FTIR bands corresponding to the oxalic acid adsorbed at the surface of the photocatalyst shows the photocatalytic degradation. Similar results has been previously reported[232] assuming the surface adsorbed or dissolved oxalic acid on TiO_2 undergo photocatalytic degradation with a zero order kinetic rate which is shown in *Scheme 3.5*
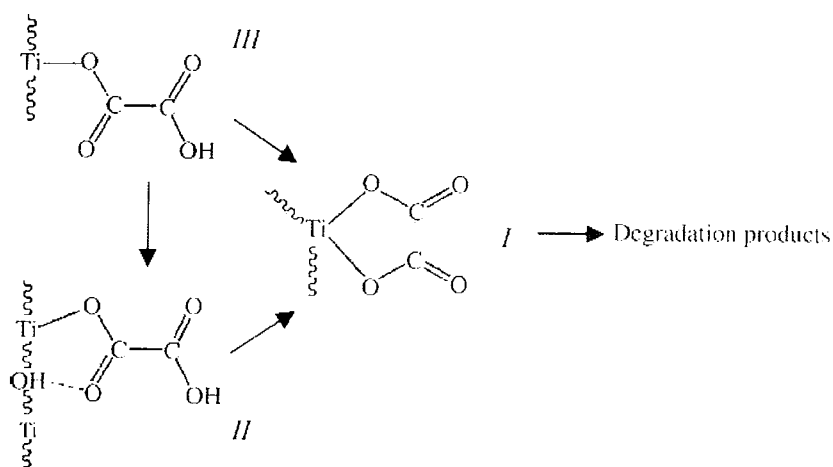
Scheme 3.5: Photocatalytic degradation of oxalic acid on TiO_2 through various surface adsorbed species.

If the photocatalytic degradation of oxalic acid on the surface of anatase TiO_2 happens, it can be through the formation of many intermediates. Though we couldn't measure other essential parameters for the assumption of those intermediates, from the similarity in spectra obtained by Mendive *et al.*[165] by using the similar laboratory experimental conditions, the possible intermediates formed as result of adsorption of oxalic acid can be supposed as a structure stated in reference 158. Using quantum chemical calculations they have assumed different species (a) and (b) formed as a result of surface adsorbed degradation of oxalic acid which is shown in *Fig. 3.18*. From the spectral analysis it could be seen that the IR band properties shows some similarity to the spectra corresponding to the species (a). This is only an assumption in light of the previous report as the experimental information obtained is insufficient to derive with precise surface species.
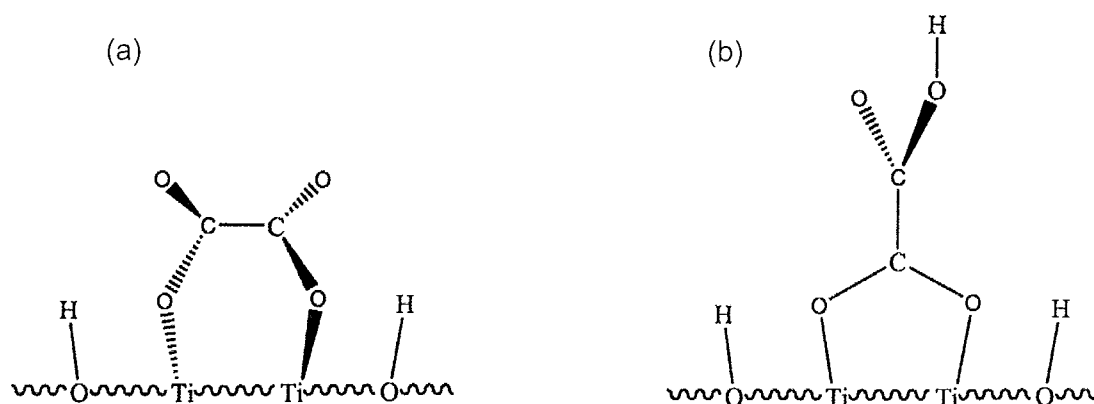
Figure 3.18: Possible structural intermediates during the adsorption of oxalic acid (Postulated pictures taken from Mendive[165]).

As described in *Section 3.2.7*, spectra of adsorption of oxalic acid on silver modified anatase TiO_2 shows similar bands as in the pure anatase. Nevertheless, a shift was observed in the band position of the prominent peaks such as 1709, 1673 and 1627 cm^{-1} and a slight in increase in the intensity of peak at 1420 cm^{-1}. These minor spectral shifts in the frequencies of the bands are expected to be due to slight changes in the bulk or surface properties of the system under steady state light illumination. It has been previously shown that change in binding modes can also cause the changes in the shifts in spectral evolution. Indeed, the silver modification caused the TiO_2 to change its surface properties as it is clear from the characterisation of the material. Additionally, literature shows that silver modification on the TiO_2 surface lead the material to increase surface area and thereby the surface adsorption sites which enable the improved adsorption of both light and adsorbent. Even if we can expect the same mode of binding of oxalic acid on TiO_2 and silver modified TiO_2, the surface intermediates formed during the light irradiation cannot be the same as the photocatalytic degradation on silver modified TiO_2 proceeds via different mechanism. As mentioned before, all these studies lack the direct information on the surface reactions. Thus, oxidation of oxalic acid is still a matter of discussion. In particular, its photocatalytic degradation mechanism is still not completely understood.

3.3.5 Photocatalysis of N-doped titania (Collaborative work noted here as an aside)

As a part of collaboration, analysis on photocatalytic activity of some unmodified and urea modified titania samples which are prepared by CREST were carried out.[†] The

[†] Centre for Research in Engineering and Surface Technology, FOCAS Institute, DIT.

samples which consisted of unmodified and urea added titania samples calcined at various temperatures (500 °C - 900 °C) where as the TTIP:urea are in 1:0.25 and 1:0.5 ratios.

The photocatalytic tests were undertaken as in the previous studies. According to the analysis, the urea modified sample (1:1 TTIP:urea) shows more than three times the activity of the unmodified titania. The full decolourization of R6G occurred within 50 min in the case of 1:1 TTIP:urea sample calcined at 900 °C whereas the standard sample takes more than 120 min to complete the degradation process. This enhanced efficiency is reflected in the kinetic analysis of the results. The degradation process, involving hydroxyl radical formation and subsequent degradation of the dye by the hydroxyl radical, obeys pseudo-first-order kinetics. First-order degradation rate constants, obtained by plotting the natural logarithm of the absorbance against irradiation time, are 0.027 min^{-1} for the standard sample and 0.073 min^{-1} for the urea-modified sample. A similar trend is observed with the urea-modified sample calcined at 800 °C, which has more than three times the degradation rate of the standard. An initial lag is also observed with this sample. This lag time was about 10 min for both samples and may be due to a slower adsorption of the dye onto the urea-modified sample. Dark studies, where the above experiments were repeated in the absence of a light source, were studied to eliminate any adsorption effects on the studies. A sample left for up to 24 h showed little change in absorbance. The kinetic plots and the progress of the reactions are shown in *Fig. 3.19.* The calcination temperature of the sample affects the catalytic efficiency. Both standard and urea-modified samples were calcined at 500, 600, 700, 800, and 900 °C. For the standard samples, the most efficient photocatalyst was found to be the sample calcined at 600 °C, whereas for the urea-modified sample the most efficient temperature was found to be 800 °C.
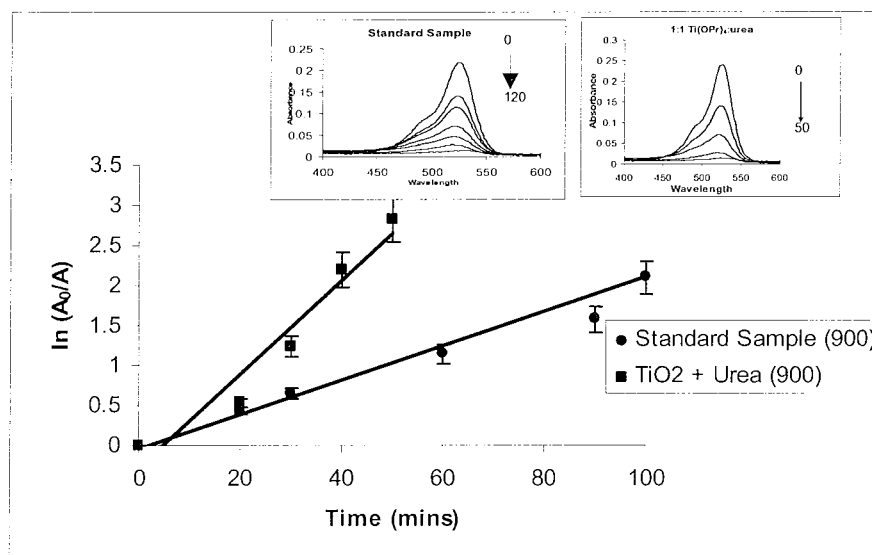
Figure 3.19: Kinetic study of standard sample and 1:1 TTIP:urea calcined sample at 900

°C. (Error bars 10%.) The best fit for the urea-modified sample is shown excluding the lag

time. Inset: Absorption spectra of rhodamine dye degradation, using standard sample

(left inset) and sample with 1:1 TTIP:urea (right inset).

Our contribution to this work is to analyse the photocatalytic activity of all the above prepared pure and urea modified samples. From the analysis, it was found that, the urea modified TiO_2 samples at high temperatures such as 800 and 900 °C shows higher photocatalytic activity than the pure TiO_2 prepared under similar conditions. It is evident from their characterisation of material that even at 800 °C the urea modified samples retains anatase phase stability up to 97% and the highly active material, 1:1 urea modified TiO_2 at 900 °C, possesses 11 % anatase phase. As already discussed, the structure of the resulting TiO_2 depends on the condensation pathway during the formation. Urea molecules chelated to the Ti ions have amino groups with a high electronegativity which retard the condensation reactions of titanium isopropoxide by

altering the reaction pathway[233] resulting in the formation of anatase having a strong network. Therefore the reason for the high photocatalytic activity of the urea modified samples at high temperature is attributed to its anatase phase stability. The more detailed discussion about the urea modification can be seen in Pillai *et al.*[182]

3.4 Conclusion

Various concentration of silver modified anatase TiO_2 have been synthesised through an acetic acid modified sol-gel route, characterised and the photocatalytic activity of the materials using various instrumental techniques analysed. Synthetic methods where the silver nitrate was not reduced by light before calcination resulted in a slightly more efficient photocatalysis over the samples prepared by light irradiation. Silver modification retains the anatase phase stability up to 700 °C. The optimum amount of silver giving the photocatalytic activity was confirmed as 5 mol% both in UV and sunlight and they show enhanced adsorption capability too. Adsorption experiments on TiO_2 using oxalic acid illustrate that oxalic acid form strong ring complexes on the surface of TiO_2 which undergo further degradation. Photcatalytic activity tests of various % of urea modified TiO_2 indicates urea modification can extend the anatase phase stability for higher temperatures and 1:1 TTIP:Urea modified sample at 900 °C shows high photocatalytic activity among other samples.

4. SILVER MODIFIED ZNO PHOTOCATALYSTS

4.1 INTRODUCTION

As we have seen from previous chapters, metal oxide mediated photocatalysis is a successful alternative to conventional methods for the removal of organic pollutants from water. Until now, many different semiconductors have been studied as photocatalysts including TiO_2, ZnO, CdS, WO_3 among others.[15, 148, 234-237] While TiO_2 is widely employed as a photocatalyst for its high efficiency, photochemical stability, non-toxic nature and low cost, ZnO is a suitable alternative to TiO_2 as it has a similar band gap energy (3.2 eV)[238] and larger quantum efficiency than TiO_2. The photocatalytic activity of ZnO has been widely explored and higher photocatalytic efficiencies for the degradation of various dyes have been reported.[131, 239-241] In terms of studying the mechanism of photocatalysis, ZnO offers some advantages over TiO_2, not least because ZnO is quite strongly luminescent. This facilitates a study of the recombination of electron-hole pairs and hence a suitable probe in the mechanistic study of highly active photocatalysts. As stated before in *Chapter 1*, the emission properties have also been used to sense the presence of organic molecules in its immediate vicinity.[133]

The modification of semiconductors with noble metals has attracted significant attention especially in heterogeneous photocatalysis.[179, 242] Incorporating silver into ZnO is an exciting area in research for developing electronic applications. In addition, silver modification is found to be effective for the fabrication of p-type conductive ZnO,[243] as the naturally occurring ZnO displays n-type conductivity due to its native defects such as zinc interstitials and oxygen vacancies. The modification with silver has influenced the photocatalytic activity of nanocrystalline photocatalysts because of its optical and electronic properties.[178, 180, 244] As mentioned in the third chapter, we found a significant enhancement in photocatalytic activity of TiO_2 by modification with silver.[158] Recently,

Kamat and co-workers have studied the interfacial electron transfer process in silver modified TiO_2.[245] Extensive research is underway to depict the exact role of silver in increasing the visible light response of metal oxides. Silver can trap the photogenerated electrons from a semiconductor and allow the holes to form hydroxyl radicals which results in the degradation reaction of organic species present. Moreover, silver can enhance the photocatalytic activity by creating a local electric field and the optical vibration of surface plasmon in silver can make a reasonable enhancement in this electric field. The increased photocatalytic activity of silver modified ZnO is reportedly due to the change in the surface properties such as oxygen vacancies and crystal defects.[246]

In the case of ZnO, there have been many studies on the effect of silver addition on the electric and optical properties of ZnO for electronic applications.[247] According to the literature, there is only a limited number of studies on silver modified ZnO as a photocatalyst for the degradation of organic contaminants. To the best of our knowledge there are no detailed studies on the effect of silver modification in ZnO based on various calcination temperatures.[134] This chapter describes a systematic study on the effect of silver modification in ZnO and consequent photocatalytic activity. The methodology of synthesis of materials reported here is through a straight-forward non-aqueous route. The enhancement in photocatalytic activity due to the presence of silver is studied by characterisation of the materials and optimisation of the reaction conditions. A possible mechanism of photocatalysis has also been presented by analysing the effect of various amounts of silver in the emission properties of both ZnO and rhodamine 6G dye. The chemical structure of rhodamine 6G is given in *Fig. 4.1*.
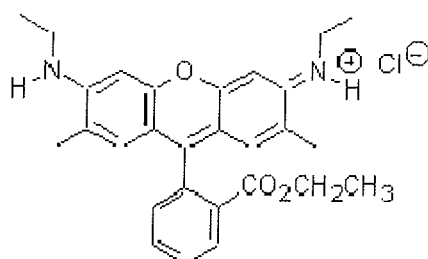
Figure 4.1: Structure of rhodamine 6G

4.2   Results

4.2.1   Characterisation of Materials

The powder X-ray diffraction patterns of unmodified and various mol% of silver modified ZnO samples calcined at 300 and 400 °C are shown in *Fig. 4.2*. The XRD pattern of 300 °C calcined samples show peaks corresponding to zinc oxalate dihydrate which were formed during the initial stage of the combination reaction between zinc acetate and oxalic acid. This agrees with the report by Yang *et al.*[248] and Pillai *et al.*[129] where they have reported the formation of zinc oxalate dihydrate at low temperature before the formation of ZnO. The Ag modified ZnO samples show peaks corresponding to Ag_2O in addition to anhydrous zinc oxalate precursors. Conversely, the spectra of 400 °C samples show typical peak patterns of ZnO wurtzite structure (JCPDS, 36-1451) and the characteristic peaks of metallic silver at 38.2.[129] No traces of impurity peeks were observed. These results confirmed the formation of single phase hexagonal ZnO and the metallic silver. During the heat treatment, the thermal decomposition of the zinc oxalate precursor resulting in the formation of ZnO where as the silver oxides also undergoes thermal decomposition to form metallic silver at 400 °C.

100
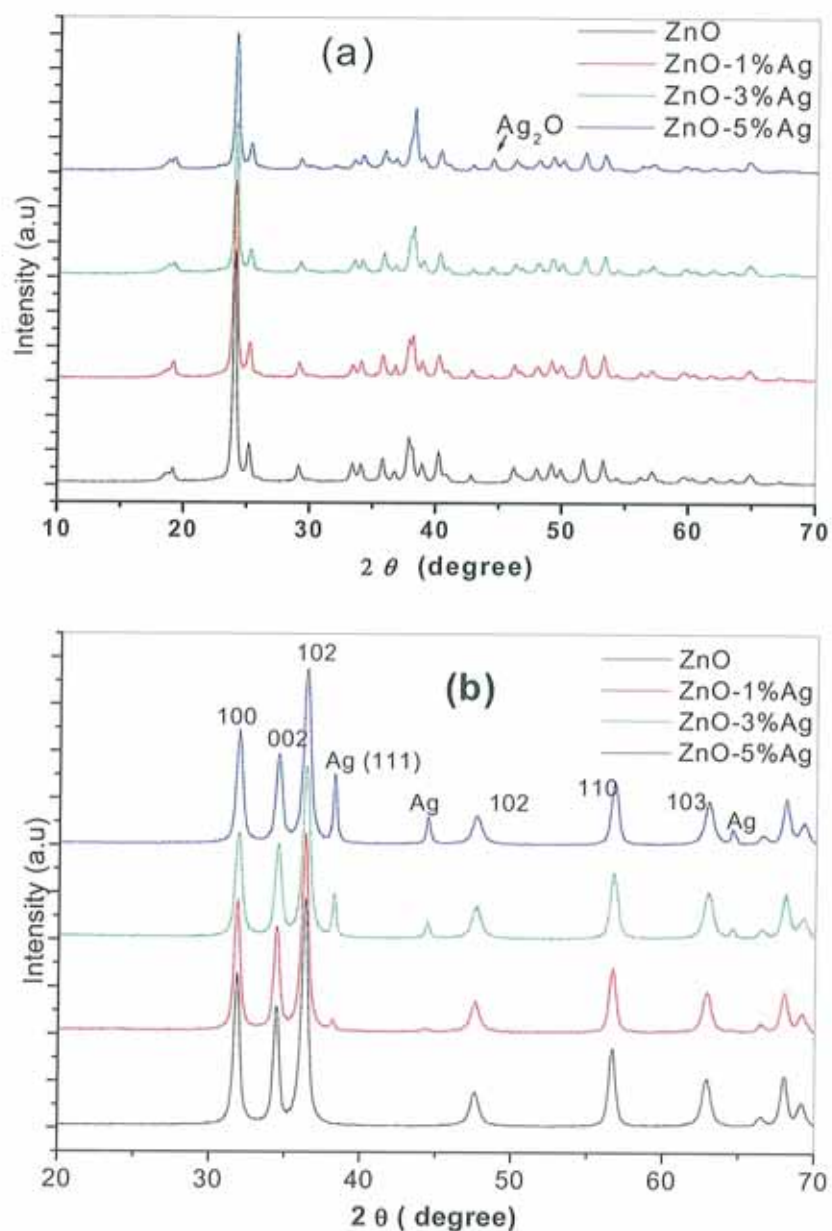
Figure 4.2: Powder XRD patterns of ZnO and various mol % of Ag modified ZnO samples calcined at (a) 300 ℃ and (b) 400 ℃.

Furthermore, a consistent increase in the intensity of silver peaks can be noted with the increase in concentration of Ag from 1 to 5 mol%. It should be noted that the formation of metallic silver and the crystalline phase of ZnO is starting at above 300 ℃. This is consistent with the thermal decomposition behaviour of zinc acetate

precursors[249] and Ag$_2$O systems.[250] The result also corresponds with a recent observation by Ahn *et al* who studied the thermal decomposition of Ag$_2$O in ZnO system.[251] Therefore, we believe that in the present ZnO system, Ag$_2$O is the stable phase at 300 °C and as the temperature increases to 400 °C, Ag$_2$O decomposes to metallic silver. According to some previous reports, Ag can be incorporated in ZnO system either as a substitute for Zn^{2+} or as an interstitial atom.[252, 253] If the silver is substituted for Zn^{2+}, a corresponding peak shift can be observed in the XRD. No such shift in the peak positions was observed in any of our modified samples. This indicates the segregation of Ag particles in the grain boundaries of ZnO crystallites rather than going into the lattice of ZnO, or only an insignificant quantity may be going to the substitutional Zn site.

The crystallite sizes of unmodified ZnO and various mol% of Ag modified ZnO samples calcined at different temperatures were calculated from the X-ray line broadening using the Scherrer equation (see *Appendix 1*). It was observed that the addition of silver causes a slight reduction in crystallite size. In general, the crystallite size of all the samples increases with increasing calcination temperature (*Fig. 4.3*), whereas silver facilitates the densification of particles at high temperatures.
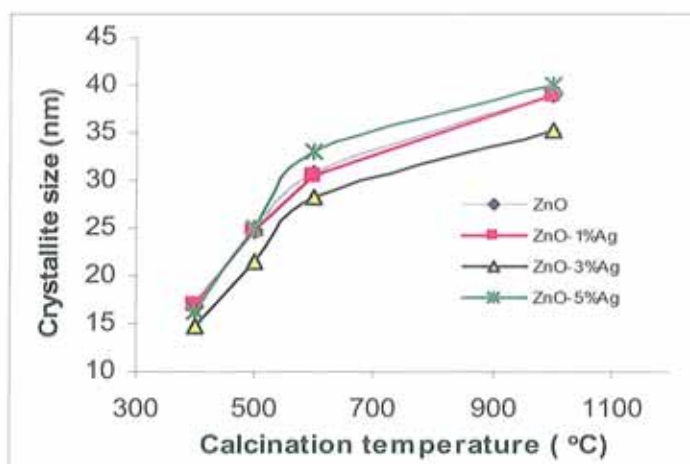
Figure 4.3: Plot of crystallite size Vs calcination temperature.

102

The surface morphology of the prepared ZnO and any changes in the surface morphology of ZnO as a result of the addition of silver were studied by analysing the scanning electron microscopy of the materials calcined at 400 °C (*Fig. 4.4*). The crystallite size analysis results shows agreement with SEM images and it is clear that unmodified ZnO shows long grains composed of nearly spherical particles though the particle distribution is not the same. Similar structural morphologies has also been previously reported.[254] However, the silver modified ZnO shows some changes in the surface morphology of the material, especially the particle size became small and the orientation growth towards the rod formation is inhibited. Moreover, the particle distribution is same which contribute to high exposed surface area for the catalyst.
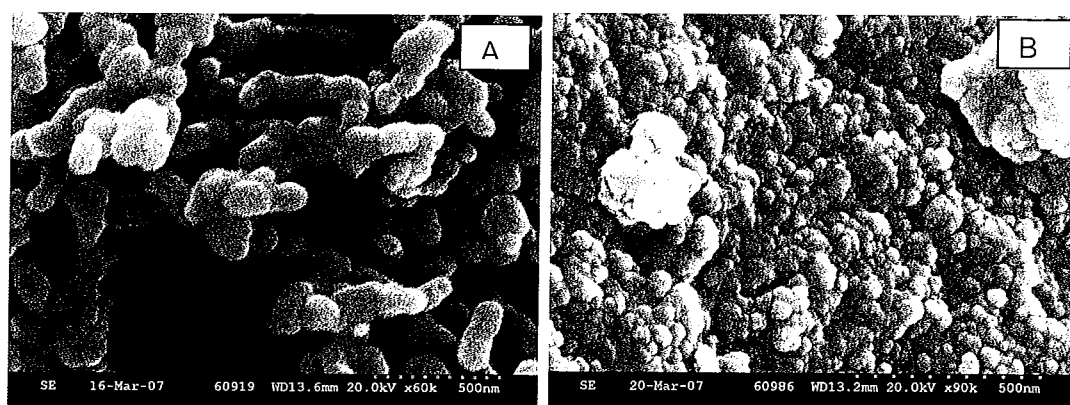
Figure 4.4: SEM images of (A) unmodified ZnO (B) 3 mol% silver modified ZnO calcined at 400 °C

In order to understand the thermal events in the samples, differential scanning calorimetry (DSC) was performed. The DSC curves of ZnO and Ag modified ZnO (AZ) samples are shown in *Fig. 4.5*. The unmodified ZnO shows three endothermic peaks starting at 68, 104 and 405 °C. On the other hand, 3 mol% Ag modified ZnO shows two endothermic peaks at 68, 112 °C and two exothermic peaks at 183 and 395 °C

103

respectively. The endothermic peak at 68 °C corresponds to the elimination of ethanol and the one at 104 °C may be attributed to the removal of structural water. The endothermic peak at 405 °C represents the removal of oxalate species.[255]

In comparison, the exothermic peak observed at 184 °C for the Ag modified ZnO is assumed to be the formation of Ag_2O where as Ag^+ is stable in the form of AgO_x or Ag_2O at these temperatures.[256] An intense exothermic peak at 390 °C shows the thermal decomposition of Ag_2O to metallic silver, which is in the same temperature region where an endothermic peak is observed for unmodified ZnO; the latter representing the formation of ZnO at this temperature. This is in good agreement with XRD results and is consistent with a previous report.[251] The exothermic formation of metallic silver is more highly energetically favourable than the endothermic evolution of ZnO. In other words, the highly exothermic nature of metal formation predominates in DSC compared to endothermic ZnO formation. In addition, an increase in silver concentration shows an increase in this peak intensity, which confirms this assumption.
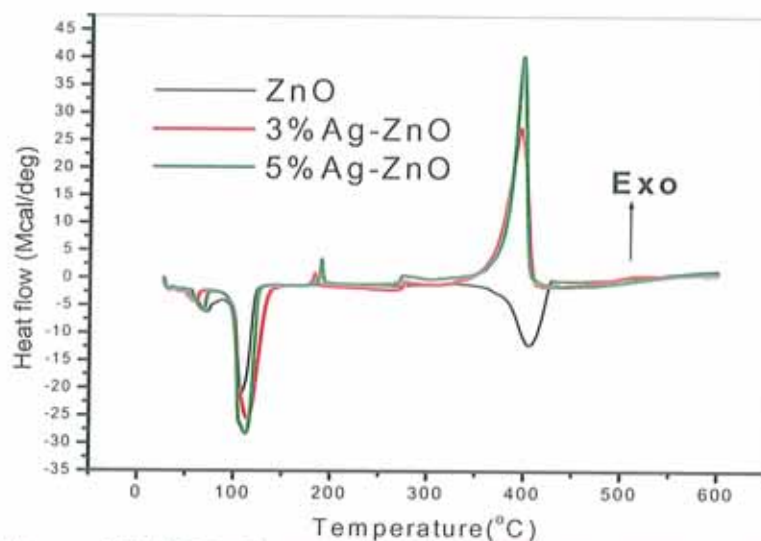
Figure 4.5: DSC of unmodified ZnO and Ag modified ZnO samples

The formation of nanocrystalline ZnO wurtzite structure and the effect of silver addition in ZnO were further confirmed by FT-IR spectral analysis, which is shown in *Fig. 4.6*. The spectrum of prepared ZnO prior to calcination shows an absorption peak at ~3400 cm^{-1} which corresponds to the O–H stretching of surface adsorbed water molecule. The band at ~2900 cm^{-1} shows the presence of C–H species. The three bands occurring in the region of 1000 – 500 cm^{-1} and the one at 1380 cm^{-1} correspond to the different modes of CO_3^{2-}.
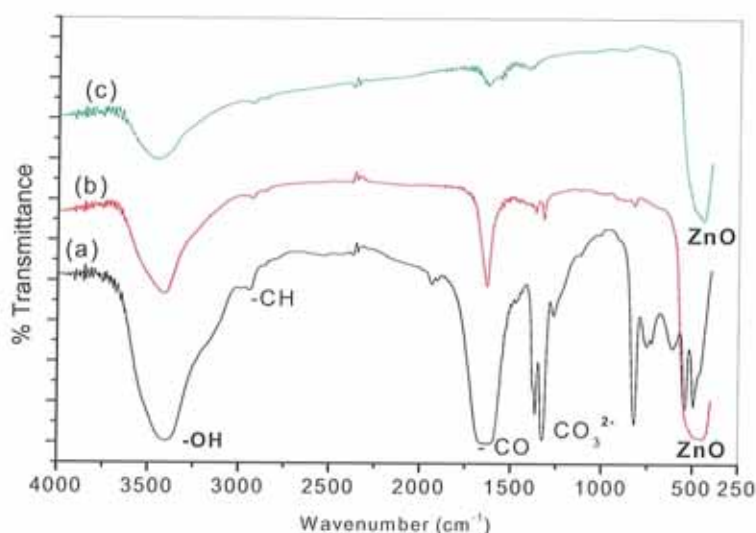
Figure 4.6: FTIR spectra of ZnO (a) as prepared at 80 °C, (b) calcined at 400 °C and (c) 3 mol% Ag modified ZnO calcined at 400 °C.

Furthermore, the symmetric and asymmetric stretching bands of acetate species can be observed at 1360 and 1600 cm^{-1}. All of these indicate that the zinc acetate precursors are present. However, in the case of ZnO at 400 °C, the peaks corresponding to the organic precursor are no longer present and the spectrum shows only the peak of nanosized ZnO at ~490 cm^{-1}. The silver modified ZnO at 400 °C as

well as the IR spectra at 300 °C, however, (see *Appendix 2*) show no bands for silver, only that of ZnO, indicating there is no chemical bonding between silver and ZnO.

In order to assess the amount of defects, Raman analysis has been carried out on the samples. Raman spectra of ZnO and silver modified ZnO at 400 °C are shown in *Fig. 4.7*. ZnO had the wurtzite structure with the C_{6v} point group symmetry. According to group theory, there were the Raman active optical modes E_2(low), E_2(high), A_1(LO), A_1(TO), E_1(LO) and E_1(TO).[257, 258] Only the two B_1 modes were not Raman active. If the incident light was exactly normal to the surface, only the E_2 modes and the A_1(LO) mode were observed, and the other modes were forbidden according to the Raman selection rules. The E_2 mode was related to a band characteristic of the wurtzite phase and in the present case the most intense peak at 436 cm^{-1} corresponds to E_2 mode of ZnO hexagonal wurtzite structure. The peak at 326 cm^{-1} should be assigned as the second order Raman spectrum arising from the zone boundary phonons $3E_{2H}$ -E_{2L}, while a smaller shoulder at 574 cm^{-1} is the contribution from E_1(LO) mode associated with oxygen deficiency.[259] A stronger E_2 mode and much lower E_1 mode indicate its good crystal quality, with only a very low oxygen vacancy. On the other hand, in addition to the ZnO peaks, the silver modified ZnO shows a weak peak at 560 cm^{-1} followed by the peak corresponding to oxygen deficiency.[250]
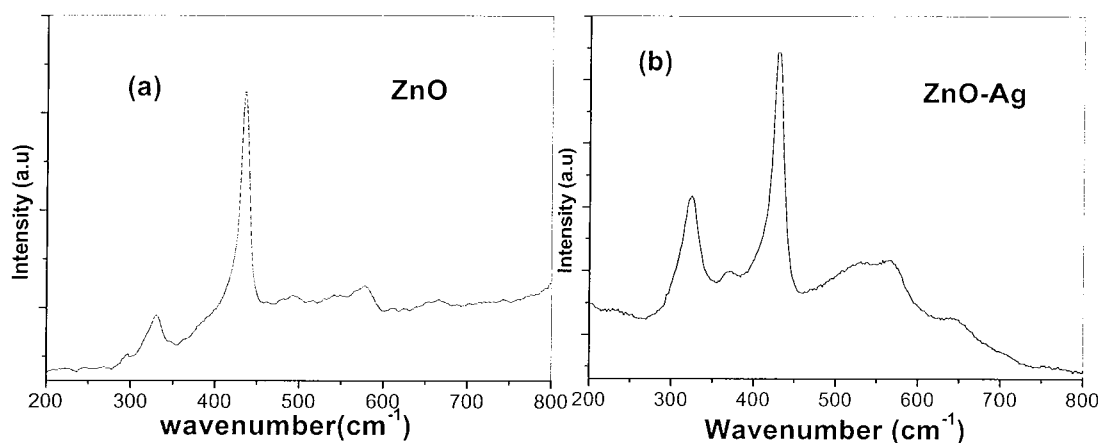
Figure 4.7: Raman spectra of ZnO and silver modified ZnO at 400 °C.

The absorption spectra of unmodified and silver modified ZnO are presented in *Fig. 4.8* and it can be seen that the silver addition does not make any significant reduction in its band gap and the highly silver modified ZnO samples extends its absorption towards the visible region, which might be due to light absorption capability of loaded silver. Also it is well demonstrated the absorption capability of the material increases as the amount of silver increases.
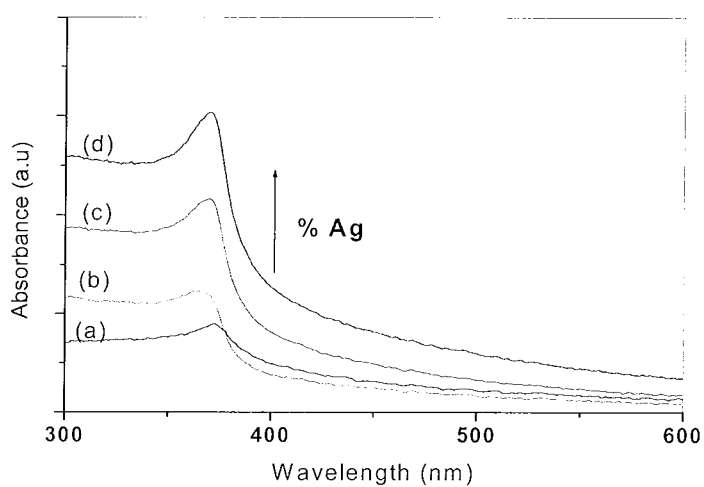
Figure 4.8: UV-visible absorption spectra of ZnO (a) and (1-5) mol% silver modified ZnO at 400 °C

4.2.2 Photocatalytic Activity

An important aim of the study involves the examination of photocatalytic activity of ZnO and various mol% of silver modified ZnO at different temperatures. The use of an aromatic compound rhodamine 6G (R6G) as a model dye for the photocatalysis study is mainly due to their recurrent occurrence in the industrial field.[260, 261] The photocatalytic activity of unmodified and various mol% of silver modified ZnO powders at temperatures ranging from 300 – 1000 °C have been studied by analysing the degradation of the dye. The absorption spectra of R6G after undergoing photocatalytic degradation by unmodified and 3 mol% silver modified ZnO at 400 °C are shown in *Fig. 4.9*. The degradation is monitored by studying the decrease in absorbance of R6G in presence of powdered sample suspensions, and quantified by plotting a first order decay plot of the absorbance at 525 nm.
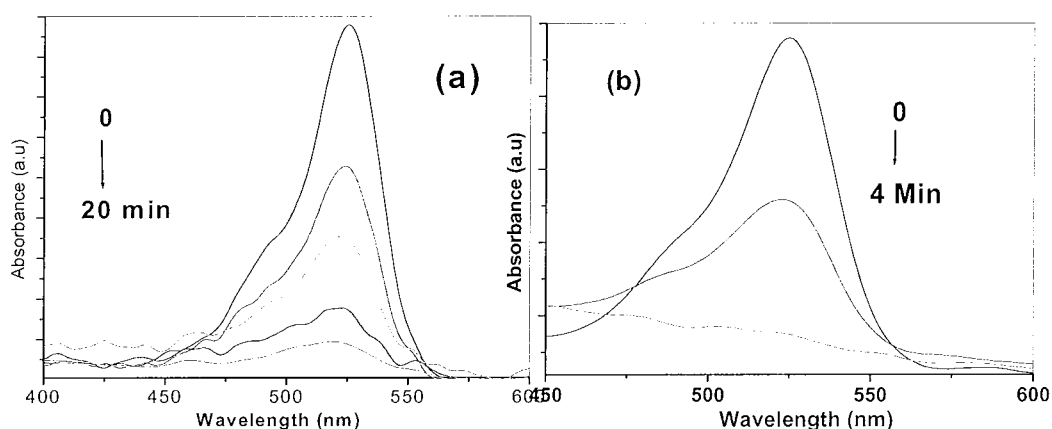
Figure 4.9: UV-visible absorption spectra of degradation of R6G by (a) ZnO and (b) 3 mol% silver modified ZnO at 400 °C

In the case of metal modification in nanoparticles, a particular concentration of metal modifier can tune the photophysical properties. From the study, it can be seen that the addition of silver enhances the photocatalytic degradation of the dye

up to 3 mol%, but above this concentration, a decrease in the rate of activity is observed. The higher percentage of silver could be unfavourable to photocatalytic efficiency. It is assumed that amount of silver below its optimum, can act as electron-hole separation centres.[262] When the Ag loading above its optimum, it can also act as charge carrier recombination centres. This is because the possibility of hole capture increases by large number of negatively charged Ag particle on ZnO which reduces the efficiency of charge separation when the silver content is above its optimum.[213] Moreover, the highly loaded silver will cover the available exposed surface of ZnO from reacting with the adsorbed substrate which contribute to reduce the photcatalytic efficiency.

Hence, in the present system, the optimum amount of silver giving the highest photocatalytic activity (*Fig. 4.10*) is determined to be 3 mol% whose rate of degradation is four times greater (0.42 min^{-1}, degrade the dye within 4 – 6 min) compared to the rate with pure ZnO (0.10 min^{-1}, degrade the dye within 20 – 25 min). A schematic representation of photocatalytic degradation of rhodamine is shown in *Fig. 4.11*. The samples at 400 °C show a better photocatalytic activity than the samples at higher temperatures, which may be attributed to the smaller crystallite size and a reasonably good surface area (*Appendix 1*). The surface area analysis (BET) of ZnO (32.05 m^2/g) and 3% silver modified ZnO (173.21 m^2/g) at this temperature shows good agreement with this activity. It should be noted that the Ag modified samples (3 & 5 mol%) showed almost similar rate of photocatalytic activity at higher temperatures such as 400 – 600 °C and hence 3 mol% silver is found to be as the optimum concentration.
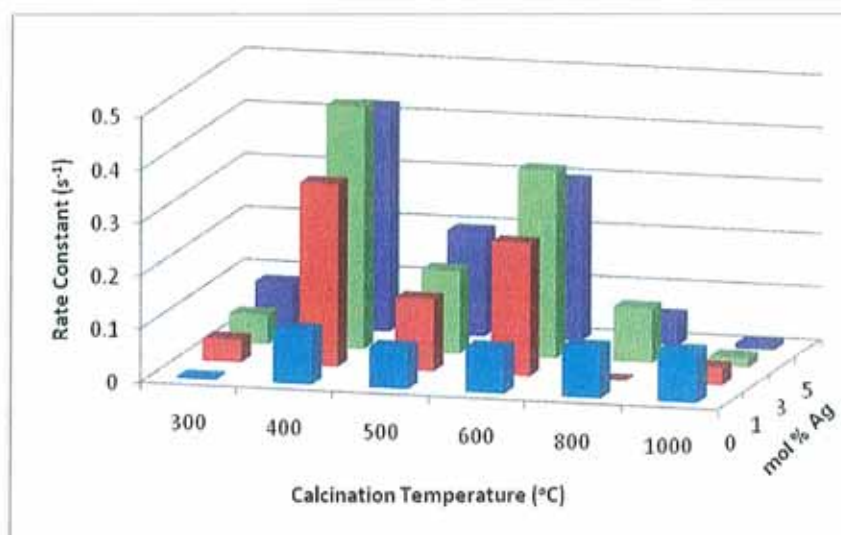
Figure 4.10: Plot of concentration of silver vs. rate constants (±10%) of degradation reaction obtained from kinetic analysis.

Nevertheless, at higher temperatures, it is found that there is no positive effect of silver addition on the photocatalytic activity (800 – 1000 °C) (*Appendix 3*). On the other hand, the silver modification is photocatalytically effective only at low temperatures. This is because the presence of silver promotes the densification and grain growth of ZnO at high temperatures[263] by forming silver island in the ZnO matrix, which causes the reduction in active surface sites of the photocatalyst for the adsorption of degradants and for the absorption of light. This conclusion has been further confirmed by BET analysis of high temperature calcined sample which shows a lesser surface area and pore volume for silver modified ZnO (2.65 m^2/g, 0.005 cc/g) than the pure ZnO (4.34 m^2/g, 0.012 cc/g) (values for 800 °C sample). The crystallite size of 3 mol% Ag modified sample showed the smallest size values among the samples and had good photocatalytic activity. 3 mol% may therefore be assumed as the optimum concentration of Ag particles for the present ZnO system.

This is similar to previous findings for silver loading in titania materials[158] and to other work involving cobalt on conbalt oxide/titania systems.[264]

Although there is no formation of ZnO at 300 °C, the silver modification causes the zinc oxalate precursor at 300 °C to show improved photocatalytic activity. This may be due to the fact that Ag_2O is present in the system, which is also a metal oxide, and can produce holes on light illumination resulting in hydroxyl radicals which subsequently degrade the dye.[265]

The visible light activity of ZnO and highly active 3 mol% silver modified ZnO materials has also been analysed in presence of Dublin sunlight and it is found that silver modified ZnO shows 5 times higher rate of degradation of the dye than the pure ZnO (*Appendix 4*) which is an indication that these silver modified materials could be utilised for sunlight driven photocatalytic processes.
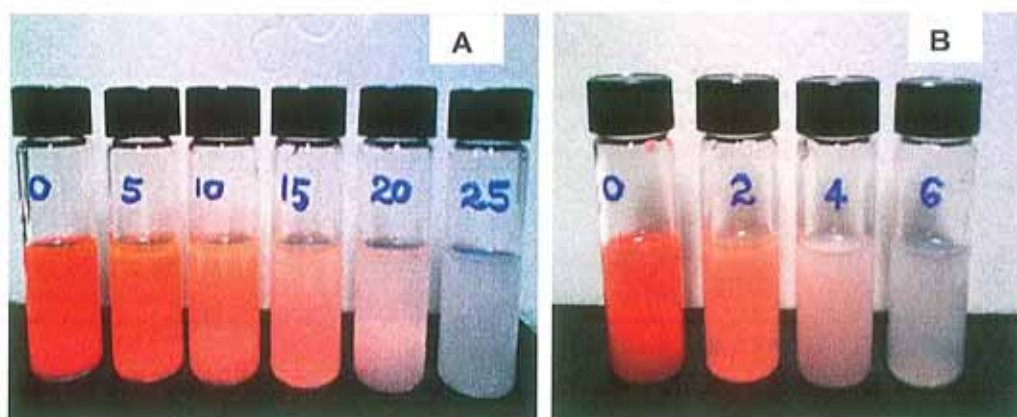
Figure 4.11: Representation of photocatalytic degradation of rhodamine dye in presence of (A) unmodified ZnO (B) 3 mol% silver modified ZnO (Time of degradation is denoted in minutes).

4.2.3 Photoluminescence Studies

Photoluminescence (PL) studies give an insight into the optical and photochemical properties of ZnO. Information on the quality of crystals, structural defects (surface oxygen vacancies, Zn interstitials *etc*) and particle surfaces can be garnered from PL spectra. The room temperature PL emission spectra (excitation at 325 nm) of ZnO and various mole % of Ag modified ZnO samples calcined at 400 °C are shown in *Fig. 4.12*. All samples emit strongly in the UV with a band centred at 390 nm, corresponding to the excitonic emission and three other less intense peaks. The weak blue band at 421 nm and 480 nm correspond to band edge free excitons and bound excitons respectively.[266] Furthermore, there is a weak green emission at 530 nm. The exact reason for this green emission is still the subject of debate. A number of hypotheses have been proposed to explain this such as transition between electron close to the conduction band and a deeply trapped hole at V_o^{++}, surface defects like Zn^{2+} vacancies, due to the transition between anti-site oxygen and donor-acceptor complexes,[267] *etc*. Surface binding of acetate ions is also known to improve the emission yield as they create vacancies that can facilitate the visible emission.[268]
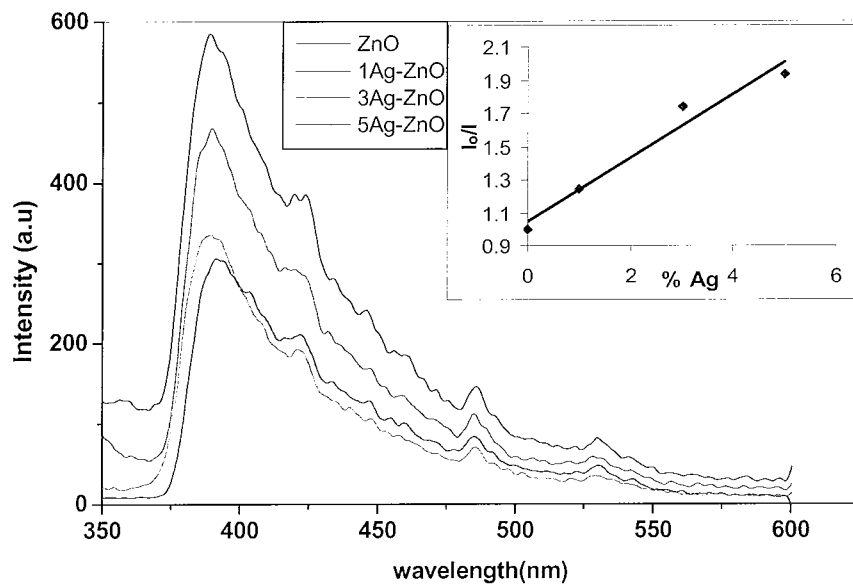
Figure 4.12: Room temperature PL spectra of ZnO and various mole % of Ag modified ZnO samples calcined at 400 °C. (Excitation at 325 nm). Inset shows the relative intensity change of emission in presence of silver. Emission intensities were measured at 390 nm.

According to some previous reports, this longer wavelength emission is due to the recombination of photogenerated hole with the singly ionized oxygen vacancy site.[269, 270] The current study agrees with this report as the presence of a lesser amount of oxygen vacancy is confirmed from the Raman study. The weak green emission and strong exciton emission of the materials demonstrate its good crystal quality. The stronger the PL intensity, the higher the photocatalytic activity.[271] During the process of PL, oxygen vacancies and defects could bind photoinduced electrons to form free or binding excitons so that PL signal could easily occur. During the process of photocatalytic reactions, oxygen vacancies and defects could become the centres to capture photoinduced electrons so that the recombination of photoinduced electrons and holes could be effectively inhibited.

Also it could be seen from the PL spectra that, the UV emission is decreasing with an increase in silver content indicating the decreased electron-hole recombination. This decrease in emission intensity is assumed to be in accordance with the Perrin's model of static quenching for silver is acting as a quencher and similar results were previously reported.[272]

4.3   Discussion

4.3.1   Effect of synthetic parameters on photocatalytic activity

The characteristic properties of ZnO powder mainly depends on its size and method of preparation. There are many methods reported for the preparation of nanosized ZnO such as aerosol, micro-emulsion, ultrasonic, sol–gel method, evaporation of solution and suspensions, evaporative decomposition of solution (EDS), solid state reaction, conventional ceramic fabrication, wet chemical synthesis and spray pyrolysis method.[273-277] Lately, room temperature UV lasing from ZnO nano-rod arrays[142] was reported by Huang et al., highlighting the prospects for the methods of fabrication of ZnO nanorods. Afterwards it was expected that some sort of morphologies of ZnO would be promising for use in a room temperature UV laser. Therefore, the development of morphologically controlled ZnO nanoparticles by a simple and economical method is an important issue. The effects of solvents are studied by many researchers[278, 279] and it was concluded that solvent not only controls the surface morphology, but also plays a vital role on the optoelectronic and electrical properties of nanosize ZnO. We chose a non-aqueous sol-gel method for the preparation of ZnO from zinc acetate and oxalic acid using ethanol as a solvent. Duffy et al. reported

similar sol-gel method for ZnO preapration where isophthalic acid was used instead of oxalic acid.[280]

An intermediate zinc oxalate was formed by the reaction between zinc acetate and oxalic acid according to the *Scheme 4.1* and *4.2*;

$$Zn(AcO)_2.2H_2O \ + \ H_2C_2O_4.2H_2O \longrightarrow ZnC_2O_4.2H_2O \ + \ 2AcOH \ + \ 2H_2O$$

$$(Scheme \ 4.1)$$

$$AcOH + C_2H_5OH \longrightarrow AcOC_2H_5 + H_2O \quad (Scheme \ 4.2)$$
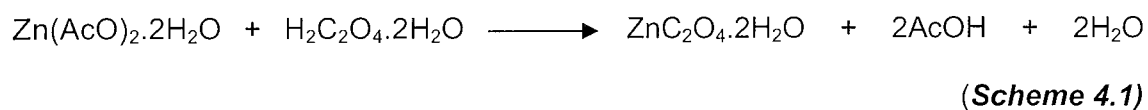
The formation of this zinc oxalate intermediate could be verified from the FTIR results of the room temperature ZnO sample. The information obtained from the XRD analysis of the samples at 300 °C corroborates with this results which shows the peaks corresponding to zinc oxalate precursor and no more peaks for wurtzite structure. The acetic acid formed according to the *Scheme 4.1* reacts further with C_2H_5OH present in the reaction mixture by the *Scheme 4.2*. This accelerated the first reaction towards the right and helped the formation of $ZnC_2O_4 .2H_2O$. The reaction of combination (*Scheme 4.1*) and esterification (*Scheme 4.2*) happened almost at the same time where the temperature of the reaction mixture was expected to be room temperature. During the heat treatment, the formed zinc oxalate dihydrate release water molecule to form ZnC_2O_4, after which it decomposed to form ZnO with the release of CO and CO_2 according to the *Scheme 4.3:*

$$ZnC_2O_4.2H_2O \longrightarrow ZnC_2O_4 + 2H_2O$$

$$ZnC_2O_4 \longrightarrow ZnO + CO + CO_2 \quad (Scheme \ 4.3)$$
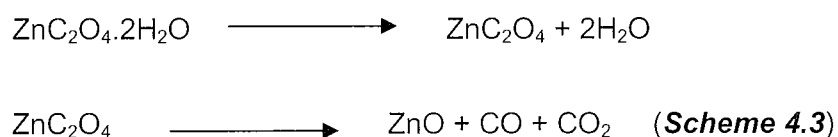
The DSC analysis clearly demonstrates this removal of structural water from zinc acetate dihydrate which is represented by the endothermic peak at 112 °C and the one at approximate 400 °C denotes the final stage (*Scheme 4.3*) of formation of ZnO.

The non-aqueous sol-gel process adopted for the present study facilitates the dispersal of Ag particles in the ZnO matrix. Such a distribution is observed to be favouring the tuning of structural features for achieving better photocatalytic activity, which was found to be better (three times) than the commercial photocatalyst, Degussa P25. The silver modified samples at 400 °C are found to be highly photoactive, with nanocrystalline ZnO formed at this temperature. The formation of nanocrystalline ZnO at 400 °C was also reported by Wang *et al*[281] where crystalline nanowires in presence of gold were observed.

The segregation of metallic Ag particles around the highly crystalline ZnO grain boundaries may be the reason for the high photocatalytic activity of the 400 °C calcined samples. The incorporation of silver can be according to *Scheme 4.4*.

$$ZnO_{(precur)} + 2Ag^+ + O_2 \rightarrow ZnO_{(precur)} + Ag_2O + \tfrac{1}{2}O_2, \quad T < 350 \quad \textbf{\textit{(Scheme 4.4)}}$$
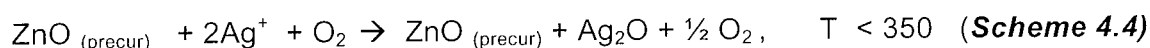
Like monovalent dopant such as K^+, Na^+, silver can perform as amphoteric dopant according to *Scheme 4.5*, where $Ag_{(Zn)}$ is the silver occupied in the Zn site and $Ag_{(i)}$ is the Ag in the interstitial site.

$$ZnO + Ag_2O \rightarrow Ag_{(Zn)} + Ag_{(i)} + ZnO + \tfrac{1}{2}O_2, \quad T > 350 \quad \textbf{\textit{(Scheme 4.5)}}$$
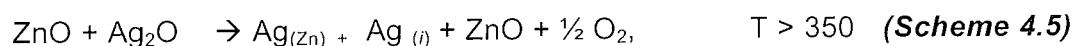
In the present case, the presence of Ag in the ZnO lattice is ruled out given the absence of a shift in the X-ray peak position. Because of the difference in ionic radii between Ag^+ (1.22 Å) and Zn^{2+} (0.72 Å), the silver particles preferentially choose to segregate around the ZnO grain boundaries. It is also observed from XRD that metallic Ag particles are formed only at 400 °C. Indeed, the 300 °C samples show the X-ray reflections corresponding to zinc acetate precursor and Ag_2O. This observation corroborates with previous reports, where the thermal decomposition behaviour of ZnO precursors was studied.[129] Also it has been reported that the thermal decomposition of AgO_x into Ag occurs in the temperature range 350 - 400 °C.[250, 282] Our observations are similar to this study and to the other reports which describe the thermal stability of chemically precipitated Ag_2O powders.[283, 284] Ahn et al. have also studied the thermal decomposition of Ag_2O in ZnO system, where they reported that the thermal decomposition of Ag_2O to metallic silver occurs above 380 °C.[251] These findings are in good agreement with the DSC result, where the crystallization of ZnO as well as the decomposition of Ag_2O occur above 380 °C. It is also evident from XRD that the incorporation of Ag into the ZnO matrix does not make a considerable change in the crystalline growth of nano ZnO compared to unmodified ZnO. However, the incorporation of 3 mol% Ag at 400 °C was found to inhibit the temperature dependent crystal growth of ZnO. Therefore, 3 mol% can be assumed as the optimum concentration of Ag particles required for the effective homogeneous distribution in the ZnO matrix by which the properties can be tuned effectively. On increasing concentration, the Ag particles can aggregate together and form localized clusters, which reduce the possibility of a homogeneous distribution and thereby reduce the surface availability for the adsorption of reactant and light.

Moreover, at high temperatures, since the Ag–O bond strength is weaker than the Ag–Ag bond strength, the formed Ag^o has higher surface energy eventually will form metallic clusters, which facilitate the densification of ZnO which reduces the surface area and hence the photocatalytic activity. The photocatalytic activity is dependent on the exposed surface area of the photocatalyst as it provides a means for the surface adsorption of the degradant. These results appear consistent with studies of Dodd et al.[285] who reported that there exists an optimum particle size for maximum photocatalytic activity of ZnO. This optimum particle size of ~15 nm, in the present study, was achieved by the suitable amount of silver addition. It is evident from the crystallite size (Fig. 4.3) that 3 mol% silver modified ZnO at 400 °C shows a smaller crystalline size among other samples. The distribution of silver in the ZnO matrix resulted in a reduction in the crystallite size. In a particular system, a smaller particle size, which causes the specific surface area to increase, is expected to increase the surface active sites where the photogenerated charge carriers are able to react with surface adsorbed molecule to form active radicals. The high crystallinity with lesser particle size results in a reasonable surface area for enhanced photocatalytic activity. In conclusion, the effect of size on the photodegradation efficiency can be ascribed to three reasons: (1) when the size of ZnO particles decreases; (2) the amount of the dispersion particles per volume in the solution will increase, resulting the enhancement of the photon absorbance; (3) at the same time, the surface area of ZnO photocatalyst will increase, which will promote the adsorption of more dye molecules on the surface. Furthermore, the simple couple of photoexcited electron–hole pairs will be suppressed.

As well as surface modification, it is evident from the absorption spectra that the silver addition can enhance the absorption capability of ZnO also. Even though there is no considerable change in the band gap (calculated from diffuse

reflectance spectra), the energy levels of silver lying in between the VB and CB of ZnO may facilitate the enhanced light absorption capability.

4.3.2 Mechanism of enhancement of photocatalytic activity by silver

One of the major aims behind the modification of semiconductors with noble metals is to improve or tune the catalytic and sensing properties. The deposition of noble metals on semiconductor nanoparticles is an effective way for improving the photocatalytic efficiency as the metal modifier can indirectly influence the interfacial charge transfer processes. As a noble metal, silver can act as electron scavenger and store them effectively. Certainly, a primary understanding of photoinduced interactions as well as the interfacial charge transfer processes in metal modified semiconductors is important to explain the exact role of metal in semiconductor photocatalysis. Light absorption of a suitable wavelength by ZnO results in the promotion of an electron from the valence band to the conduction band. The resulting hole is primarily responsible for the formation of hydroxyl radicals, which subsequently degrade the pollutants adsorbed onto the surface of the photocatalyst.[286] In such a photocatalytic process, the separation and recombination of photoinduced charge carriers are competitive pathways and photocatalytic activity is effective when recombination between them is prevented. The extent of recombination can be gauged by the intensity of luminescence.

In the present case, the UV emission at 390 nm of ZnO reduces as a function of mol % of silver (*Fig. 4.12*). This gradual decrease can be ascribed to the electron trapping effect of Ag, which acts as an acceptor species, hindering the recombination of charge carriers on ZnO.[287] Similar results were found with titanium dioxide.[288] The Fermi level of silver, which lies below the conduction band of ZnO, energetically

favours the transfer of electrons from ZnO. In order to assess the nature of photocatalytic degradation of R6G, we analysed the emission spectra of ZnO and silver modified ZnO in presence of R6G which is shown in *Fig. 4.13*.
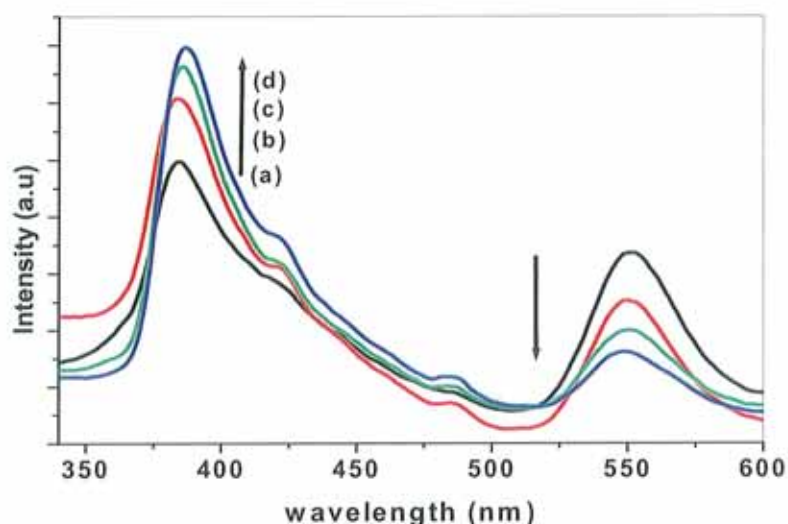
Figure 4.13: Room temperature PL spectra of (a) ZnO and (b), (c), (d) are 1, 3 & 5 mol% Ag modified ZnO respectively in presence of R6G. Emission at 390nm corresponds to ZnO emission and at ~550 nm corresponds to R6G.

An increase in intensity of UV emission (390 nm) of ZnO, as a function of amount in silver was observed, which is reverse in the case of samples without R6G. Interestingly, this increase in ZnO emission coincides with the decrease in emission of R6G at ~550 nm indicating that there is an additional photoelectrochemical process that dominates the electron capturing by silver at the time of photodegradation of R6G. These findings indicate the degradation of R6G on the silver modified ZnO surfaces may be occuring by a simultaneous two stage charge transfer processes.

The possible interfacial charge transfer events in the silver modified semiconductor at the time of degradation of dye can be explained by using the diagram presented

120

in *Fig. 4.14*. After the initial events such as the (1) ground state singlet to singlet excitation in dye and (2) band-gap excitation in ZnO, the possible electron transfer processes that can happen in the Ag-ZnO system in photocatalytic degradation of R6G are transfer of elctrons from (3) sensitized dye to the conduction band of ZnO, (4) sensitized dye to Ag particles, (5) from the CB of ZnO to Ag, (6) from the CB of ZnO to its VB (recombination) and sensitized dye to the shallow trap levels in the band gap of ZnO.
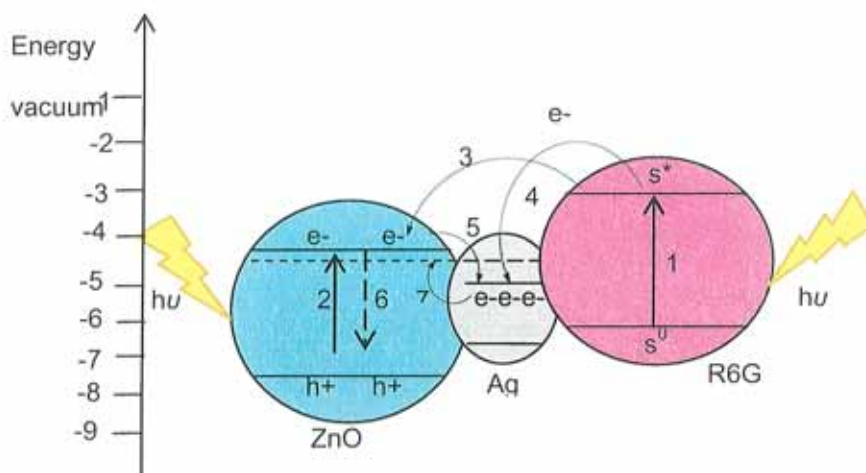
Figure 4.14: Schematic showing the electron transfer events of Ag-ZnO system in presence of R6G. (1) S^0 to S^*; (2) VB to CB in ZnO (charge carrier generation; (3) S* to CB of ZnO; (4) S* to Ag; (5) CB of ZnO to Ag and (6) CB to VB of ZnO (charge carrier recombination (7) Shifting of Fermi level of silver. The high reduction potential of S*, CB of ZnO and of Ag (according to literature data)[289, 290] drives its electron injection reactions.

From the UV-vis and PL spectra it is found that an increase of Ag concentration in the system enhances the UV emission of ZnO in presence of R6G, while diminishes in the absence of dye. This could be ascribed to the extent of VB hole formation as a function of Ag concentration.[160] The greater the formation of VB holes, the more intense the UV emission, provided all charge carriers are recombining effectively.

However, in the absence of R6G, the CB electrons of ZnO generated as a result of the band-gap excitation are captured by the Ag particles and the recombination is reduced significantly; hence we observe a decrease in emission intensity as the Ag concentration increases. Furthermore, an increase in the VB hole concentration formed as a function of Ag addition also found to enhace the UV emission by a similar mechanism. In presence of R6G, however, the CB electron population in ZnO is retained by the electron injection from the dye, which also simultaneously populates the electron level in Ag. The process (3) is facilitated by rhodamine as a sensitizing dye adsorbed on the surface of a semiconductor can act as electron donor. Kamat and co-workers[291-293] and Kalyanasundaram et al.[294] have shown that dyes with carboxylate group or hydroxyl group can interact with TiO_2/ZnO surface and the induced electron transfer can be from the excited state of the dye to the CB of the semiconductor. Both processes (4) and (5) are possible in the case of silver because of the position of its energy level.[295] Mulvaney and co-workers reported the dependency of Fermi-level equillibration with the nature of metal particle used for modification.[296] For example, if the metal is Pt, it will encourage the discharge of electron towards the electrolyte (solution) where as if it is Au it will unusually store the electrons between the semiconductor-metal layers. Hence keeping that in mind, for the present system, we would expect that this electron transfer will continue until the overall Fermi level of the metal modified ZnO system shifts towards more negative potential (7) and ultimately equillibrates with that of ZnO.[177] Once this level is reached, Ag discharges the stored electrons in to the solution where they react with dissolved oxygen to form the superoxides and OH radicals in turn. These active oxygen species react with the dye molecules and degrade them effectively.

If there was back electron transfer between the excited dye cation radical (dye$^{+\bullet}$) and ZnO (e$^-$), the dye would have regenerated. However, no dye regeneration was observed which indicates suppression of this back electron transfer by silver. Hence, there is a role for silver in utilising the captured electrons and thereby the free holes in the case of a system containing sensitizing dye. The enhanced photocatalytic activity of semiconductors modified with Ag were previously reported to be due to the generation of more free VB holes as a function of silver addition. However, in the present case, active oxygen species such as OH radicals and $O_2^{\bullet-}$ generated by the CB electrons are found to be major species responsible for the dye degradation. Both the sensitizing property of dye and electron scavenging ability of silver together contribute to the interfacial charge transfer process in such a way to utilise the photo-excited electrons, in addition to the VB holes, to form this active oxygen species. The high reduction potential of the dye used is found to be the key factor that governs the electron transfer process and thereby defines the mechanism of photocatalytic degradation.

4.5   Conclusions

Various mol% of highly active silver modified and unmodified ZnO photocatalysts at different temperatures were prepared through a non-aqueous sol-gel route. The structural and optical properties of the resultant materials were characterised by XRD, DSC, FT-IR, Raman, UV-Vis, and PL spectroscopy. The materials synthesised were shown to have a high crystallinity. The silver modification was effective at low temperatures such as 400 – 600 °C and results in a reduction of the crystallte size of the 3% Ag material relative to ZnO. Photocatalytic activity of all samples were determined by analysing the degradation of rhodamine 6G in presence of the powdered suspensions. Silver modification caused the material to show significant improvement in the photocatalytic activity. 3 mol% silver at 400 °C

was considered as the optimum concentration which shows four times higher rate of degradation of dye than that of unmodified ZnO. The mechanism of photocatalytic activity was studied by analysing the emission properties and it was found that the presence of silver facilitates the interfacial charge transfer processes in such a way to utilise the CB electron for enhancing the photocatalytic activity. This results show that silver has a significant role to play in the trapping of electrons in these materials, and as such these materials applications could be extend to the development of a photocatalyst which is applicable in both environmental purification and energy production processes.

5. SILVER-CERIA CO-DOPED VISIBLE-LIGHT ACTIVE TiO$_2$ PHOTOCATALYSTS

5.1 Introduction

As the widespread application of semiconductor photocatalysis becomes closer to reality, increased attention has been focused on visible light mediated technologies. The development of photocatalysts exhibiting high reactivity under visible light (λ> 400 nm) should allow the main part of the solar spectrum, even under poor illumination of interior lighting, to be used. Much effort has been taken by researchers to design visible light active titania semiconductors by adopting various modification methods. Doping is an effective way, among many methods described in *Chapter 1*, to create highly optically and electrochemically active semiconductors for various applications. Numerous research reports are available to account for this. Metals, non-metals, transition metals, rare earth elements *etc.* were used as the dopants in different laboratory preparation condition and some of them reported an enhancement in the visible light activity of TiO_2. Doping with transition metals have been investigated by researchers,[297, 298] and though it could extend the optical absorption, the thermal instability and an increase in the charge carrier recombination centres have limited the performance of these materials.[299]

On the other hand, doping with anionic non-metals like fluorine (F – see Yu *et al.* [64, 300]), carbon (C – see Khan *et al.* [301]), nitrogen (N – see Asahi *et al.* [302]), sulfur (S – see Umebayashi *et al.* [303]), boron (B – see Moon *et al.* [304]) *etc.* have also been investigated widely, aimed at extending photocatalytic activity into the visible-light region. Conclusions from these studies were that this visible light activity was a result of band gap reduction, as discussed in *Chapter 1*. Furthermore, co-doping with these dopants was also found useful for the improved visible light activity.[305] Modification with noble metals has been reported as an effective method to increase the photocatalytic efficiency. Titania that contains platinum (IV), and Au (III) exhibit photocatalytic activity in the visible light in the aqueous suspension, degrading organic pollutants.[306, 307] Lin *et*

al. have explored the visible light photoactivity of Pt-doped TiO_2 for the degradation of nitrogen oxides.[308] There is literature available on the silver modification and we already have seen in Chapters *3* and *4* that silver metal could significantly enhance the photcatalytic performance of TiO_2 and ZnO.

Alternatively, the photocatalytic activity could be significantly enhanced by rare earth metals,[309] especially lanthanide ions with 4*f* electron configuration, for they could form complexes with various Lewis bases.[310, 311] Sibu *et al.*[312] investigated the effect of lanthanum doping in TiO_2 and they observed a huge increment in surface area of the catalyst about 1-160 m^2/g. Among the lanthanide oxides, the catalytic property of ceria received much attention due to its properties including: (1) redox couple Ce^{3+}/Ce^{4+} with the ability of ceria to shift between CeO_2 and Ce_2O_3 under oxidizing and reducing conditions; and (2) the easy formation of labile oxygen vacancies with the relatively high mobility of bulk oxygen species. Structural and optical investigations on ceria-doped TiO_2 have been done by many researchers and it was proven that ceria doping can remarkably influence structural properties of TiO_2, especially, in high temperature conditions.[313, 314]

CeO_2 itself is widely studied and accepted as an additive in the so-called three way catalyst (TWC) for automobile exhaust treatment.[315] It stabilizes and keeps a high surface area of other catalysts by preventing the sintering. It is previously reported that the presence of CeO_2 in mixed oxides can promote various catalytic reactions such as CO_2 activation,[316] CO oxidation[317] and CO/NO removal.[318] It is, therefore, not surprising that ceria based oxide systems are of great interest for the photocatalytic degradation purposes. It has become gradually recognised that cerium oxide and noble metals are subjected to mutual interaction, which depend on the noble metal, and that can influence the catalytic activity. Given these characteristic properties of ceria and in light

of the results observed from the previous studies of silver modification on TiO_2, we were motivated to make TiO_2 a 'multi-purpose catalyst' by co-doping with silver and ceria. Though visible light activity is the primary goal of research, analysis on how silver-ceria interaction can influence the catalytic properties of TiO_2 will be the principal consideration. There is a good deal of research available about ceria doped TiO_2,[319] silver doped TiO_2,[158] and silver doped CeO_2 (for three-way catalysts).[320] However, there is no report in research literature on the study of effect of silver-ceria co-doping on TiO_2. To the best of our knowledge, this is the first study making use of the characteristic properties of both ceria and silver to enhance the photo-catalytic property of TiO_2.

This chapter describes results of analysis on the effect of silver-ceria co-doping on TiO_2 to enhance the photo-response towards visible region. The methodology selected for the synthesis is a sol-gel process and optimised the ratio of amount of co-dopant in TiO_2 matrix for both UV and visible light activity. Structural properties were characterised and a red shift is observed in the absorption of silver-ceria co-doped TiO_2 towards visible region. In addition to the visible light response, the silver-ceria doped materials stabilizes the anatase phase stability up to a temperature such as 800 °C and reduces the percentage of rutile at 900 °C. In addition, the effect on photocatalytic activity is discussed in light of physical and structural properties of the materials synthesised.

5.2 Results

5.2.1 Characterisation of the materials

5.2.1.1 X-ray diffraction analysis

The crystal phase composition and crystallite size estimation of silver-ceria doped samples were analysed by dividing the samples into low temperature region and high temperature region. The low temperature samples ranged from 400—600 °C. and high temperature samples ranged from 700—900 °C. The concentration of ceria (1 mol%) was kept constant and various mol% (1,3 and 5) of silver were used throughout the preparation. The X-ray powder diffraction pattern of pure (undoped) and silver-ceria co-doped TiO$_2$ (ACT) samples calcined at various temperatures are shown in *Fig. 5.1*.
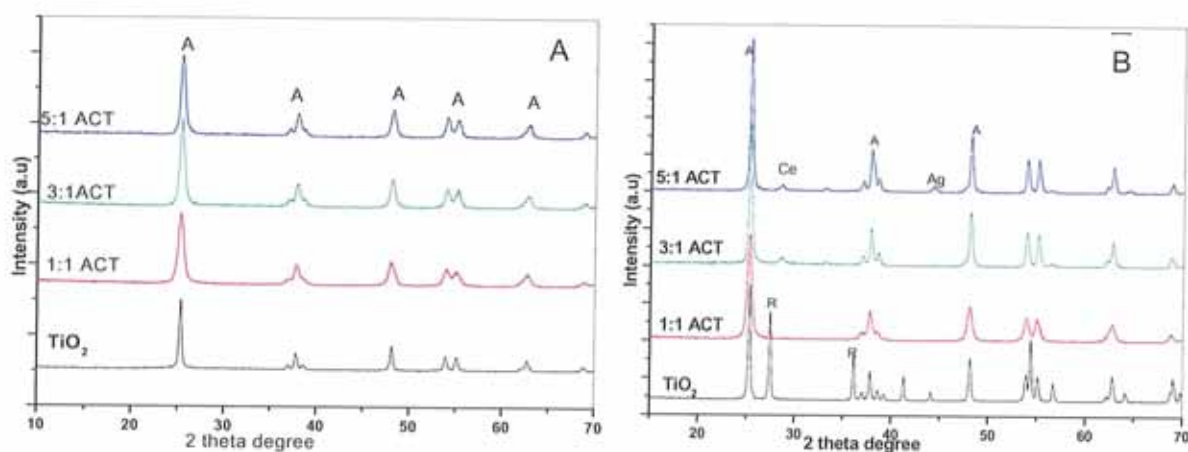
Figure 5.1: XRD of pure and silver-ceria co-doped TiO$_2$ samples calcined at (A) 600 °C and (B) at 700 °C

All the spectra at 600 °C show typical anatase structure (JCPDS, No. 21-1272) both for the pure and doped TiO$_2$ materials. Additionally, no peaks associated with cerium oxide and silver were observed which hinted at uniform dispersion of silver and ceria in the TiO$_2$ matrix. Similar spectra were obtained from the samples at 400 °C. In fact the ionic

radii of Ag^+, Ce^{3+} and Ce^{4+} are 1.28, 1.03 and 1.02 Å respectively are much bigger than that of Ti^{4+} (0.68 Å). Therefore, it is not easy for Ce^{3+}/Ce^{4+} to enter the TiO_2 lattice. The relative intensity of the main (101) anatase peak became sharper and stronger with silver-ceria content in the oxide mixture, which means that CeO_2 phase could also undermine the crystallization of anatase phase as well as preventing generation of rutile phase. On the other hand, if silver alone was used as the dopant, an opposite trend could be observed, as already shown in previous results (Chapter 3). As in the case of silver-modified TiO_2, average crystallite sizes were calculated from XRD analysis (Scherrer formula), and are summarised in Table 5.1. It appears that ACT samples show a tremendous decrease in the crystallite size for lower temperature as well as at high temperature up to 800 °C. For samples at 400 °C, it shows no remarkable increment almost similar crystallite sizes because of poor crystallinity.

Table 5.1: Crystallite sizes of pure and silver-ceria co-doped TiO_2 samples at various temperatures.

Temperature (°C)	Crystallite sizes (nm) (± 10%)				
	TiO_2	1:1 ACT	3:1 ACT	5:1 ACT	3:3 ACT
400	9.6	8.6	7.3	9.2	7.1
600	26.7	12.1	13.0	13.5	9.5
700	32.8	13.9	22.8	25.0	23.5
800	41.4	31.0	36.3	36.3	33.5
900	45.3	31.6	37.5	34.5	39.8

When the temperature increases to 700 and 800 °C, peaks associated with rutile are present (at 2θ = 27.45 and 54.5) although anatase is still the dominant crystallite phase. The amount of rutile present in the anatase rutile mixture was calculated using the Spurr equation (Chapter 2) and it was found that samples at 700 °C contains 49% and at 800 °C contains 99% of rutile. However, silver-ceria co-doping reduces the percentage of rutile to zero at these temperatures. This means the presence of ceria hinders the phase transformation from anatase to rutile. The average crystallite sizes also show reduction for silver–ceria modified samples.

As indicated in the Fig. 5.1 (B) and Fig. 5.2 (A), new peaks appeared at 28.58, 33.1, and 56.3 for the silver-ceria co-doped TiO_2 samples at high temperatures accredited to CeO_2 cubic phase[321] (JCPDS, No. 43-1002) and peaks at 38.2 and 44.1 represent the metallic silver. According to previous results from Chapter 3, it is clear that rutile phase is present at 700 °C even in presence of silver, though it could reduce the percentage of rutile. Hence, in the present system containing both silver and ceria, the existence of anatase phase up to 800 °C and reduction in crystallite size is not only because of silver, but the suitable amount of ceria (1 mol %) required for phase stabilization. It was further confirmed by analysing the XRD pattern of samples consisting of higher percentages of ceria in presence of silver (3:3 ACT) at all these temperatures which is presented in Fig.5.2 (B) and it shows that ceria in presence of silver can act as a crystallinity promoter when temperature increases. More details are provided in the discussion, below. Furthermore, it should be noted that for the samples at 900 °C (Appendix 5) there is no formation of anatase even with silver ceria co-doping which may be due to the presence of agglomerated metallic silver at this temperature.
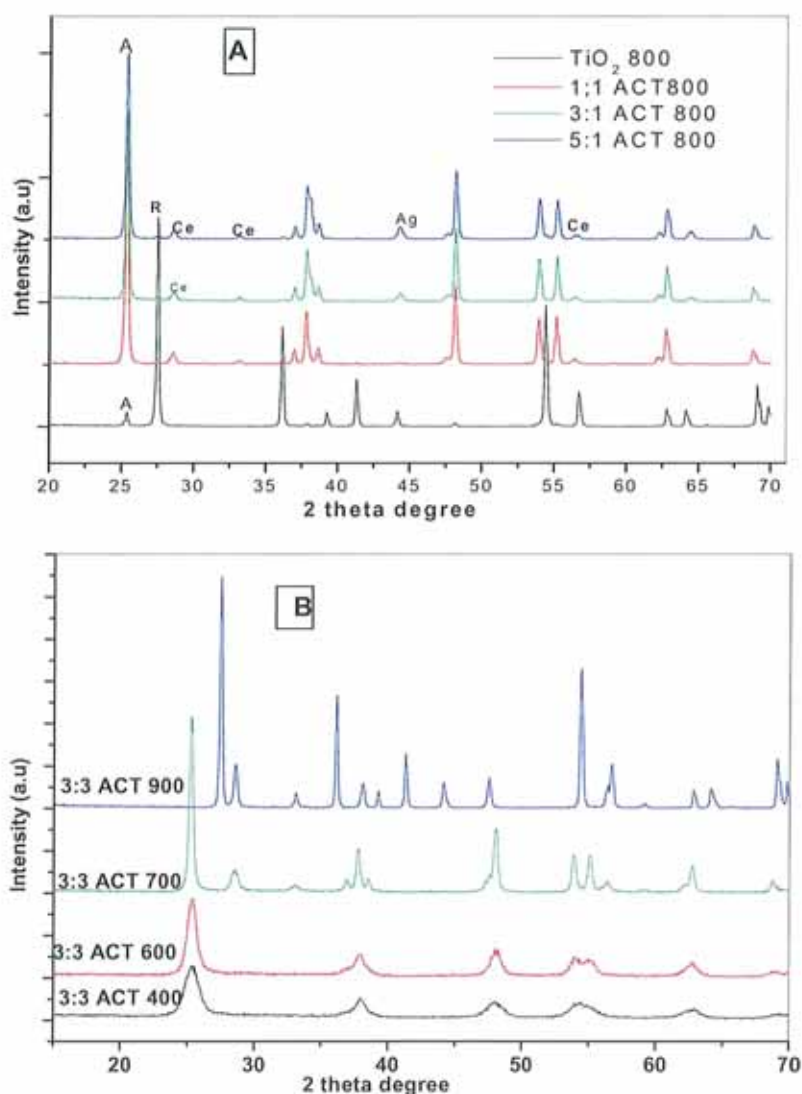
Figure 5.2: XRD of pure and silver-ceria co-doped TiO₂ samples calcined at (A) 800 °C and (B) 3:3 ACT at various temperatures.

5.2.1.2 Differential scanning calorimetry

The thermal events and phase changes that occur during the heat treatment in the undoped and doped TiO_2 materials were studied by recording the differential scanning calorimetry. DSC curves of all the precursor materials were presented in *Fig. 5.3.* (A) and show a small endotherm occurred below 100 °C for all the samples, due to the removal of free adsorbed water and residual organic compounds. For undoped TiO_2,

an exotherm with a lower enthalpy of dissociation present at *ca.* 351 °C could be due to the decomposition of acetate groups associated with the gel and also due to the removal of chemisorbed water.
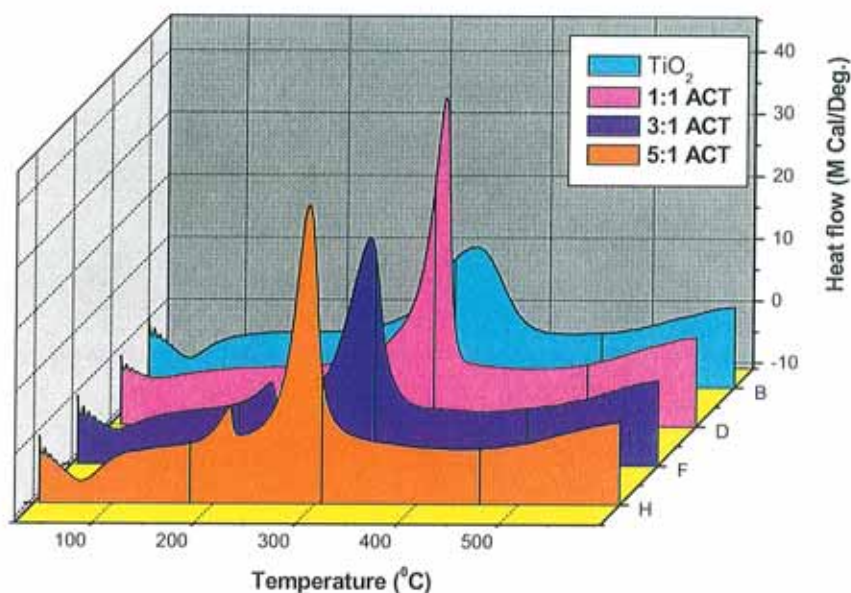
Figure 5.3: DSC of undoped and silver- ceria co-doped TiO$_2$ samples

For 3:1 and 5:1 ACT materials, a small exothermic peak at 215 – 220 °C is detected which can be ascribed to the combustion /decomposition of the organic matters associated with dopants. Thus, for the present case it can be due to the decomposition of cerium nitrate or due to the formation of Ag$_2$O from silver nitrate where both processes are expected to happen at this temperature. On the other hand, the lack of this exotherm for the 1:1 ACT implies that, it might be due to the formation of Ag$_2$O which is energetically more favourable than the decomposition of cerium nitrate.

As stated earlier, the main exothermic peak at ~350 °C for undoped TiO_2 which represents the anatase phase evolution, shifts towards the lower the temperature region such as 350, 315 and 290 °C for 1:1, 3:1 and 5:1 ACT samples . This variation may be due to the structural evolution that happens by the addition of co-dopants. As we have seen in *Chapter 4* the thermal decomposition of Ag_2O is happening in this temperature range and which is highly energetic than other phase evolution of metal oxide present in the system. It is already reported that Ag_2O loses its oxygen in presence of ceria even at lower temperatures.[320] Therefore the present study indicates that early phase transition from amorphous phase for silver-ceria co-doped TiO_2 is not due to the ceria, but the presence of ceria on silver enhances the early crystallization. This was further confirmed by studying the DSC of 3:3 ACT and a 3 mol% ceria doped TiO_2 material (3CeT) and it was observed that higher percentage of ceria with silver doped TiO_2 shows an early phase formation (*Fig. 5.4*). Previous research about the high temperature phase transformation[322] using similar amount of ceria doped TiO_2 agree with this confirmation.
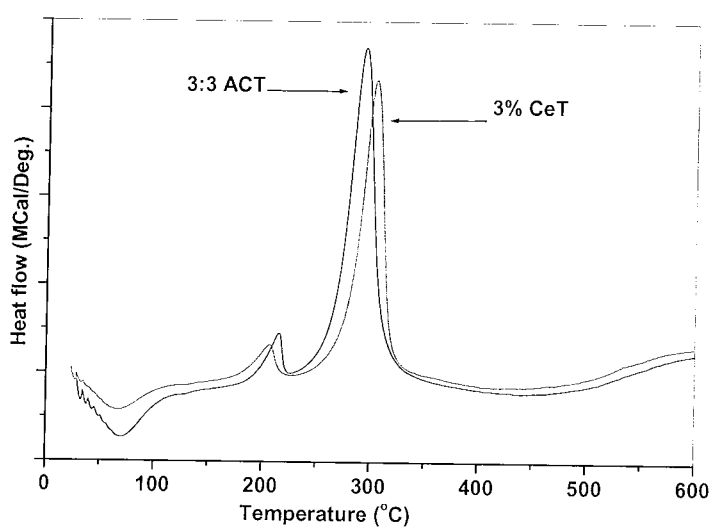
Figure 5.4: DSC of 3:3 ACT and 3 mole% Ce doped TiO_2

134

5.2.1.3 Microstructure analysis

Fig. 5.5 shows the transmission electron microscopic (TEM) analysis of undoped and 3:1 ACT sample calcined at 700 °C. The particles for undoped TiO_2 shows a mixture of spherical particle collapsed with clusters of rutile where as the 3:1 ACT sample shows a well defined spherical particle having reduced crystallite sizes which is in good agreement with the crystallite size calculated using XRD.
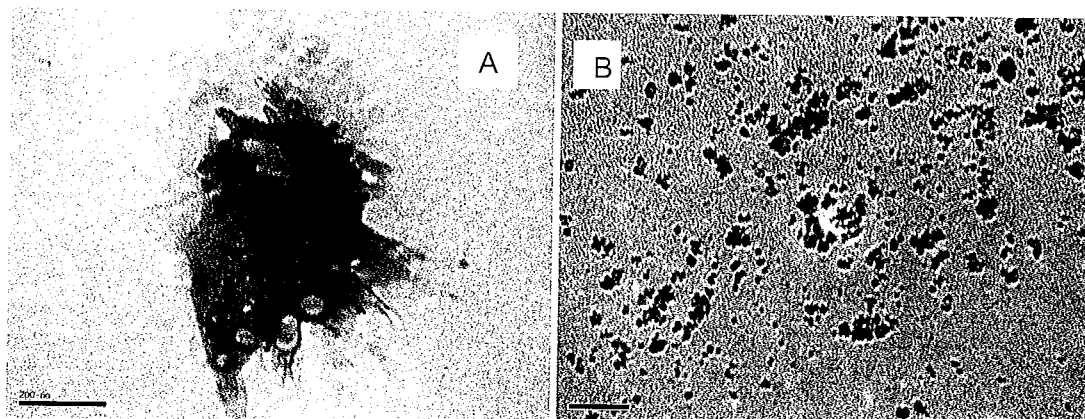
Figure 5.5: TEM images of (a) undoped TiO_2 and (B) 3:1 ACT at 700 °C.

5.2.1.4 FTIR spectra

FTIR spectra of undoped and various mol% of silver-ceria doped TiO_2 samples at 700 °C are shown in *Fig. 5.6*. All the samples show a broad band in the region 3300 – 3600 cm^{-1} which indicate the stretching vibration of OH group. Bands in the region 1600 – 1620 cm^{-1} represent the bending vibrations of surface adsorbed water. Interestingly, all the ACT samples show an increase in intensity of this band which indicates the presence of more surface hydroxyls, as a result of the improved surface area. There is a large frequency separation appeared in the range 1424 – 1620 cm^{-1} which denotes the presence bridging acetate ligands. A big shoulder at 1094 cm^{-1} for undoped TiO_2 represents the anatase Ti—O bond vibration, which is formed during the gelation time,

and which is shifted towards ~1227 cm^{-1}, 1159 cm^{-1}, and 1110 cm^{-1} for 1:1, 3:1 and 5:1

ACT samples respectively that hinted to the effect of ceria to stabilize the Ti—O bond

from further transformation. The undoped TiO$_2$ sample show a strong band at 530 cm^{-1}

which is the characteristic peak of titania, and interestingly for the ACT samples this

peak is shifted to ~ 468 cm^{-1} – 490 cm^{-1} which indicate the fact that there is Ti—O—Ce

bond formation. Similar results were reported in the literature where La was used as

the dopant.[312] From the results it is evident that at high temperatures the interaction of

Ce is not with silver but with the TiO$_2$ support.
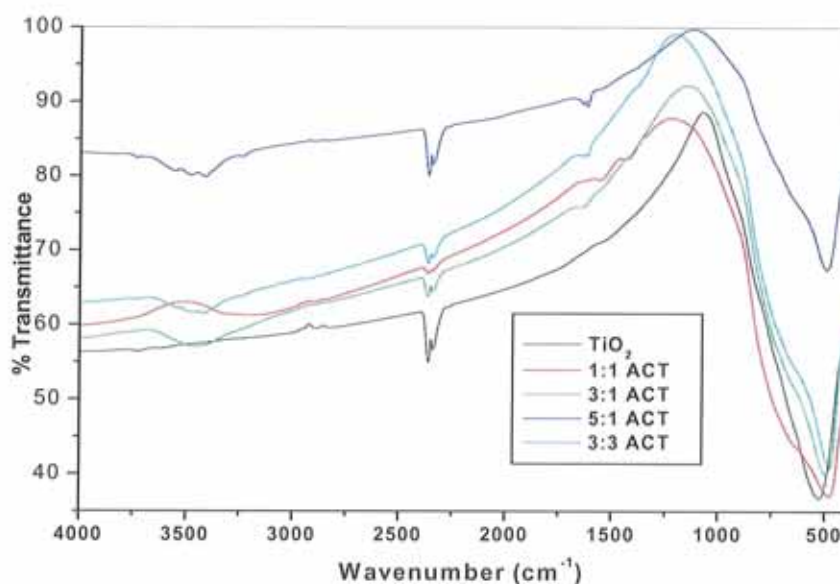
Figure 5.6: FTIR spectra of undoped and various mol% ACT sample at 700 °C

5.2.1.5 Visible absorption

To investigate the optical absorption properties of prepared ACT materials, we

examined the diffuse reflectance spectra of all the powders calcined at 700 °C. The

spectra of undoped, 1:1, 3:1 and 5:1 ACT samples are presented in *Fig. 5.7*. From the

results, it is clear that silver-ceria co-doping results in a significant shift in the optical absorption towards the visible region. The band gap calculated from the spectra for undoped TiO_2 is 3.17 eV and that of 1:1 ACT, 3:1 ACT and 5:1 ACT are 2.7, 2.3 and 2.4 eV respectively. It was reported that for a system consisting of Ti—O—Ce type of bonding, the red shift in the absorption is due to the charge transfer between the impurity band and conduction band of TiO_2.[103, 309] From the FTIR spectra, it has already been observed that there is a Ti—O—Ce bonding possibility. In addition, from the previous study (*Chapter 3*) with which only silver was used as the dopant, no band gap change was observed as a result of doping. Researchers reported the increment in red shift with respect to the increment in amount of ceria.[323] Though the same amount of ceria was used in all the samples with various amount of silver, an increase in shift is observed corresponding to the increment in silver, where it is believed for the present system 1 mol% ceria as the optimum.
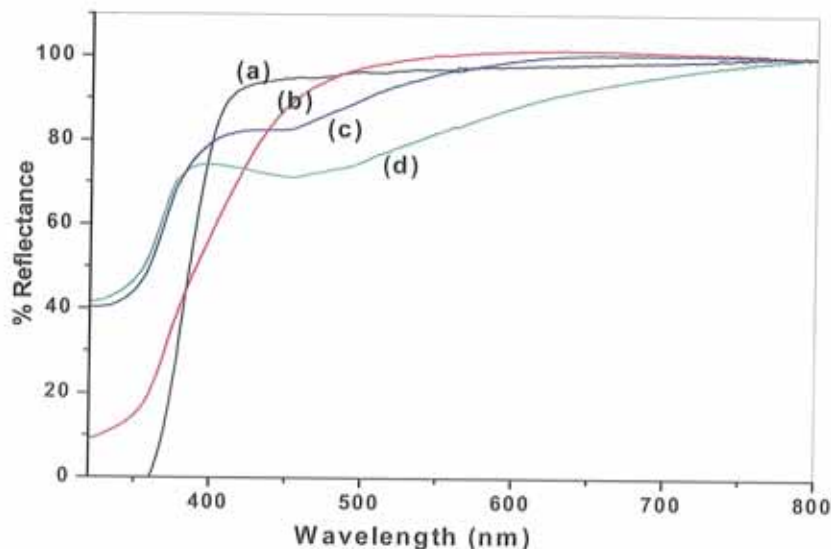
Figure 5.7: Diffuse reflectance spectra of (a) undoped (b) 1:1 ACT (c) 3:1 ACT and (d) 5:1 ACT calcined at 700 °C.

137

This may be due to the fact that the higher amounts of silver facilitate the crystallization/densification of CeO_2 at high temperatures, which causes the CeO_2 phases to increase. This assumption agrees with the results from the XRD of samples at 700 °C where peaks corresponding to CeO_2 were observed. As the concentration of CeO_2 phases increases, the impurity band would become broader and thus the charge separation gap become narrower which enables the material to have an absorption in the visible region. This was further confirmed by measuring the band gaps of ACT samples at lower temperature (not shown) and it was observed that there wasn't a significant reduction in the band gap.

5.2.2 Photocatalytic activity

The photocatalytic activity of undoped and ACT samples at low temperatures and high temperatures were studied by using rhodamine 6G. It was found that with suitable amount of silver and ceria, the TiO_2 material can be active in both UV and visible light. For comparison, spectra of the photocatalytic degradation of rhodamine are shown – one from low temperature range and one from higher temperature (*Fig. 5.8 and Fig. 5.9*). For undoped TiO_2, the 700 °C sample shows the highest rate of degradation compared to others at 400, 600, 800 and 900 °C. This may be due to the presence of rutile with anatase. There have been reported previously that titania contains a small fraction of rutile with anatase can show better photocatalytic activity than that of anatase.
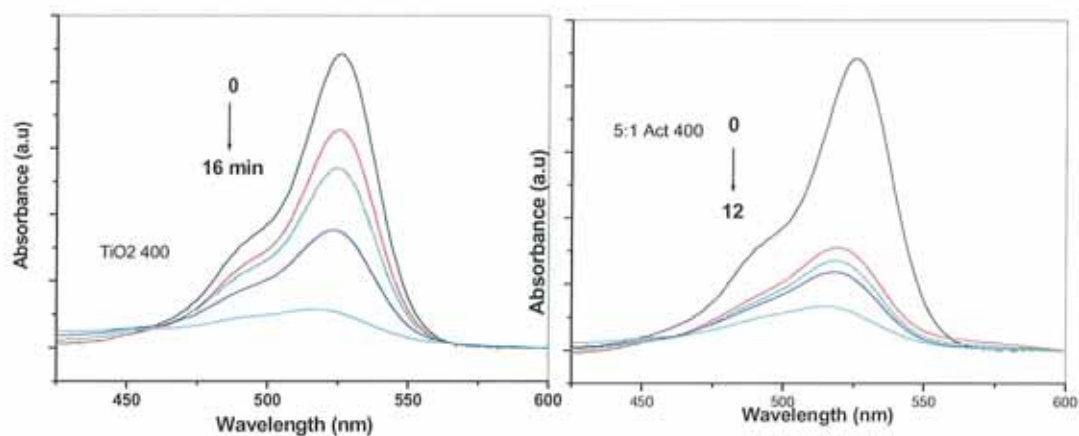
Figure 5.8: UV-Vis absorption spectra of the degradation of rhodamine using undoped TiO₂ and 5:1 ACT at 400 ℃
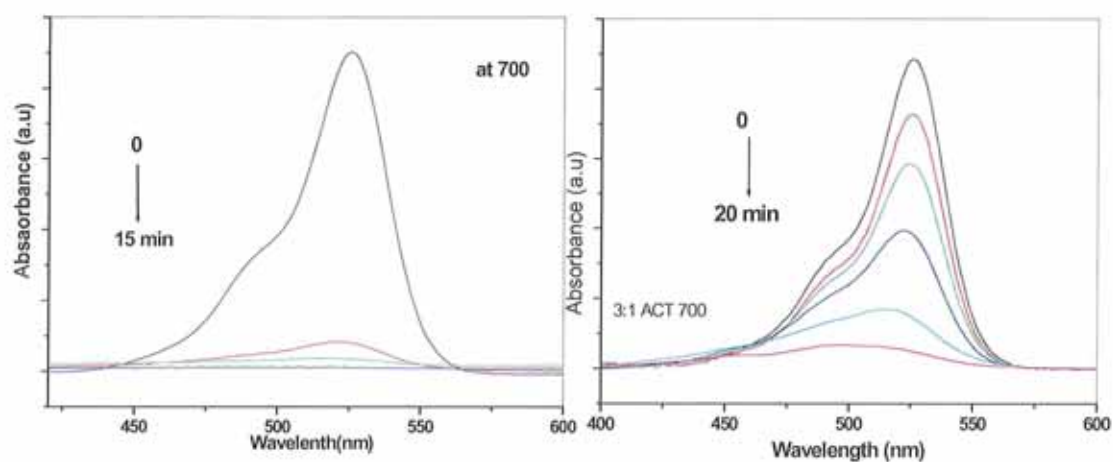
Figure 5.9: UV-Vis absorption spectra of the degradation of rhodamine 6G using undoped TiO₂ and 3:1 ACT at 700 ℃

But in the case of silver-ceria modified samples, no considerable increase in the rate of degradation of rhodamine for high temperature calcined samples in the UV light was observed. The 5:1 ACT sample at low temperature, say at 400 – 600 °C, shows an

increase in the photocatalytic activity relative to the undoped one at the same temperature whereas the 3:1 ACT gives the highest rate at high temperature such as 700 °C. The rate of degradation is calculated from the first order rate kinetics, which is represented in *Table 5.2*, and it is assumed that in the case of silver-ceria co-doping, low temperature doped samples show UV activity and high temperature such as 700 °C samples with big band gap reduction would expected to have visible light activity. More details will be discussed below. From the degradation experiments, it is noticeable that the entire ACT samples with a suitable amount of silver at low temperatures also show visible light activity.

According to the characterisation analysis, the ACT samples which were not active in the UV light show a band gap reduction and so high activity in the visible light region would be expected. Many factors are there to account for this visible light activity. This point is addressed shortly. The lower photcatalytic activity of silver-ceria co-doped TiO_2 relative to the undoped TiO_2 at high temperature is probably due to the partial blocking of the surface sites available for rhodamine where the interaction of rare earth element with TiO_2 changes the amount of surface hydroxyls and thus reduces the OH radicals.

Temperature (°C)	Rate constant k (min^{-1}) of TiO$_2$ samples with various mol % of silver-ceria			
	0	1:1 ACT	3:1 ACT	5:1 ACT
400	0.102	0.02	0.017	0.180
600	0.121	0.018	0.02	0.02
700	0.30	0.036	0.144	0.013
800	0.170	0.10	0.12	0.06
900	0.019	0.007	0.005	0.006

5.3   Discussion

5.3.1   Textural and phase formation

The influence of dopant on the structural and textural properties of metal oxides can be explained on the basis of changes caused by the dopant on defect structure of the TiO$_2$ lattice. Several studies[208, 209, 324] have reported that a sol-gel sample of TiO$_2$ should undergo a phase transformation from high photocatalytic anatase phase to thermodynamically favourable rutile phase during calcination. In this study, all the samples were calcined from 400 to 900 °C and it was found that all the samples at 600 °C were of anatase phase. When the temperature increases to 800 °C, the undoped TiO$_2$ starts to show the formation of rutile phase where as the silver ceria co-doped material show no peaks of rutle in addition to the peaks for CeO$_2$ and metallic silver.

That means a suitable amount of ceria could prevent the rutile formation. It is known that anatase-rutile phase transformation is related to many factors such as preparation conditions, impurity present, dopants, precursor *etc*. Various research reports[325-327] shows the variety of rare earth elements used to get the high temperature stability for TiO_2. The rutile formation temperature is raised to 900 °C for the silver-ceria co-doped samples from that of undoped TiO_2 at 700 °C. This inhibition of phase transformation was ascribed to the anatase phase stabilization due to the surrounding Ce atoms through the formation of Ti—O—Ce bond[328] and evidence for the Ti—O—Ce bond formation from the FTIR spectra further confirms this observation. Also, there is a possibility for the titanium ions to substitute for the cerium ions in the lattice of cerium oxide to form octahedral Ti sites. The interaction between the tetrahedral Ti and octahedral Ti atom retarded the phase transformation from anatase to rutile. Anderson and Bard explained the phase transformation in TiO_2-SiO_2 in a similar way.[329]

In addition, the Ce–O–Ti interaction blocks the Ti–O species at the interface with TiO_2 domains stabilizing them to prevent structural re-organisation for further phase transformation. This will cause TiO_2 to inhibit agglomeration, which prevents the growth of titania nanocrystallites and results in a high surface area. Our crystallite size calculation results (*Table 5.1*) shows agreement with this assumption. The BET surface area analysis of undoped TiO_2 and 3:1 ACT at a lower temperature region are 34.56 m^2/cc and 86.44 m^2/cc which corroborate these calculations. As we stated earlier, due to the mismatch of ionic radius of Ce^{4+} and Ag^+ with respect to Ti^{4+}, there is also a chance for the Ce^{4+} and Ag^+ ions to go to the interstitial sites. The slow rate of grain growth for ACT compared to an undoped one may also be attributed to the presence of interstitial Ce ions. Thus the stabilization of Ti-O bond will in turn retard the anatase-

rutile transformation (A—R) temperature because the A—R transformation requires breakage of Ti-O bonds,[330] and in the case of Ce containing system it is difficult to break the Ti—O bond which is strengthened by Ce atoms.

It is interesting to note that, in the low temperature region, there is no peak for either silver or ceria which indicates a uniform distribution of these dopants into the TiO_2 matrix. It is well known fact in the literature that the CeO_2 has an effect in dispersing the Ag metal and preventing its agglomeration to bigger particles.[331] Only limited research literature is available about the surface interaction of silver and ceria though it is an interesting research subject in the area of automotive pollution catalyst since Yao et al. reported the Pt- CeO_2 linkage.[332] Diwell et al. reported that under oxidising conditions, formed Pt-ceria complex maintains the Pt stability against sintering.[333] As we have seen from the DSC analysis, because of the oxygen storage property of ceria, it can accelerate the reduction of silver, but keeps the metallic silver in a well-dispersed state. According to the previous reports, the silver–ceria interaction is more feasible at lower temperatures.[334] Our results also show good agreement with this conclusion. When the temperature goes above 800 °C, the agglomerated silver island can accelerate the crystallinity of CeO_2 which further facilitate the rutile formation.

5.3.2 Visible light absorption and photocatalytic activity

Photocatalytic degradation experiments reveal the fact that the silver-ceria co-doping is an effective method of modification for developing both UV and visible light active TiO_2 catalysts. The low temperature calcined ACT sample especially, at 400 °C, shows the increase in the rate of photocatalytic degradation whereas the samples at high temperature shows no significant increase in the degradation. The low temperature activity of the silver-ceria co-doped samples may be due to the presence of optimum

143

amount of silver present in the system, not due to ceria. Though we can consider the increase in surface area as a result of ceria as one factor, silver does the same function at this temperature. Many previous studies[319] explains the increase activity of ceria doped TiO_2 in a concept that CeO_2 can act as an electron scavenger to trap the photogenerated electron forming at the CeO_2-TiO_2 interface, and converted in to Ce^{3+} resulting in the prevention of electron –hole recombination (*Scheme 5.1*).

$$Ce^{4+} + e^{-} (TiO_2) \quad \rightarrow \quad Ce^{3+} \quad \textbf{\textit{(Scheme 5.1)}}$$

The electrons trapped in the Ce^{4+}/Ce^{3+} site subsequently transferred to the surrounding adsorbed O_2 which further continues the OH radical formation as follows: (*Scheme 5.2 and 5.3*)

$$Ce^{3+} + O_2 \quad \rightarrow \quad O_2^{\cdot -} + Ce^{4+} \quad \textbf{\textit{(Scheme 5.2)}}$$

$$O_2^{\cdot -} + 2H+ \quad \rightarrow \quad 2 \, OH^{\cdot} \quad \textbf{\textit{(Scheme 5.3)}}$$
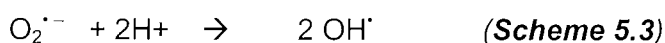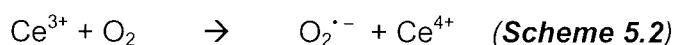
Because of the high oxygen storage property, the excited electron may more rapidly be transferred to the Ce^{3+}-TiO_2 surface.

But in the case of the silver-ceria co-doped TiO_2 system, different mechanisms are expected for the lower temperature and higher temperature samples. CeO_2 is an n-type semiconductor having multiple oxidation states like Ce^{3+} and Ce^{4+} The oxidation state of Ce in lower temperature sample is unclear as we have no XRD peaks of Ce or silver in low temperature samples because of its fair dispersion. However, previous reports shows that in the sol-gel synthesised Ce-TiO_2 at lower temperature, Ce exists mainly as Ce^{3+}.[335] It is evident from XRD results that at high temperature, it exists as mainly Ce^{4+}. In addition, it is assumed that at low temperatures Ce^{3+}/Ce^{4+} co-existed in TiO_2 and similar results were reported. As mentioned, at lower temperatures, there is a possibility for the silver-ceria interaction to occur rather than the interaction of Ce and

144

TiO$_2$. The interaction with ceria makes with silver, for a particular concentration, to form silver nanoparticle that can disperse well in the TiO$_2$ matrix. These silver nanoparticles at this temperature range will show an apparent increase in the absorption due to the surface plasmon resonance of Ag nanoparticle. It is obvious from the report that metallic Ag has high activity if it is dispersed and stabilized on the surface of CeO$_2$.[320] This assumption was further confirmed by recording the absorption spectra of a lower temperature sample which shows good agreement (*Fig. 5.10*) where the strong absorption band at ~400 nm represents the surface plasmon absorbance of silver. There was previous study about the effect of ceria on the precipitation of silver, but not on the TiO$_2$ system.[334]
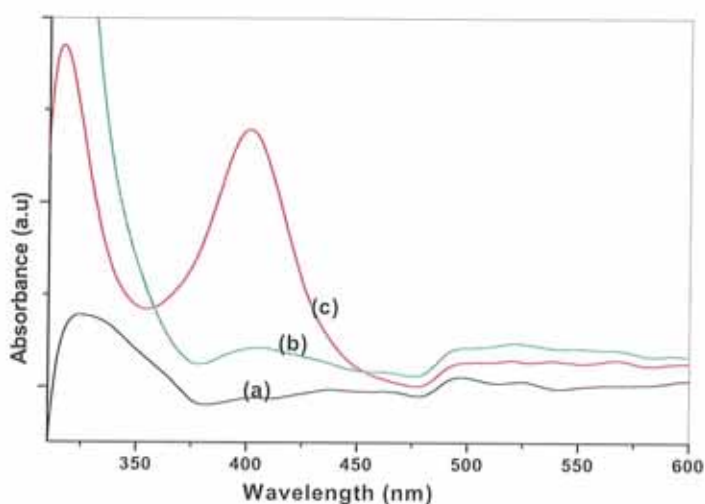
Figure 5.10: UV-Vis absorption spectra of (a) undoped (b) 3:1 and (c) 5:1 ACT samples at 500 ℃.

Hence, for the present case, at lower temperatures, silver-ceria interactions cause the material to enhance the photocatalytic activity. These samples are expected to show both UV and visible light activity. Since it is known that noble metals can promote the Ce^{IV} to Ce^{III} reaction,[336, 337] it is assumed that there is feasible charge transfer between

Ce^{3+} and Ag during the calcination processes. There was a previous study about the effect of ceria on the precipitation of silver, not on the TiO_2 system, where they could observe an increase in the absorbance of Ce^{3+} during light absorption process.[334] Earlier studies about the noble metal–ceria interaction show that it may form species like M–O–Ce where both metal and ceria are in oxidised state. In the case of Pt–O–Ce, ceria stablilzes the metal in a high oxidation state that led to a superior interaction. By taking metal-ceria interaction into consideration, the possible electronic transfer that can be happened in the case of silver-ceria co-doped TiO_2 at low temperature is given below.

$$Ce^{3+} + Ag^0 \rightarrow Ce^{4+} + Ag^0 \qquad \textit{(Scheme 5.4)}$$

$$Ag^{+/0} + (e^-)\,TiO_2 \rightarrow Ag^{0/e-} + TiO_2\,(h^+) \qquad \textit{(Scheme 5.5)}$$
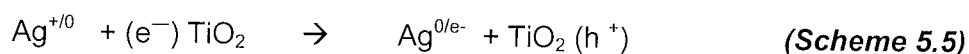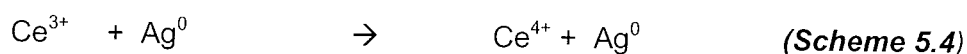
Scheme 5.4 is possible, as it is accepted in the case of TiO_2/Ag system previously because of the Fermi level difference, which prevent further agglomeration of silver nanoparticles and hence keeps silver in a highly dispersed state. Scheme 5.5 thus inhibits the electron-hole recombination and which results in increased photocatalytic activity for an optimal content of silver. The possibility of reverse reaction of Scheme 5.4 results in the increase in the concentration of Ce^{3+} and which can later facilitate the OH radical formation and hence the photocatalysis. Another possibility is the direct interaction between CeO_2 and noble metal resulting in a synergetic effect which causes the removal of surface oxygen from CeO_2 with subsequent reoxidation leading to the formation of highly active O_2 radicals.[338] The possibility of all these electronic transitions is minimal in the case of degradation of a sensitizing dye.

At high temperatures, for the undoped TiO_2 at 700 °C compared to other samples we could see an increased photocatalytic activity. It is established, based on the difference in the position of conduction band between anatase and rutile, that the presence of suitable amount of rutile with anatase can enhance the photocatalytic electronic transitions.[339] Based on this hypothesis, one explanation for high photocatalytic activity is that the existence of rutile causes an increase in charge-separation resulting from interfacial electron transfer from anatase to rutile. Another explanation is that due to the presence of small rutile crysallites, rapid electron transfer from rutile to lower energy anatase lattice which lead to a charge separation. However, the stabilization of the charge separation caused by the two phases can activate the total catalyst and holes can participate in the oxidative degradation.[340] But this is not fully applicable in the case where surface area is a measure of photcatalytic activity as surface area will reduce at high temperature.

To explain the photocatalytic activity for ACT samples at high temperatures, the interaction can be assumed as being between ceria and the TiO_2 support. The information we obtained from diffuse reflectance spectra shows that there is a band gap reduction for ACT samples. As aforementioned, Ti^{4+} ions could be in place of $Ce^{4+/3+}$ site to form an interfacial phase Ce—Ti(IV)—O_2. It can be considered as an impurity band of interfacial Ce—Ti(IV)—O_2 with n-type identity. This is because when Ti^{4+} takes up one Ce^{3+} hole, one electron will be generated. Red shifts of this type can be attributed to the charge-transfer between the CeO_2 band and the conduction band of TiO_2. Possible electronic transition in addition to *Scheme 5.1* and *Scheme 5.2* that can happen in this case is given as *Scheme 5.6*. The Ce^{3+} formed according to *Scheme 5.1* traps photogenerated holes in TiO_2 resulting in the inhibition of recombination or it can transfer the electron to surface adsorbed oxygen. An additional

possibility, namely, the reverse reaction of *Scheme 5.4* can not be neglected at high temperatures as there is the residual aggregated metallic silver.

$$Ce^{3+} + h^+ (TiO_2) \longrightarrow Ce^{4+} \qquad (\textit{Scheme 5.6})$$

The low photocatalytic activity in the UV light for the ACT samples than the undoped samples can be due to many factors. First, due to the reduction in band gap, there is a chance to get increased rate of electron-hole recombination and to reduce the redox potential of the total system. Second is, the impurity atom substituted in the lattice of TiO_2 may act as the trapping or recombination centres for electrons and holes, accounting for the decreased photodegradation efficiency. In terms of increment in surface area caused by silver-ceria co-doping, a more likely explanation for the visible light activity of ACT samples is as follows. The quantity of light that can be absorbed by a spherical particle depends on the particle size and optical property of the TiO_2 crystals. Also penetration of light into the particle is influenced by the morphology of the particles.[341] It is well known that the smaller crystals are generally poorer light scatterers than larger crystals. Particles formed from large TiO_2 crystals have smoother surface than the particles made from small crystals. On the smooth surface, the incident photons are scattered and lost mostly by reflection. The rougher surface formed by the small crystals allows a greater number of scattered photons to penetrate into the particles and also have more adsorption sites for the degradant. From *Table 5.1*, it can be seen that the crystallite size TiO_2 decreased as a result of silver-ceria co-doping. This suggests that the effect of photon penetration as a result of silver-ceria co-doping is also a likely explanation for the enhanced visible light absorption.

5.4 Conclusion

In conclusion, it is considered that silver-ceria co-doping is an effective way to design photocatalysts that can be active both in UV and visible light. All the high temperature ACT samples show a red shift towards visible region and this visible light absorption was attrributed to the reduction in band gap energy of TiO_2 as a result of silver-ceria co-doping. From the current study, it is found that all the ACT samples at high temperature show visible light absorption and the higher amount of silver is detrimental to the effect in red shift caused by ceria. From the results obtained it is believed that in the case of silver-ceria co-doping on TiO_2, for low temperature calcined ACT samples, the activity was due to the interaction between silver and ceria whereas at high temperature ACT samples, the activity was due to the band gap reduction created by the interaction between CeO_2 and TiO_2 – which was further confirmed from DRS and IR spectra. These findings would help to improve the application of TiO_2 from as a photocatalyst to a multipurpose catalyst.

6. FUTURE WORK

6.1 Analyse photocatalytic degradation of a range of dyes

It is well-known that photocatalytic reactions are governed by various parameters including pH, surface area, catalyst loading, light intensity/wavelength, surface charge, substrate concentration, *etc.* Photcatalytic activities studies were done with large number of substrates and many different methods under widely varying conditions. So, the activity comparison among different photocatalytic samples is often not straightforward. Therefore, many researchers have made efforts to provide a standard protocol for the estimation of photocatalytic activities. Recently, several workers in the area have argued that in order to determine whether a photocatalyst is "highly active" or "not active", it is necessary to test the material against a range of degradants, with different functional groups and charges. After analysing a range of TiO_2 samples with various substrates, Choi *et al.* concluded that the highly substrate specific activity of TiO_2 hold back the comparison of which TiO_2 is better than others.[342]

Currently we use an organic model dye R6G, which have an absorption in the visible region, for the photocatalytic activity study. Nevertheless, in order to study the exact mechanism of photocatalysis, whether it is due to the photosensitization or dye sensitization, it is imperative to study the photocatalytic activity in presence of such dyes having absorption in the UV region (for example, benzaldehyde, formaldehyde *etc*). The comparative study of mechanisms of degradation of both these type of dyes will be helpful for the future work.

6.2 OH radical Quantification

The property of charge separation in semiconductors is used in many important technological applications such as the conversion of solar energy, detoxification of pollutants, imaging, sensors and optoelectronics. In the case of environmental

application, a proper understanding of the reaction mechanisms in the semiconductor photocatalysis will lead to the development of efficient photocatalytic systems specific to particular chemical species and new photocatalysts based on the TiO_2 nanomaterials. Furthermore, the clarification of the excited state dynamics on TiO_2 surface is important subject for the design of the highly active photocatalysts. It is accepted that in the case of heterogeneous photocatalysis, hydroxyl radicals formed on the surface of TiO_2 during photocatalysis are considered to be responsible for many oxidation reactions like degradation of the pollutant. For the reason that OH radical generation is the primary step that leads to the destruction of the pollutant, the measurement of rate of OH radical generation is one of the most important parameters to be studied for the evaluation of newly developing photocatalysts. Also this would be useful for the comparison of various photocatalysts. Similar analysis has been reported.[343] In *Chapter 4* an attempt was made to predict the mechanism of increased photocatalytic activity of silver modified TiO_2. The OH radical quantification and further lifetime study of the corresponding species in that case would give more useful information to determine the difference in mechanism of degradation in presence of pure and silver modified TiO_2.

6.3   Modification of TiO₂ and ZnO using separately prepared nanosilver

Silver nanoparticles with various sizes and shape have the ability to absorb visible light because surface resonance frequency strongly depends on their size, shape and dielectric environment of the nanoparticles.[344] Still it is a challenge to synthesis highly concentrated, various size and shaped silver nanoparticles having absorption in the visible region.[185] Based on work completed for the previous chapters, some other results we obtained which show promising for future work. In *Chapter 3* we discussed about the silver doping through direct calcination of silver salt with TiO_2 precursor.

Hence a study on the effect of silver, which is prepared through different method, on the photocatalytic activity of TiO_2 would be interesting. Here, various colured (shaped) stable silver sol such as yellow, red, blue and green were synthesised through an easy single step method. This is the first time report on the preparation of various coloured silver sol through single step. In order to make utilize the size and shape dependant properties of prepared nanosilver to enhance the photocatalytic activity of semiconductors, we doped it in both TiO_2 and ZnO. The Uv-Vis absorption spectra of all the sol and their corresponding TEM are shown in *Fig.6.1.*

Yellow silver sol show only spherical particles, where as the higher absorption silver sol shows triangles in addition to small amount spherical silver nanoparticles. When the absorption shifts to higher wavelength, triangle particles show change in size and shape, namely, truncated triangles. As a part of preliminary analysis, TiO_2 and ZnO at 600 °C were doped with yellow silver sol and the photocatalytic activity investigated. The results show significant enhancement in activity and hence the visible light activity would be expected for the samples doped with rest of the visible light absorbed sols. Uv-vis absorption spectra of degradation of methylene blue using pure TiO_2, yellow silver sol doped anatase TiO_2, pure ZnO and yellow silver sol doped ZnO are shown in *Fig.6.2* and *Fig.6.3*.
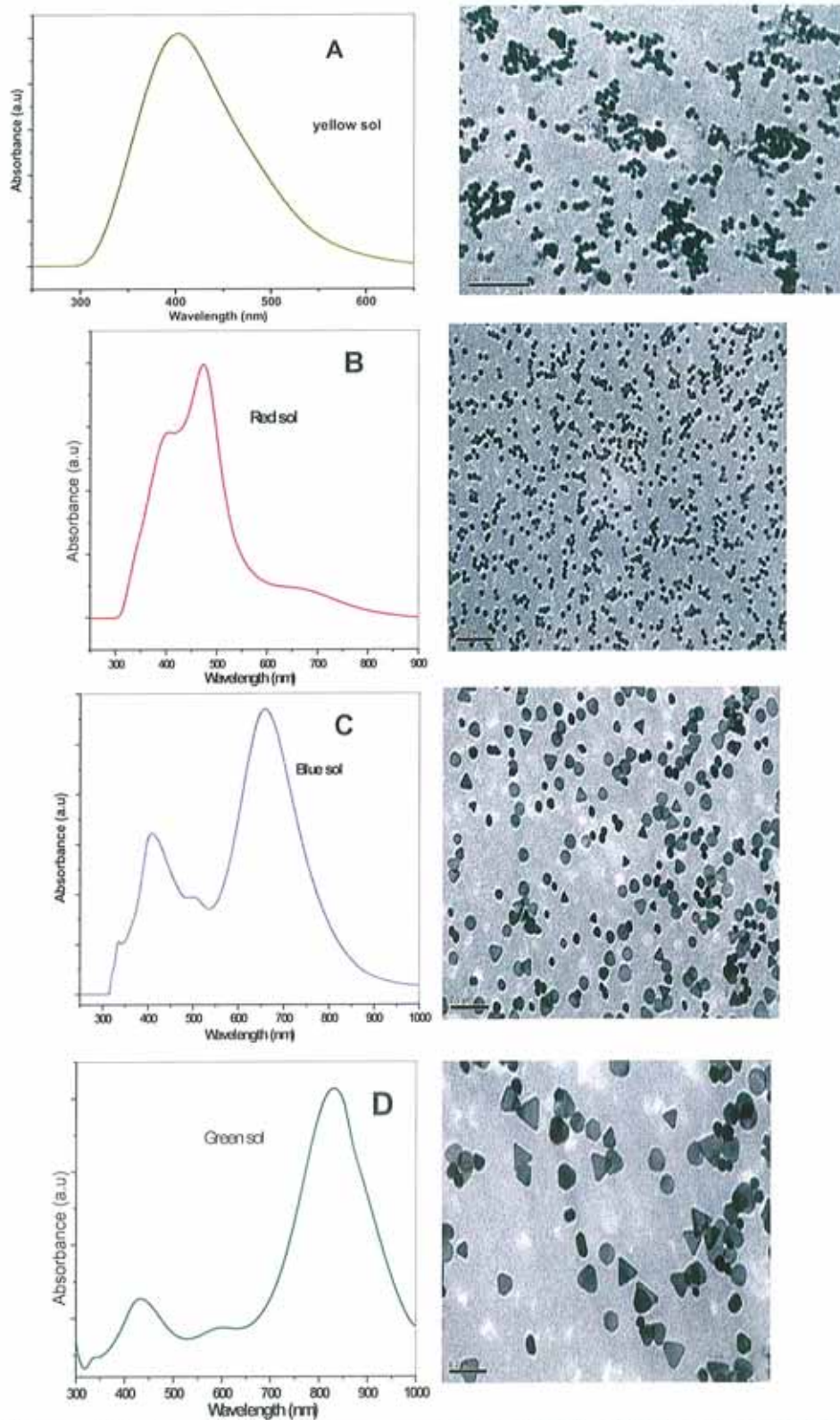
Figure 6.1: Uv-vis absorption spectra and TEM of (A) yellow sol (B) red sol (C)

blue sol and (D) green silver sol.

154
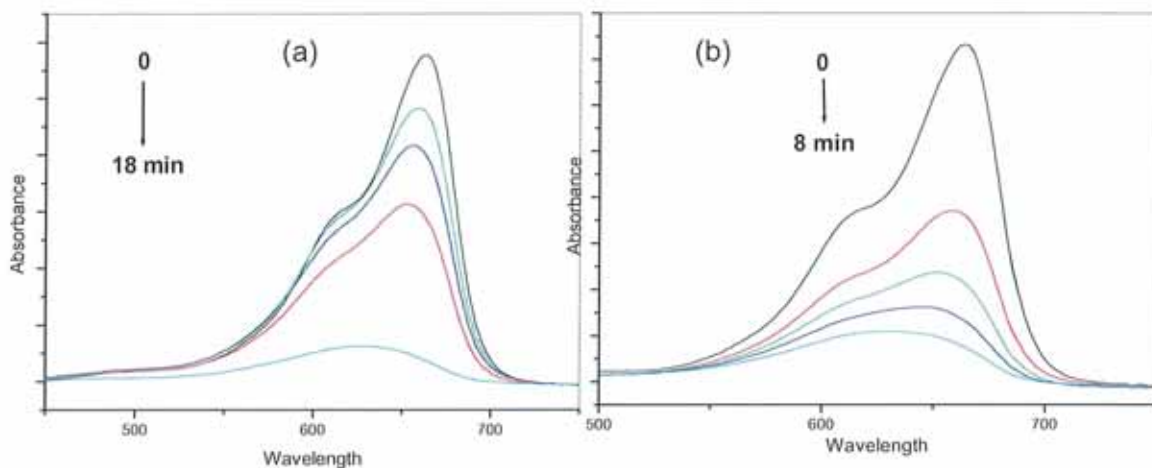
Figure 6.2: Uv-vis absorption spectra of the degradation of methylene blue in presence of (a) pure TiO₂ and (b) TiO₂ doped with yellow silver sol.
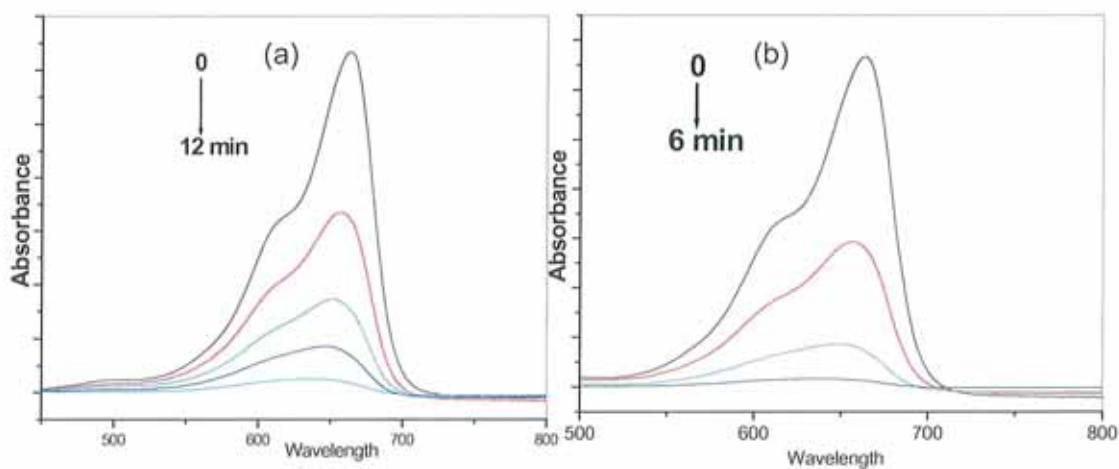
Figure 6.3 Uv-Vis absorption spectra of degradation of methylene blue in presence of (a) pure ZnO and (b) ZnO doped with yellow silver sol.

6.4 Study on the sensing property of ZnO

The photocatalytic properties of ZnO have already been shown in *Chapter 4*. Photocatalytic remediation of pollutants in presence of semiconductors can be in its most useful (operational) level, if one can detect the presence/nature of pollutants in

the reaction media. A desirable feature for the detoxification of air and water is to develop a catalyst system that can simultaneously sense and destroy toxic chemicals.

A recent study reported that ZnO can sense same time the presence of pollutants and degrade it effectively, because of its emission property.[162] The visible emission of ZnO is very sensitive to hole scavengers. The quenching of visible emission in presence of hole scavengers will be an indication of presence of trace organic contaminants in the aqueous media. Some initial experiments have been carried out on the sensing property of ZnO using 4-chlorophenol as the pollutant. We could observe a quenching in emission of ZnO in presence of 4-chlorophenol. After the degradation of the pollutant ZnO recovered the initial emission intensity (*Fig. 6.4*). Making use and developing the dual role of the ZnO systems in this work as a sensor and a photocatalyst would be another useful object for the future work.
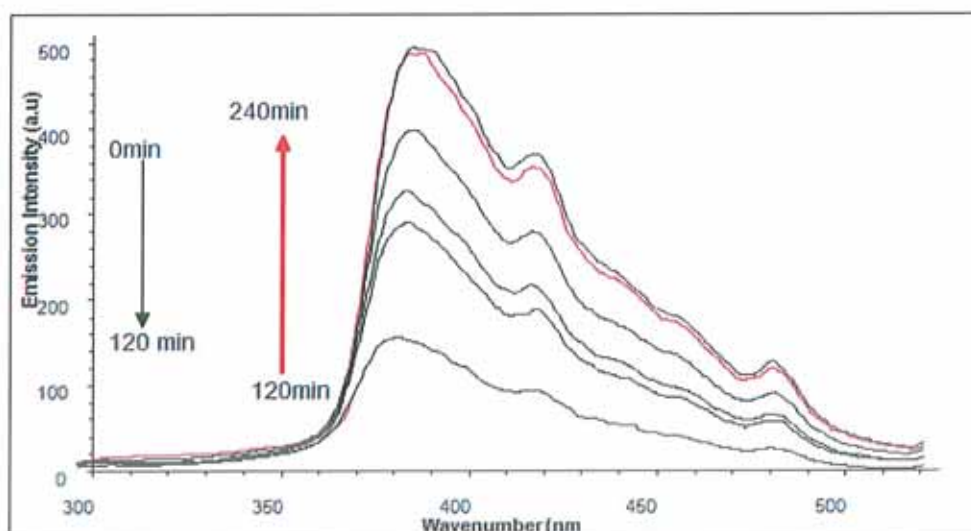
Figure 6.4: Photocatalytic sensing of ZnO in presence of 4-chlorophenol.The red line indicates the emission recovery of ZnO after degrading the pollutant.

6.5   Analysis of thin films

An important subsequent development of this type of research is its successful application. In the beginning, researchers employed titania nanoparticles as suspended powders to study its activity. However, the difficulty in the recycling of particles and the need for long term utilization made researchers to think of using them as immobilized surfaces. Therefore the recent research is focused on the preparation as immobilized surfaces, *e.g.* as thin films on a solid support. As described in *Chapter 2*, we fabricated thin coatings of TiO_2 and silver modified TiO_2, present samples under study, on glass slides (*Fig. 6.5*). Photocatalytic activity analysis shows better efficiency for these thin films and so further analysis on the surface morphology, contact angle and optimisation on preparation method would be advantageous.
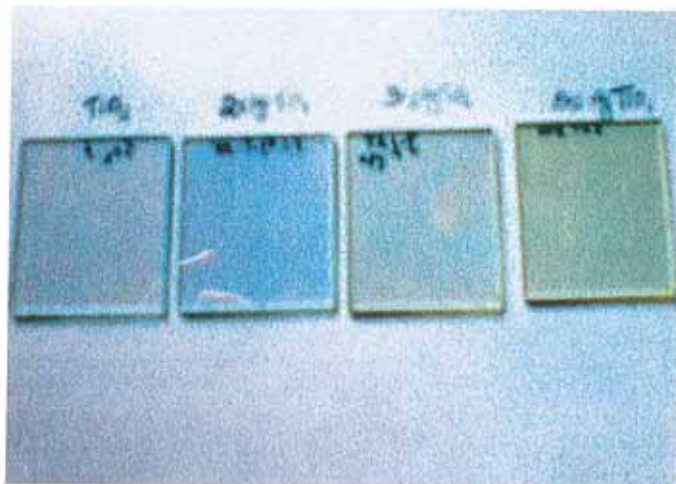
Figure 6.5 Photograph of TiO_2 and silver modified TiO2 coatings on glass slides calcined
at 500 °C (from left: TiO_2, 2% Ag, 3% Ag and 5% Ag).

REFERENCES

1. M. Fox, in *Health and Science*, 2006.
2. P. Toner, L. Stapleton and M. Lehane, *Ireland's Environment: A Millennium Report*, Environmental Protection Agency, Wexford, 2000.
3. in *EPA News*, 2007, p. 3.
4. A. G. Collins and A. I. Johnson, *Ground water contamination*, ASTM International, 1988.
5. A. Mills, R. H. Davies and D. Worsley, *Chem. Soc. Rev.*, 1993, **22**, 417.
6. NASA, *Environment and Resource Management*, Spinoff, 2005.
7. J. W. Verhoeven, *Pure Appl. Chem.*, 1996, **68**, 2223.
8. A. Mills and S. L. Hunte, *J. Photochem. Photobiol. A: Chemistry* 1997, **108**, 1-35.
9. U. Stafford, K. A. Gray and P. V. Kamat, *Chem. Rev.*, 1996, **3**, 77.
10. O. Legrini, E. Oliveros and A. M. Braun, *Chem. Rev.*, 1993, **3**, 671.
11. H. Hidaka, J. Zhao, E. Pelizzetti and N. Serpone, *J. Phys. Chem.*, 1992, **96**, 2226.
12. A. Fujishima and K. Honda, *Nature*, 1972, **238**, 37.
13. M. Saito, *Tech. Report Rev.*, 1998, 28.
14. K. W. Boer, *Survey of Semiconductor Physics*, Van Nostrand Reinhold, New York, 1990.
15. M. R. Hoffmann, S. T. Martin, W. Choi and D. W. Bahnemann, *Chem. Rev.*, 1995, **95**, 69.
16. R. Nakamura and Y. Nakato, *J. Am. Chem. Soc.*, 2004, **126**, 1290.
17. M. Gratzel, *Heterogeneous Photochemical Electron Transfer*, CRC Press, Boca Raton, 1989.
18. M. Mrowetz and E. Selli, *New J. Chem.*, 2006, **30**, 108.
19. A. J. Hoffmann, E. R. Carraway and M. R. Hoffmann, *Environ. Sci. Technol.*, 1994, **28**.
20. C. Kormann, D. W. Bahnemann and M. R. Hoffmann, *Environ. Sci. Technol.*, 1991, **25**, 494.
21. S. Tunesi and M. Anderson, *J. Phys. Chem.*, 1991, **95**, 3399.
22. M. Kaneko and I. Okura, *Photocatalysis - Science and Technology*, Springer, 2002.
23. M. Gratzel, *Nature*, 2001, **414**, 338.
24. A. Fujishima and K. Honda, *Bull. Chem. Soc. Jap.*, 1971, **44**, 1148.
25. X. Z. Ding and X. K. Liu, *J. Mater. Res.*, 1998, **13**, 9.
26. X. Z. Ding and X. K. Liu, *J. Alloys Comp.*, 1997, **143**, 248.
27. Y. Hwu, Y. D. Yao, N. F. Cheng, C. Y. Tung and H. M. Lin, *Nanostruct. Mater.*, 1997, **9**, 355.
28. H. Zhang and J. F. Banfield, *J. Mater. Chem.*, 1998, **8**, 2073.
29. D. V. Bavykin, S. N. Gordeev, A. V. Moskalenko, A. A. Lapkin and F. C. Walsh, *J. Phys. Chem. B*, 2005, **109**, 8565.
30. A. N. Enyashin and G. Seifert, *Physica Status Solidi B*, 2005, **242**, 1361.
31. R. F. Howe and M. Gratzel, *J. Phys. Chem.*, 1985, **89**, 4495.
32. R. F. Howe and M. Gratzel, *J. Phys. Chem.*, 1987, **91**, 3906.
33. S. H. Szczepankiewicz, A. J. Colussi and M. R. Hoffmann, *J. Phys. Chem. B*, 2000, **104**, 9842.

34. N. Serpone, D. Lawless, R. Khairutdinov and E. Pelizzetti, *J. Phys. Chem.*, 1995, **99**, 16655.
35. A. Chemseddine and T. Moritz, *Eur. J. Inorg. Chem.*, 1999, 235.
36. S. Y. Chae, M. K. Park, S. K. Lee, T. Y. Kim, S. K. Kim and W. I. Lee, *Chem. Mater.*, 2003, **15**, 3326.
37. X. Feng, J. Zhai and L. Jiang, *Angew. Chem. Int. Ed.*, 2005, **44**, 5115.
38. Q. Huang and L. Gao, *Chem. Lett.*, 2003, **32**, 638.
39. Q. Zhang and L. Gao, *Langmuir*, 2003, **19**, 967.
40. A. R. Armstrong, G. Armstrong, J. Canales, R. Garcia and P. G. Bruce, *Angew. Chem. Int. Ed.*, 2004, **43**, 2286.
41. A. R. Armstrong, G. Armstrong, J. Canales, R. Garcia and P. G. Bruce, *Adv. Mater.*, 2005, **7**, 862.
42. T. Kasuga, M. Hiramatsu, A. Hoson, T. Sekino and K. Niihara, *Langmuir*, 1998, **14**, 3160.
43. D. V. Bavykin, J. M. Friedrich and F. C. Walsh, *Adv. Mater.*, 2006, **18**, 2807.
44. D. V. Bavykin, V. N. Parmon, A. A. Lapkin and F. C. Walsh, *J. Mater. Chem.*, 2004, **14**, 3370.
45. T. Kasuga, M. Hiramatsu, A. Hoson, T. Sekino and K. Niihara, *Adv. Mater.*, 1999, **11**, 1307.
46. J. Wang, Q. Zhuang, Y. Peng and D. Li, *Nature*, 2005, **437**, 121.
47. B. Wen, C. Liu and Y. Liu, *J. Phys. Chem. B*, 2005, **109**, 12372.
48. J. M. Wu, *J. Cryst. Growth*, 2004, **269**, 347.
49. J. M. Wu, S. Hayakawa, K. Tsuru and A. Osaka, *Scripta Mater.*, 2002, **46**, 101.
50. X. Peng and A. Chen, *J. Mater. Chem.*, 2004, **14**, 2542.
51. M. D. Blesic, Z. V. Saponjic, J. M. Nedeljkovic and D. P. Uskokovic, *Mater. Lett.*, 2002, **54**, 298.
52. V. Jokanovic, A. M. Spasic and D. Uskokovic, *J. Coll. Interfac. Sci.*, 2004, **278**, 342.
53. H. Xia and Q. Wang, *Chem. Mater.*, 2002, **14**, 2158.
54. W. Huang, X. Tang, W. Y., Y. Koltypin and A. Gedanken, *Chem. Commun.*, 2000, 1415.
55. Y. Zhu, H. Li, Y. Koltypin, Y. R. Hacohen and A. Gedanken, *Chem. Commun.*, 2001, 2616.
56. G. Ma, X. Zhao and J. Zhu, *Int. J. Mod. Phys. B*, 2005, **19**, 2763.
57. X. Wu, Q. Z. Jiang, Z. F. Ma, M. Fu and W. F. Shangguan, *Solid State Commun.*, 2005, **136**, 513.
58. W. Choi, A.Termin and M. R. Hoffmann, *J. Phys. Chem.*, 1994, **98**, 13669.
59. F. B. Li, X. Z. Li and M. F. Hou, *Appl. Cat. B: Environmental*, 2004, **48**, 185.
60. M. Anpo, S. Kishiguchi, Y. Ichihashi, M. Takeuchi, H. Yamashita, K. Ikeue, B. Morin, A. Davidson and M. Che, *Res. Chem. Intermed.*, 2001, **27**, 459.
61. S. U. M. Khan, M. Al-Shahry and W. B. Ingler, *Science*, 2002, **297**, 2243.
62. X. Chen, Y. Lou, A. C. S. Samia, C. Burda and J. L. Gole, *Adv. Funct. Mater.*, 2005, **15**, 41.
63. A. Hattori, M. Yamamoto, H. Tada and S. Ito, *Chem. Lett.*, 1998, 707.
64. J. C. Yu, J. G. Yu, W. K. Ho, Z. T. Jiang and L. Z. Zhang, *Chem. Mater.*, 2002, **14**, 3808.
65. T. Ohno, T. Mitsui and M. Matsumura, *Chem. Lett.*, 2003, **32**, 364.
66. T. Umebayashi, T. Yamaki, H. Itoh and K. Asai, *Appl. Phys. Lett.*, 2002, **81**, 454.
67. R. Asahi, T. Morikawa, T. Ohwaki, K. Aoki and Y. Taga, *Science*, 2001, **293**, 269.

68. T. Yamaki, T. Umebayashi, T. Sumita, S. Yamamoto, M. Maekawa, A. Kawasuso and H. Itoh, *Nucl. Instrum. Methods Phys. Res. Sect. B*, 2003, **206**, 254.

69. R. Vogel, P. Hoyer and H. Weller, *J. Phys. Chem.*, 1994, **98**, 3183.

70. P. A. Sant and P. V. Kamat, *Phys. Chem. Chem. Phys.*, 2002, **4**, 198.

71. I. Robel, V. Subramanian, M. Kuno and P. V. Kamat, *J. Am. Chem. Soc.*, 2006, **128**, 2385.

72. Y. Tian and T. Tatsuma, *Chem. Commun.*, 2004, 1810.

73. P. D. Cozzoli, M. L. Curri and A. Agostiano, *Chem. Commun.*, 2005, 3186.

74. K. Kawahara, K. Suzuki, Y. Ohko and T. Tatsuma, *Phys. Chem. Chem. Phys.*, 2005, **7**, 3851.

75. H. A. Macleod, *Thin Film Optical Filters*, MacMillan, New York, 1986.

76. P. T. Moseley and B. C. Tofield, *Solid State Gas Sensors*, Adam Hilger, Bristol, 1987.

77. E. M. Logothetis, *Ceram. Proc. Eng. Sci.*, 1980, **1**, 281.

78. L. D. Birkefeld, A. M. Azad and S. A. Akbar, *J. Am. Ceram. Soc.*, 1992, **75**, 2964.

79. N. Savage, B. Chwieroth, A. Ginwalla, B. R. Patton, S. A. Akbar and P. K. Dutta, *Sensors Actuators B*, 2001, **79**, 17.

80. S. L. Pugh and J. T. Guthrie, *Dyes and Pigments*, 2002, **55**, 109.

81. Y. Kubota, C. Niwa, T. Ohnuma, Y. Ohko, T. Tatsuma and T. Mori, *J. Photochem. Photobiol. A: Chemistry*, 2001, **141**, 225.

82. J. C. Ireland, P. Klostermann, E. W. Rice and R. M. Clark, *Appl. Environ. Microbiol.*, 1993, **59**, 1668.

83. J. C. Sjogren and R. A. Sierka, *Appl. Environ. Microbiol.*, 1994, **60**, 344.

84. R. Cai, K. Hashimoto, Y. Kubota and A. Fujishima, *Chem. Lett.*, 1992, 427.

85. K. Suzuki, in *Photocatalytic Purification and Treatment of Water and Air*, eds. D. F. Ollis and H. Al-Ekabi, 1993.

86. M. Gratzel, *Acc. Chem. Res.*, 1981, **14**, 376.

87. A. Wold, *Chem. Mater.*, 1993, **5**, 280.

88. H. Gerischer and A. Heller, *J. Electrochem. Soc.*, 1992, **68**, 139.

89. E. F. Duffy, F. A. Touati, S. C. Kehoe, O. A. McLoughlin, L. Gill, W. Gernjak, I. Oller, M. I. Maldonado, S. Malato, J. Cassidy, R. H. Reed and K. G. McGuigan, *Solar Energy*, 2004, **77**, 657.

90. K. G. McGuigan, T. M. Joyce, R. M. Conroy, J. B. Gillespie and M. Elmore-Meegan, *J. Appl. Microbiol.*, 1998, **84**, 1138.

91. K. G. McGuigan, F. Méndez-Hermida, J. A. Castro-Hermida, E. Ares-Mazás, S. C. Kehoe, M. Boyle, C. Sichel, P. Fernández-Ibáñez, B. P. Meyer, S. Ramalingham and E. A. Meyer, *J. Appl. Microbiol.*, 2006, **101**, 453.

92. F. Méndez-Hermida, E. Ares-Mazás, K. G. McGuigan, M. Boyle, C. Sichel and P. Fernández-Ibáñez, *J. Photochem. Photobiol. B: Biology*, 2007, **88**, 105.

93. G. N. Schrauzer and T. D. Guth, *J. Am. Chem. Soc*, 1977, **99**, 7189.

94. S. N. Frank and A. J. Bard, *J. Am. Chem. Soc*, 1977, **99**, 303.

95. B. Kreutler and A. J. Bard, *J. Am. Chem. Soc*, 1978, **100**, 4317.

96. A. L. Pruden and D. F. Ollis, *J. Catal.*, 1983, **82**, 404.

97. T. Matsunaga, R. Tomato, T. Nakajima and H. Wake, *FEMS Microbiol. Lett.*, 1985, **29**, 211.

98. A. Fujishima, J. Ohtsuki, T. Yamashita and S. Hayakawa, *Photomed. Photobiol.*, 1986, **8**, 45.

99. B. O'Regan and M. Gratzel, *Nature*, 1991, **353**, 737.

100. N. Negishi, T. Iyoda, K. Hashimoto and A. Fujishima, *Chem. Lett.*, 1995, **24**, 841.

101. R. Wang, K. Hashimoto, A. Fujishima, M. Chikuni, E. Kojima and A. Kitamura, *Nature*, 1997, **388**, 431.
102. K. Sayama and H. Arakawa, *Faraday Trans.*, 1997, **93**, 1647.
103. E. Borgarello, J. Kiwi, M. Gratzel, E. Pelizzetti and M. Visca, *J. Am. Chem. Soc*, 1982, **104**, 2996.
104. A. Hagfeldt, N. Vlachopoulos and M. Gratzel, *J. Electrochem. Soc.*, 1994, **141**, L82.
105. F. Campus, P. Bonhote, M. Gratzel, S. Heinen and L. Walder, *Sol. Energy Mater. Sol. Cells*, 1999, **56**, 281.
106. K. D. Schierbaum, U. K. Kirner, J. F. Geiger and W. Goepel, *Sensors Actuators B*, 1991, **B4**, 87.
107. T. Takeuchi, *Sensors Actuators*, 1988, **14**, 109.
108. L. Zheng, M. Xu and T. Xu, *Sensors Actuators B*, 2000, **B66**, 28.
109. V. Demarne, S. Balkanova, A. Grisel, D. Rosenfeld and F. Levy, *Sensors Actuators B*, 1993, **14**, 497.
110. A. Trinchi, Y. X. Li, W. Wlodarski, S. Kaciulis, L. Pandolfi, S. Viticoli, E. Comini and G. Sberveglieri, *Sensors Actuators B*, 2003, **B95**, 145.
111. R. K. Sharma and M. C. Bhatnagar, *Sensors Actuators B*, 1999, **B56**, 215.
112. Y. Chen, J. C. Crittenden, S. Hackney, L. Sutter and D. W. Hand, *Environ. Sci. Technol.*, 2005, **39**, 1201.
113. in *Japan Chemical Week*, 2006, p. 4.
114. D. Robert and S. Malato, *Sci. Tot Env.*, 2002, **291**, 85.
115. http://es.epa.gov/ncerqa, Field Testing of a Solar Assisted System for Detoxification of Water, Accessed December, 2008.
116. D. M. Blake, National Renewable Energy Laboratory, Colorado, 2001.
117. N. Sakai, A. Fujishima, T. Watanabe and K. Hashimoto, *J. Phys. Chem. B*, 2003, **107**, 1028.
118. A. Fujishima and X. Zhang, *C. R. Chimie*, 2006, **9**, 750.
119. in *Japan Nanonet Bulletin 44th Issue*, 2005.
120. in *Japan Chemical Week*, 2003, p. 7.
121. *Polymers, Paint, Colour Journal*, 2006, **196**, 16.
122. D. W. Bahnemann, C. Kormann and M. R. Hoffmann, *J. Phys. Chem.*, 1987, **91**, 3789.
123. L. Bahadur and T. N. Rao, *J. Photochem. Photobiol. A: Chemistry*, 1995, **91**, 233.
124. J. B. Lee, H. J. Lee, S. H. Seo and J. S. Park, *Thin Solid Films*, 2001, **398-399**, 641.
125. B. J. Norris, J. Anderson, J. F. Wager and D. A. Keszler, *J. Phys. D. Appl. Phys.*, 2003, **36**, 105.
126. Z. W. Pang, Z. R. Dai and Z. L. Wan, *Science*, 2001, **291**, 1947.
127. Z. Hu, S. Chen and S. Peng, *J. Coll. Interfac. Sci.*, 1996, **182**, 457.
128. S. C. Pillai, J. M. Kelly, D. E. McCormack, P. O'Brien and R. Raghavendra, *J. Mater. Chem.*, 2003, **13**, 2586.
129. S. C. Pillai, J. M. Kelly, D. E. McCormack and R. Raghavendra, *J. Mater. Chem.*, 2004, **14**, 1572.
130. S. C. Pillai, J. M. Kelly, D. E. McCormack and R. Ramesh, *Mater. Sci. Tech.*, 2004, **20**, 964.
131. C. A. K. Gouvea, F. Wypych, S. G. Moraes, N. Duran, N. Nagata and P. Peralta-Zamora, *Chemosphere*, 2000, **40**, 433.
132. B. Sang and M. Konagai, *J. Appl. Phys.*, 1996, **35**, 602.
133. P. V. Kamat, R. Huehn and R. Nicolaescu, *J. Phys. Chem. B*, 2002, **106**, 788.

134. M. J. Height, S. E. Pratsinis, O. Mekasuwandumrong and P. Praserthdam, *Appl. Cat. B: Environmental*, 2006, **63**, 305.
135. L. Roselin, G. R. Rajarajeswarl, R. Selvin, V. Sadasivam, B. Sivasankar and K. Rengaraj, *Solar Energy*, 2002, **73**, 281.
136. D. F. Ollis, in *Photocatalysis - Fundamentals and Applications*, eds. E. Pelizzetti and N. Serpone, Wiley Interscience, New York, 1989.
137. A. Akyol and M. Bayramoglu, *J. Haz. Mat.* , 2005, **124**, 241.
138. J. Nishio, M. Tokumura, H. T. Znad and Y. Kawase, *J. Haz. Mat.*, 2006, **138**, 106.
139. S. Chakrabarti and B. K. Dutta, *J. Haz. Mat. B*, 2004.
140. B. Neppolian, H. C. Choi, S. Sakthivel, B. Arabindoo and V. Murugesan, *J. Haz. Mat.*, 2002, **89**, 303.
141. som.web.cmu.edu/structures/S014-ZnO.html Accessed December, 2008.
142. M. H. Huang, S. Mao, H. Feick, H. Q. Yan, Y. Y. Wu, H. Kind, R. Russo and P. D. Yang, *Science*, 2001, **292**, 1897.
143. Y. C. Kong, D. P. Yu, Z. B., W. Fang and S. Q. Feng, *Appl. Phys. Lett.*, 2003, **78**, 407.
144. W. I. Park, Y. H. Jun, S. W. Jung and G. C. Yi, *Appl. Phys. Lett.*, 2003, **82**, 964.
145. C. H. Liu, J. A. Zapien, Y. Yao, X. Meng, C. S. Lee, S. Fan, Y. Lifshitz and S. T. Lee, *Adv. Mater.*, 2003, **15**, 838.
146. A. B. Hartanto, X. Ning, Y. Nakata and T. Okada, *Appl. Phys. A*, 2003, **78**, 299.
147. B. Liu and H. C. Zeng, *J. Am. Chem. Soc*, 2003, **125**, 4430.
148. L. Vayssieres, *Adv. Mater.*, 2003, **15**, 464.
149. J. Wang and L. Gao, *J. Mater. Chem.*, 2003, **13**, 2551.
150. P. Jiang, J. J. Zhou, H. F. Fang, C. Y. Wang and S. S. Xie, *Mater. Lett.*, 2006, **60**, 2516.
151. C. X. Xu and X. W. Sun, *J. Cryst. Growth*, 2005, **277**, 330.
152. G. C. Yi and W. I. WangPark, *Semicond. Sci. tech.*, 2005, **20**, S22.
153. T. Yoshida, in *23rd European Photovoltaic Solar Energy Conference and Exhibition*, Valencia, Spain, 2008.
154. W. D. Ketola and D. Grossman, *Organic Materials ASTM International*, 1994, 69.
155. P. V. Kamat and N. M. Demitrijevic, *Solar Energy*, 1990, **44**, 83.
156. P. V. Kamat, *Langmuir*, 1985, **1**, 608.
157. V. Subramanian, E. E. Wolf and P. V. Kamat, *J. Am. Chem. Soc*, 2004, **126**, 4943.
158. M. K. Seery, R. George, P. Floris and S. C. Pillai, *J. Photochem. Photobiol. A: Chemistry*, 2007, **189**, 258.
159. H. Jia, J. Zeng, W. Song, J. An and B. Zhao, *Thin Solid Films*, 2006, **496**, 281.
160. S. X. Liu, Z. P. Qu, X. W. Han and C. L. Sun, *Catal. Today*, 2004, **93**, 877.
161. B. Connolly, DIT, Dublin, 2005.
162. R. Georgekutty, M. K. Seery and S. C. Pillai, *J. Phys. Chem. C*, 2008, **112**, 13563.
163. A. S. R. Juo and K. Franzluebbers, *Tropical Soils - Properties and management for sustainable agriculture*, Oxford University Press, Oxford, 2008.
164. P. A. Connor, K. D. Dobson and A. J. McQuillan, *Langmuir*, 1999, **15**, 2402.
165. C. B. Mendive, T. Bredow, M. A. Blesa and D. W. Bahnemann, *Phys. Chem. Chem. Phys.*, 2006, **8**, 3232.
166. A. J. McQuillan, *Adv. Mater.*, 2001, **13**, 1034.
167. R. A. Spurr and H. Myers, *Anal. Chem.*, 1957, **29**, 760.
168. M. S. Reisch, *Chemical Engineering News*, 2003, **81**, 13.

169. T. Sakata, in *Photocatalysis - Fundamentals and Applications* eds. N. Serpone and E. Pelizzetti, Wiley, New York, 1989.
170. Y. Bessekhouad, N. Chaoui, M. Trzpit, N. Ghazzal, D. Robert and J. V. Weber, *J. Photochem. Photobiol. A: Chemistry*, 2006, **183**, 218.
171. D. Dvoranova, V. Brezova, M. Mazur and M. A. Malati, *Appl. Cat. B: Environmental*, 2002, **37**, 91.
172. H. Yamashita, Y. Ichihashi, M. Takeuchi, S. Kishiguchi and M. Anpo, *J. Synchotron Rad.*, 1999, **6**, 451.
173. F. Kiriakidodu, D. I. Kondarides and X. E. Verykios, *Catal. Today*, 1999, **54**, 119.
174. P. D. Cozzoli, R. Comparelli, E. Fanizza, M. L. Curri, A. Agostiano and D. Laub, *J. Am. Chem. Soc*, 2004, **126**, 3868.
175. Y. Ohko, T. Tatsuma, T. Fujii, K. Naoi, C. Niwa, Y. Kubota and A. Fujishima, *Nature Mat.*, 2003, **2**, 29.
176. M. Machida, K. Norimoto and T. Kimura, *J. Am. Ceram. Soc.*, 2005, **88**, 95.
177. M. Jakob, H. Levanon and P. V. Kamat, *Nano Lett.*, 2003, **3**, 353.
178. E. Stathatos, T. Petrova and P. Lianos, *Langmuir*, 2001, **17**, 5025.
179. P. V. Kamat, *J. Phys. Chem. B*, 2002, **106**, 7729.
180. H. E. Chao, Y. U. Yun, H. U. Xiangfang and A. Larbot, *J. Eur. Ceram. Soc.*, 2003, **23**, 1457.
181. V. Vamathevan, R. Amal, D. Beydoun, G. Low and S. McEvoy, *J. Photochem. Photobiol. A: Chemistry*, 2002, **148**, 233.
182. S. C. Pillai, P. Periyat, R. George, D. E. McCormack, M. K. Seery, H. Hayden, J. Colreavy, D. Corr and S. J. Hinder, *J. Phys. Chem. C*, 2007, **111**, 1605.
183. B. Xin, L. Jing, Z. Ren, B. Wang and H. Fu, *J. Phys. Chem. B*, 2005, **109**, 2805.
184. Y. Wang and N. Herron, *J. Phys. Chem.*, 1991, **95**, 525.
185. D. M. Ledwith, A. M. Whelan and J. M. Kelly, *J. Mater. Chem.*, 2007, **17**, 2459.
186. C. Hu, Y. Q. Lan, J. H. Qu, X. X. Hu and A. M. D. Wang, *J. Phys. Chem. B*, 2006, **110**, 4066.
187. A. Chen, M. C. Bartelt, S. M. Seutter and K. F. McCarty, *Surf. Sci.*, 2000, **464**, L708.
188. C. B. Mendive, University of Hannover, 2007.
189. M. E. Calvo, R. J. Candal and S. A. Bilmes, *Environ. Sci. Technol.*, 2001, **35**, 4132.
190. D. P. Birnie and N. J. Bendzko, *Mater. Chem. Phys.*, 1999, **59**, 26.
191. A. Leaustic and R. E. Riman, *J. Non-Cryst. Solids*, 1991, **135**, 259.
192. P. P. Phule and F. Khairulla, in *Better Ceramics Through Chemistry IV*, eds. B. J. J. Zelinski, C. J. Brinker, D. E. Clark and D. R. Ulrich, MRS Symposium Proceedings, 1990, p. 527.
193. G. Yi, Z. Wu and M. Sayer, *J. Appl. Phys.*, 1988, **64**, 2717.
194. D. C. Bradley, R. C. Mehrotra and D. P. Gaur, in *Metal Alkoxides*, Academic Press, New York, 1978.
195. S. Doeuff, M. Henry, C. Sanchez and J. Livage, *J. Non-Cryst. Solids*, 1987, **89**, 206.
196. I. Laaziz, A. Larbot, A. Julbe, C. Guizard and L. Cot, *J. Sol. State Chem.*, 1992, **98**, 393.
197. D. P. Birnie, *J. Mater. Sci.*, 2000, **35**, 367.
198. R. Parra, M. S. Góes, M. S. Castro, E. Longo, P. R. Bueno and J. A. Varela, *Chem. Mater.*, 2008, **20**, 143.
199. J. Livage, C. Sanchez, M. Henry and S. Doeuff, *Solid State Ionics*, 1989, **32/33**, 633.

200. C. Sanchez, F. Babonneau, S. Doeuff and A. Leaustic, in *Innovative Processing and Synthesis of Ceramics, Glasses, and Composites*, ed. A. C. Society, Wiley, New York, 1998.

201. H. Choi, E. Stathatos and D. D. Dionysiou, *Appl. Cat. B: Environmental*, 2006, **63**, 60.

202. J. C. S. Wu and C. Y. Yeh, *Mater. Today*, 2001, **16**, 615.

203. W. D. Kingery, H. K. Bowen and D. R. Uhlmann, *Introduction to Ceramics*, Wiley, New York, 1976.

204. A. Henglein, *J. Phys. Chem.*, 1979, **83**, 2209.

205. V. Iliev, D. Tomova, L. Bilyarska, A. Eliyas and L. Petrov, *Appl. Cat. B: Environmental*, 2006, **63**, 266.

206. J. P. Jolivet, *De la solution à l'oxyde: Condensation des cations en solution aqueuse. Chimie de surface des oxydes*, CNRS, Paris, 1994.

207. Y. U. Ahn, E. J. Kim and S. H. Hahn, *Mater. Lett.*, 2003, **57**, 4660.

208. H. Z. Zhang and J. F. Banfield, *J. Phys. Chem. B*, 2000, **104**, 3481.

209. J. Ovenstone and K. Yanagisawa, *Chem. Mater.*, 1999, **11**, 2770.

210. C. P. Sibu, Cochin University of Science And Technology, 2004.

211. J. M. Coronado, *J. Photochem. Photobiol. A: Chemistry*, 2002, **150**, 213.

212. M. Gratzel and R. F. Howe, *J. Phys. Chem.*, 1990, **94**, 2566.

213. A. Sclafani and J. M. Hermann, *J. Photochem. Photobiol. A: Chemistry*, 1998, **113**, 181.

214. T. Watanabe, T. Takizava and K. Honda, *J. Phys. Chem.*, 1977, **81**, 1845.

215. H. Tran, K. Chiang, J. Scott and R. Amal, *Photochem. Photobiol. Sci.*, 2005, **4**, 565.

216. H. Tran, J. Scott, K. Chiang and R. Amal, *J. Photochem. Photobiol. A: Chemistry*, 2006, **183**, 41.

217. H. M. Sung-suh, J. R. Choi, H. J. Hah, S. M. Koo and Y. C. Bae, *J. Photochem. Photobiol. A: Chemistry*, 2004, **163**, 37.

218. X. Yan, T. Ohno, K. Nishijima, R. Abe and B. Ohtani, *Chem. Phys. Lett.*, 2006, **429**, 606.

219. M. A. Blesa, R. J. Candal and S. A. Bilmes, *Surf. Coll. Sci.*, 2004, 1783.

220. C. Guillard, C. Hoang-Van, P. Pichat and F. Marme, *J. Photochem. Photobiol. A: Chemistry*, 1995, **89**, 221.

221. G. Lapidus, D. Barton and P. E. Yankwich, *J. Phys. Chem.*, 1964, **68**, 1863.

222. D. E. Wobbe and W. A. Noyes, *J. Am. Chem. Soc*, 1928, **48**, 2858.

223. W. L. Clark, *J. Phys. Chem.*, 1957, **61**, 699.

224. A. Dinglinger and E. Z. Schroer, *Physik Chem. A*, 1937, **179**, 401.

225. E. O. Wiig, *J. Am. Chem. Soc*, 1930, **52**, 4737.

226. S. Yamamoto and R. A. Back, *J. Phys. Chem.*, 1985, **89**, 622.

227. M. M. Kosanic, *J. Photochem. Photobiol. A: Chemistry*, 1998, **119**, 119.

228. F. P. Rotzinger, J. M. Kesselman-Truttmann, S. J. Hug, V. Shklover and M. Gratzel, *J. Phys. Chem. B*, 2004, **108**, 5004.

229. S. J. Hug and B. Sulzberger, *Langmuir*, 1994, **10**, 3587.

230. A. D. Weisz, L. Garcia-Rodenas, P. J. Morando, A. E. Regazzoni and M. A. Blesa, *Catal. Today*, 2002, **76**, 103.

231. S. J. Hug and D. W. Bahnemann, *J. Electron. Spec. Relat. Phen.*, 2006, **150**, 208.

232. C. B. Mendive, D. W. Bahnemann and M. A. Blesa, *Catal. Today*, 2005, **101**, 237.

233. P. Cheng, J. Qiu, M. Gu and W. Shangguan, *Mater. Lett.*, 2004, **58**, 3751.

234. M. Afzaal, M. A. Malik and P. O'Brien, *New J. Chem.*, 2007, **31**, 2029.

235. P. V. Kamat, *J. Phys. Chem. C*, 2007, **111**, 2834.

236. A. Mills and J. Wang, *J. Photochem. Photobiol. A: Chemistry*, 2006, **182**, 181.
237. P. Periyat, S. C. Pillai, D. E. McCormack, J. Colreavy and S. J. Hinder, *J. Phys. Chem. C*, 2008, **112**, 44.
238. S. Sakthivel, B. Neppolian, M. V. Shankar, B. Arabindoo, M. Palanichamy and V. Murugesan, *Sol. Energy Mater. Sol. Cells*, 2003, **77**, 65.
239. S. Dindar and J. Icli, *J. Photochem. Photobiol. A: Chemistry*, 2001, **140**, 263.
240. C. Hariharan, *Appl. Cat. A: General*, 2006, **304**, 55.
241. A. A. Khodja, T. Sehili, J. F. Pilichowski and P. Boule, *J. Photochem. Photobiol. A: Chemistry*, 2001, **141**, 231.
242. J. M. Hermann, H. Tahiri, Y. Ait-Ichou, G. Lossaletta, A. R. Gonzalez-Elipe and A. Fernandez, *Appl. Cat. B: Environmental*, 1997, **13**, 219.
243. H. S. Kang, B. D. Ahn, J. H. Kim, G. H. Kim, S. H. Lim, H. W. Chang and S. Y. Lee, *Appl. Phys. Lett.*, 2006, **88**, 202108.
244. P. Pathak, M. J. Meziani, L. Castillo and Y. P. Sun, *Green Chemistry*, 2005, **7**, 667.
245. T. Hirakawa and P. V. Kamat, *J. Am. Chem. Soc*, 2005, **127**, 3928.
246. R. Wang, J. H. Xina, Y. Yang, H. Liu, L. Xu and J. Hu, *Appl. Surf. Sci.*, 2004, **227**, 312.
247. S. H. Jeong, B. N. Park, S. B. Lee and B. J. H., *Surf. & Coating Tech.*, 2005, **193**, 340.
248. L. Yang, G. Wang, C. Tang, H. Wang and L. Zhang, *Chem. Phys. Lett.*, 2005, **409**, 337.
249. L. Spanhel and M. A. Anderson, *J. Am. Chem. Soc*, 1991, **113**, 2826.
250. G. I. N. Waterhouse, G. A. Bowmaker and J. B. Metson, *Phys. Chem. Chem. Phys.*, 2001, **3**, 3838.
251. B. D. Ahn, H. S. Kang, J. H. Kim, H. W. Chang and S. Y. Lee, *J. Appl. Phys.*, 2006, **100**, 093701.
252. D. J. Blinks and R. W. Grimes, *J. Am. Ceram. Soc.*, 1993, **76**, 2370.
253. J. Fan and R. Freer, *J. Appl. Phys.*, 1995, **77**, 9.
254. P. Tonto, O. Mekasuwandumrong, S. Phatanasri, V. Pavarajarn and P. Praserthdam, *Ceramics International*, 2008.
255. S. C. Pillai, J. M. Kelly, D. E. McCormack and R. Ramesh, *J. Mater. Chem.*, 2008, DOI:10.1039/b804793f.
256. H. J. Chuang and H. W. Ko, *Proc. Nat. Sci. Council. Rep. China A: Phys. Sci. Eng.*, 1989, **13**, 145.
257. S. K. Sharma and G. J. Exarhos, *Sol. State. Phen.*, 1997, **55**, 32.
258. Z. C. Zhang, B. B. Huang, Y. Q. Yu and D. L. Cui, *Mater. Sci. Eng. B*, 2001, **86**, 109.
259. J. J. Wu and S. C. Liu, *J. Phys. Chem. B*, 2002, **106**, 9546.
260. T. Aarthi and G. Madras, *Ind. Eng. Chem. Res.*, 2007, **46**, 7.
261. Y. Qiu, F. Zhang, F. Zhao, Y. Tang and X. Song, *J. Photochem. Photobiol. A: Chemistry*, 1995, **85**, 281.
262. J. M. Hermann, J. Disdier and P. Pichat, *J. Phys. Chem.*, 1986, **90**, 6028.
263. S. T. Kuo, W. H. Tuan, J. Shieha and S. F. Wang, *J. Eur. Ceram. Soc.*, 2007, **27**, 4521.
264. Q. J. Yang, H. Choi and D. D. Dionysiou, *Appl. Cat. B: Environmental*, 2007, **74**, 170.
265. L. Zhang, J. C. Yu, H. Y. Yip, Q. Li, K. W. Kwong, A. W. Xu and P. K. Wong, *Langmuir*, 2003, **19**, 10372.
266. K. Vanheusden, W. L. Warren, C. H. Seager, D. R. Tallant and J. A. Voigt, *J. Appl. Phys.*, 1996, **79**, 7983.

165

267. A. B. Djurisic, Y. H. Leung, C. W. C. H. Choy, K. W. Cheah and W. K. Chan, *Appl. Phys. Lett.*, 2004, **84**, 2635.
268. P. V. Kamat and B. Patrick, *J. Phys. Chem.*, 1992, **96**, 6829.
269. S. Manticone, R. Tefeu and A. V. Kanaev, *J. Phys. Chem. B*, 1998, **102**, 2854.
270. B. D. Yao, Y. F. Chan and N. Wang, *Appl. Phys. Lett.*, 2002, **81**, 757.
271. H. Liu, S. Cheng, M. Wu, H. Wu, J. Zhang, W. Li and C. Cao, *J. Phys. Chem. A*, 2000, **104**, 7016.
272. V. Subramanian, E. E. Wolf and P. V. Kamat, *J. Phys. Chem. B*, 2003, **107**, 7479.
273. S. M. Haile, D. W. Johnson, G. H. Wiseman and H. K. Bowen, *J. Am. Ceram. Soc.*, 1989, **72**, 2004.
274. S. Hingorani, V. Pillai, P. Kumar, M. S. Multani and D. O. Shah, *Mater. Chem. Res. Bull.*, 1993, **28**, 1303.
275. K. Okuyama, *J. Mater. Sci.*, 1997, **32**, 1229.
276. R. Okuyama, *J. Aerosol Sci.*, 1998, **22**, 5.
277. E. Sonder, T. C. Quinky and L. Kinser, *Am. Ceram. Soc. Bull.*, 1984, **63**, 278.
278. Y. J. Kwon, K. H. Kim, C. S. Lim and K. B. Shim, *J. Ceram. Proc. Res.*, 2002, **3**, 146.
279. J. Zhang, L. Sun, J. Yin, H. Su, C. Liao and C. Yan, *Chem. Mater.*, 2002, **14**, 4172.
280. G. M. Duffy, S. C. Pillai and D. E. McCormack, *Smart Mater. Struct.*, 2007, **16**, 1379.
281. X. Wang, Q. Li, Z. Liu, J. Zhang and Z. Liu, *Appl. Phys. Lett.*, 2004, **84**, 4941.
282. Y. Kanai, *J. Appl. Phys.*, 1991, **30**, 2021.
283. S. Dallek, B. F. Larrick and W. A. West, *J. Electrochem. Soc.*, 1986, **133**, 245.
284. B. V. L'vov, *Thermochim. Acta*, 1999, **13**, 333.
285. A. C. Dodd, A. J. Mckinley, M. Saunders and T. Tsuzuki, *J. Nano Res.*, 2006, **8**, 43.
286. D. W. Bahnemann, *Solar Energy*, 2004, **77**, 445.
287. L. Q. Jing, Y. Qu, B. Wang, S. Li, B. Jiang, L. Yang, F. Wei and H. Fu, *J. Sun, Solar Energy Mater. & Solar Cell*, 2006, **90**, 1773.
288. Z. Zhou, S. Quian, S. Yao and Z. Zhang, *Rad. Phys. Chem.*, 2002, **65**, 241.
289. J. Bandara, K. Tennakone and P. Binduhewa, *New J. Chem.*, 2001, **25**, 1302.
290. J. Zhao, T. K. Wu, K. Oikawa, H. Hidaka and N. Serpon, *Environ. Sci. Technol.*, 1998, **32**, 2394.
291. P. V. Kamat, J. P. Chauvet and R. W. Fessenden, *J. Phys. Chem.*, 1986, **90**, 1389.
292. P. V. Kamat, S. Das, K. G. Thomas and M. V. George, *Chem. Phys. Lett.*, 1991, **178**, 75.
293. P. V. Kamat and M. A. Fox, *Chem. Phys. Lett.*, 1983, **102**, 379.
294. K. Kalyansundaram, N. Vlachopoulos, V. Krishnan, A. Monnier and M. Gratzel, *J. Phys. Chem.*, 1987, **91**, 2342.
295. P. V. Kamat, *Pure Appl. Chem.*, 2002, **74**, 1693.
296. A. Wood, M. Giersig and P. Mulvaney, *J. Phys. Chem. B*, 2001, **105**, 8810.
297. E. Hendry, F. Wang, J. Shan, T. F. Heins and M. Bonn, *Phys. Rev. B*, 2004, **69**, 81.
298. Y. Ichihashi, H. Yamashita and M. Anpo, *Funct. Mater.*, 1996, **16**, 12.
299. Y. Choi, T. Umebayashi and M. Yoshikawa, *J. Mat. Sci.*, 2004, **39**, 1837.
300. A. Hattori and H. Tada, *J. Sol-Gel Sci. Technol.*, 2001, **22**, 47.
301. S. U. M. Khan, M. Al-Shahry and W. B. Ingler Jr, *Science*, 2002, **297**, 2243.
302. R. Asahi, Y. Taga, W. Mannstadt and A. J. Freeman, *Phys. Rev. B*, 2000, **61**, 7459.

303. T. Umebayashi, T. Yamaki, H. Itoh and K. Asai, *Chem. Lett.*, 2003, **32**, 330.
304. S. C. Moon, H. Mametsuka, S. Tabata and E. Suzuki, *Catal. Today*, 2000, **58**, 125.
305. H. Luo, T. Takata, Y. Lee, J. Zhao, K. Domen and Y. Yan, *Chem. Mater.*, 2004, **16**, 846.
306. W. Macyk and H. Kisch, *Chem. Eur. J.*, 2001, **7**, 1862.
307. L. Zang, C. Lange, I. Abraham, S. Stork, W. F. Maier and H. Kisch, *J. Phys. Chem. B*, 1998, **102**, 10765.
308. C. Yu, J. Lin and R. W. M. Kwok, *J. Phys. Chem. B*, 1998, **102**, 5094.
309. A. W. Xu, Y. Gao and H. Q. Liu, *J. Catal.*, 2002, **207**, 151.
310. K. T. Ranjit, I. Willner, S. H. Bossmann and A. M. Braun, *J. Catal.*, 2001, **204**, 305.
311. K. T. Ranjit, I. Willner, S. H. Bossmann and A. M. Braun, *Environ. Sci. Technol.*, 2001, **35**, 1544.
312. C. P. Sibu, S. R. Kumar, P. Mukundan and K. G. K. Warrier, *Chem. Mater.*, 2002, **14**, 2876.
313. P. Periyat, K. V. Baiju, P. Mukundan, P. K. Pillai and K. G. K. Warrier, *J. Sol-Gel Sci. Technol.*, 2007, **43**, 299.
314. TBA.
315. J. G. Nunan, H. J. Robota, M. J. Cohn and S. A. Bradley, *J. Catal.*, 1992, **133**, 309.
316. A. Trovarelli, G. Dolcetti, C. de Leitenburg, J. Kaspar, P. Finetti and A. Santoni, *J. Chem. Soc. Faraday Trans.*, 1992, **88**, 1311.
317. C. Serre, F. Garin, G. Belot and G. Marie, *J. Catal.*, 1993, **141**, 9.
318. M. F. M. Zwinkels, S. G. Jaras and P. G. Menon, *Catal. Rev. Sci. Eng.*, 1993, **35**, 319.
319. F. B. Li, X. Z. Li, M. F. Hou, K. W. Cheah and W. C. H. Choy, *Appl. Cat. A: General*, 2005, **285**, 181.
320. S. Imamura, H. Yamada and K. Utani, *Appl. Cat. A: General*, 2000, **192**, 221.
321. T. Lopez, F. Rojas, R. Alexander-Katz, F. Galindo, A. Balankin and A. Buljan, *J. Sol. State Chem.*, 2004, **177**, 1873.
322. J. Xiao, T. Peng, R. Li, Z. Peng and C. Yan, *J. Sol. State Chem.*, 2006, **179**, 1161.
323. Z. Liu, B.Guo, L. Hong and H. Jiang, *J. Phys. Chem. Sol.*, 2005, **66**, 161.
324. S. J. Kim, S. D. Park and Y. H. Jeong, *J. Am. Ceram. Soc.*, 1999, **82**, 927.
325. R. Gopalan and Y. S. Lin, *Ind. Eng. Chem. Res.*, 1995, **34**, 1189.
326. C. A. LeDuc, J. M. Campbell and J. A. Rossin, *Ind. Eng. Chem. Res.*, 1996, **34**, 1189.
327. J. Lin, J. C. Yu, D. Lo and S. K. Lam, *J. Catal.*, 1999, **183**, 368.
328. E. L. Crepaldi, G. J. d. A. A. Soler-Illia, D. Grosso, F. Cagnol, F. Ribot and C. Sanchez, *J. Am. Chem. Soc*, 2003, **125**, 9770.
329. C. Anderson and A. Bard, *J. Phys. Chem.*, 1994, **98**, 1769.
330. J. A. Gamboa and D. M. Pasquevich, *J. Am. Ceram. Soc.*, 1992, **75**, 2934.
331. S. E. Paje, M. A. Garcia, M. A. Villegas and J. Llopis, *Optical Mater.*, 2001, **17**, 459.
332. Y. F. Yu Yao, *J. Catal.*, 1984, **87**, 152.
333. A. F. Diwell, R. R. Rajaram, H. A. Shaw and T. J. Treux, *Catalysis and automotive pollution control*, Elsevier, Amsterdam, 1991.
334. Y. Dai, J. Qiu, X. Hu, I. Yang, X. Jiang, C. Zhu and B. Yu, *Appl. Phys. B*, 2006, **84**, 501.
335. J. Rynkowski, J. Farbotko, R. Touroude and L. Hilaire, *Appl. Cat. A: General*, 2000, **203**, 335.

336. A. S. Sass, V. A. Shvets, G. A. Savel'eva, N. M. Popova and V. B. Kazanskii, *Kinetic Katal.*, 1984, **25**, 924.

337. A. S. Sass, V. A. Shvets, G. A. Savel'eva, N. M. Popova and V. B. Kazanskii, *Kinetic Katal.*, 1987, **28**, 777.

338. A. L. Tarasov, L. K. Przheval'skaya, V. A. Shvets and V. B. Kazanskii, *Kinetic Katal.*, 1988, **29**, 1020.

339. T. Kawahara, Y. Konishi, H. Tada, N.Tohge, J. Nishii and S. Ito, *Angew. Chem. Int. Ed.*, 2002, **15**, 41.

340. L. Zhao, M. Han and J. Lian, *Thin Solid Films*, 2008, **516**, 3394.

341. A. J. Maira, K. L. Yeung, C. Y. Lee, P. L. Yue and C. K. Chan, *J. Catal.*, 2000, **192**, 18.

342. J. Ryu and W. Choi, *Environ. Sci. Technol.*, 2008, **42**, 294.

343. J. Marugan, D. Hufschmidt, M. J.-. Lopez-Munoz, V. Selzer and D. Bahnemann, *Appl. Cat. B: Environmental*, 2006, **62**, 201.

344. S. Malynych and G. Chumanov, *J. Am. Chem. Soc*, 2003, **125**, 2896.

PUBLICATIONS BY THE AUTHOR

1. M. K. Seery, R. George, P. Floris and S. C. Pillai, *J. Photochem. Photobiol. A: Chemistry*, 2007, **189**, 258.

2. S. C. Pillai, P. Periyat, R. George, D. E. McCormack, M. K. Seery, H. Hayden, J. Colreavy, D. Corr and S. J. Hinder, *J. Phys. Chem. C*, 2007, **111**, 1605.

3. R. Georgekutty, M. K. Seery and S. C. Pillai, *J. Phys. Chem. C*, 2008, **112**, 13563.

4. R. Georgekutty, M. K. Seery and S. C. Pillai, *Chem. Mater.* 2009 (Submitted)

PRESENTATIONS BY THE AUTHOR

1. *Metal Oxide Photocatalysis: Study of the Mechanism of Action*, (Oral Presentation) R. Georgekutty, 59th Irish Universities Chemistry Research Colloquium, Dublin.

2. *Synthesis of silver doped ZnO for enhanced photocatalytic applications*, R. George, M. K. Seery, S. C. Pillai, April 2008, Materials Ireland, Athlone.

3. *Synthesis of silver doped ZnO for enhanced photocatalytic applications*, (Poster Presentation) R. George, M. K. Seery, S. C. Pillai, Aug 2007, SP-2, Second International Conference in Semiconductor Photochemistry, Aberdeen.

4. *Silver doped ZnO for enhanced photocatalytic application*, (Poster Presentation) R. George, M. K. Seery, S. C. Pillai, Jun 2007, 59th Irish Universities Chemistry Research Colloquium, Dublin.

5. *Silver doped sol-gel titania for efficient visible light catalysed photocatalysis*, (Poster Presentation) R. George, M. K. Seery, S. C. Pillai, 23rd International Manufacturing Conference, Aug 2006, University of Ulster, Belfast, UK.

APPENDICES

Appendix 1: Table of crystallite sizes of ZnO and various mol% silver modified ZnO.

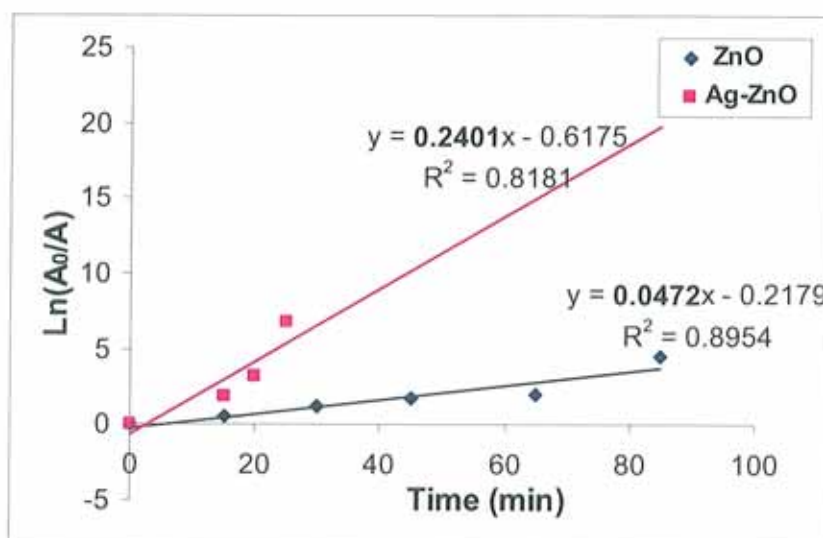|	Crystallite sizes (nm)			
Temperature (^{o}C)	ZnO	ZnO-1%Ag	ZnO-3%Ag	ZnO-5%Ag
400	16.85	16.9	14.8	16.3
500	24.73	24.7	21.4	25.1
600	30.62	30.6	28.2	32.9
1000	39.07	39.1	35.3	40

Appendix 2: FT-IR spectra of ZnO and silver modified ZnO (a), 3Ag-ZnO (b) and 5Ag-ZnO (c) at 300 °C
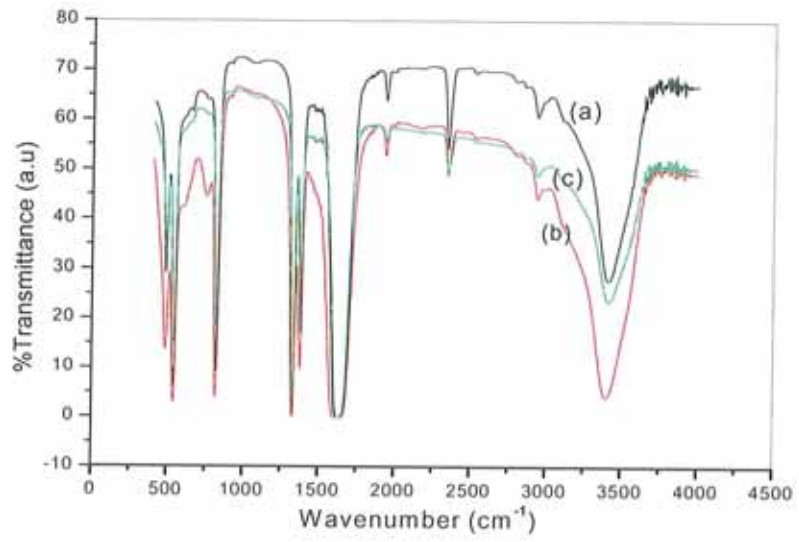
Appendix 3: Table of rate constants for photocatalytic degradation of R6G in presence of silver modified ZnO at higher temperatures.

Temperature (°C)	Rate constant (min^{-1}) of ZnO samples with various mol % of silver			
	0	1	3	5
300	0.003	0.043	0.056	0.083
400	0.101	0.345	0.457	0.423
500	0.076	0.136	0.156	0.197
600	0.084	0.250	0.353	0.300
800	0.095	--	0.103	0.055
1000	0.096	0.0344	0.019	0.010

Appendix 4: Kinetic data showing the sunlight driven photcatalytic degradation of rhodamine in presence of ZnO and 5 mol% silver modified ZnO.

A plot of $Ln(A_0/A)$ versus Time (min) showing two data series: ZnO (blue diamonds) and Ag-ZnO (pink squares).

For Ag-ZnO: $y = \mathbf{0.2401}x - 0.6175$, $R^2 = 0.8181$

For ZnO: $y = \mathbf{0.0472}x - 0.2179$, $R^2 = 0.8954$

Appendix 5: XRD of TiO$_2$ and silver-ceria co-doped TiO$_2$ at 900 °C.